

THESIS

c.2

LIBRARY
Michigan State
University



This is to certify that the

dissertation entitled

SYSTEMATIC STUDIES OF CHARGED DERIVATIVES OF PEPTIDES ANALYZED BY MASS SPECTROMETRY

presented by

Kenneth David William Roth

has been accepted towards fulfillment of the requirements for

Ph.D. degree in Chemistry

Date 21 Feb 1999

0-12771

PLACE IN RETURN BOX to remove this checkout from your record. TO AVOID FINES return on or before date due. MAY BE RECALLED with earlier due date if requested.

DATE DUE	DATE DUE	DATE DUE
17212101 002001	MAR 2 6 2004 ;	
SEP 1 9 2004		

1/98 c/CIRC/DateDue.p85-p.14

SYSTEMATIC STUDIES OF CHARGED DERIVATIVES OF PEPTIDES ANALYZED BY MASS SPECTROMETRY

Ву

Kenneth David William Roth

A DISSERTATION

Submitted to
Michigan State University
in partial fulfillment of the requirements
for the degree of

DOCTOR OF PHILOSOPHY

Department of Chemistry

ABSTRACT

SYSTEMATIC STUDIES OF CHARGED DERIVATIVES OF PEPTIDES ANALYZED BY MASS SPECTROMETRY

By

Kenneth David William Roth

Mass spectrometry is a powerful analytical technique for sequence analysis of peptides and proteins. However, the fragmentation patterns of peptides are often complex and difficult to interpret. Charge derivatization was developed as an approach to simplify the fragmentation patterns of peptides and to increase the sequence information available from analysis by mass spectrometry. This dissertation provides an introduction to several types of mass spectrometers, the use of mass spectrometry for peptide sequencing, and common types of peptide fragment ions. A review of charge-derivatization techniques is also included with special attention given to the tris(2,4,6-trimethoxyphenyl)-phosphonium-acetyl (TMPP*-Ac) derivatization technique.

The fragmentation of TMPP⁺-Ac-derivatized peptides is described in detail with special attention paid to fragmentation during analysis by FAB-CAD-MS/MS. The preparation of a weighable quantity of a purified TMPP⁺-Ac-derivatized peptide is also described. Based on the UV absorbance of the derivatized and underivatized peptide, reaction yields as high as 98.5% were observed. The selectivity of the TMPP⁺-Ac reagent for the N-terminus was studied in the presence of lysine, cysteine, and tyrosine. The derivatization reaction was studied in an unbuffered solution containing 4-dimethyl-aminopyridine and in a pH 8.3 Tris-HCl buffer solution. The reagent reacted with lysine,

cysteine, and tyrosine to some extent in both the buffered and unbuffered solution. Derivatization in the buffered solution did not provide enhanced selectivity and resulted in a decrease in the desired N-terminal-derivatized product. Derivatization of the cysteine side-chain was more complete than derivatization of the N-terminus. Derivatization of lysine and tyrosine was less complete than derivatization of the N-terminus. No signal enhancement was observed for a TMPP*-Ac-derivatized peptide analyzed by MALDI-MS compared to the signal obtained from an equal amount of the underivatized peptide. However, when a mixture of the derivatized and underivatized peptide was analyzed by MALDI-MS, the signal intensity of the underivatized peptide was suppressed.

The use of mass spectrometry and charge derivatization to distinguish between normal and isomeric forms of aspartate (Asp) and glutamate (Glu) was studied. Small underivatized peptides containing the isomeric residues β -Asp or γ -Glu produced more intense y ions and less intense [MH⁺-H₂O] fragment ions than analogous peptides containing normal Asp or Glu. The fragmentation differences were more dramatic for pairs of charge-derivatized peptides. Charge-derivatized peptides containing β -Asp or γ -Glu produced *b_n and *b_{n-1}+H₂O fragment ions that were more intense, and *d_n fragment ions that were less intense, than those produced from analogous charge-derivatized peptides containing normal Asp or Glu. Fragmentation mechanisms were proposed to rationalize these differences in fragment ion intensities.

Copyright by Kenneth David William Roth 1999

ACKNOWLEDGMENTS

I want to thank my research advisor, Professor J. Throck Watson for his guidance and support during my graduate career. I want to thank Professor John Allison for his constructive criticism of, and suggestions for, my dissertation. I also want to thank the students in Prof. Watson's lab and the staff of the Mass Spectrometry Facility for their assistance and friendship during my time at Michigan State.

Most importantly, I want thank my wonderful wife, Jennifer, for her love and support. She has worked and sacrificed just as much as I have in order to complete my studies. Even in the difficult times, she never stopped believing in me, loving me, and encouraging me. I couldn't have done it without you, Jennifer. I also want to thank our children, Nathan and Maggie, for sacrificing time with their Dad, so that he could finish school.

I want to thank my parents, Professor R. Waldo Roth and Mrs. Marlene Roth for teaching me the importance of an education and for giving me a love for learning. Mom and Dad, thank you for modeling unconditional love and for teaching me that character is more important than status or degrees. Thank you also to my other parents, Monty and Kathy Riffer for treating me like a son and for their support. In addition, I want to thank the other members of my family and my friends who helped support our family during the long process of completing my studies. I am humbled by, and grateful for, your support.

TABLE OF CONTENTS

LIST	OF TABLES	viii
LIST	OF FIGURES	ix
CHAI	PTER 1: INTRODUCTION	1
I.		
П.	Ionization Techniques	
	A. Fast Atom Bombardment (FAB) and Liquid Secondary-Ionization	
	Mass Spectrometry (LSIMS)	2
	B. Matrix-assisted Laser Desorption/Ionization (MALDI)	3
	C. Electrospray Ionization (ESI)	
Ш.		
	A. Sector Analyzers	
	B. Time-of-Flight (TOF) Analyzers	
	C. Quadrupole Analyzers	
	D. Ion Trap Analyzers	
IV.	•	
v .	Peptide Fragmentation	
VI.	N-Terminal-Charged Derivatives	
	A. Quaternary Ammonium Derivatives	
	B. Quaternary Phosphonium Derivatives	
VII.	N-Terminal Derivatives with High Proton Affinities	
VIII.	C-Terminal-Charged Derivatives	
IX.	Side-Chain Derivatives	
Χ.	Negatively-Charged Derivatives	
XI.	Concluding Commentary	
XII.	Summary	
XIII.	References	
ACET	PTER 2: STUDIES OF TRIS(2,4,6-TRIMETHOXYPHENYL)PHOSPHONI TYL (TMPP ⁺ -AC) DERIVATIZATION FOR PEPTIDE SEQUENCING BY I TROMETRY	MASS
SPEC I.	Introduction	
	Experimental	
П.		
	B. Preparation of TMPP ⁺ -Ac-S-Pentafluorophenyl Bromide	
	([TMPP ⁺ -Ac-SPf][Br-])	65
	C. TMPP ⁺ -Ac Derivatization of Peptides in Unbuffered Solution	
	D. TMPP ⁺ -Ac Derivatization of Peptides in Buffered Solution	
	E. HPLC Separation	
	F. Analysis	
	Fast Atom Bombardment (FAB)	
	MALDI	70

		ESI-MS on an Ion Trap Instrument	70
		ESI-MS on a Triple Quadrupole Instrument	71
		ESI-In-Source Fragmentation (ISF)-MS	71
III.	Fra	gmentation of TMPP+-Ac-derivatized Peptides	72
	Α.		
	В.	Sequence-specific Fragmentation of TMPP ⁺ -Ac-derivatized Peptides by	
		FAB-CAD-MS/MS	
	C.	Sequence-specific Fragmentation of TMPP ⁺ -Ac-derivatized Peptides by	
		MALDI-PSD, ESI-CAD-MS/MS, and ESI-ISF-MS	85
IV.	Pre	paration of a Weighable TMPP+-Ac Derivative Standard	86
V.		ction Yields and Selectivity	
		Reaction Yields in Buffered and Unbuffered Solutions	
	В.	TMPP ⁺ -Ac Derivatization of Lysine	89
		TMPP ⁺ -Ac Derivatization of Cysteine	
	D.		
VI.	Ion	ization Efficiency and Signal Supression	
VII.		erences	
CHAP	TER	3: FRAGMENTATION BEHAVIOR OF PEPTIDES AND CHARGE-	
DERI	VAT	IZED PEPTIDES CONTAINING ISOMERIC ACIDIC RESIDUES	106
I.	Intr	oduction	106
	A.	Isomeric Residues	106
	В.	Formation of β-Aspartate and γ-Glutamate	107
	C.	Conventional Analysis of β-Aspartate and γ-Glutamate	111
	D.	Mass Spectrometric Analysis of β-Aspartate and γ-Glutamate	113
П.	Exp	perimental	
	Α.	Reagents	116
	В.	Charge Derivatization	
	C.	Analysis	118
III.	Res	ults and Discussion	120
	A.	Underivatized Peptides	120
		y Ions	
		[MH ⁺ -H ₂ O] and [MH ⁺ -NH ₃] Ions	131
		w and v Ions	
		c _{n-1} , b _{n-1} +H ₂ O, and b _n Ions	
		Internal Ions	136
	В.	Charge-derivatized Peptides	136
		*b _n Ions	138
		*d _n Ions	145
		*b _{n-1} +H ₂ O Ions	150
		*c _{n-1} Ions	
		*a _n Ions	155
		[C-H ₂ O] ⁺ and [C+H-H ₂ O] ²⁺	157
IV.	Cor	iclusions	
V.		erences	

LIST OF TABLES

Table 2.1	Common TMPP ⁺ -Ac fragment ions observed in MS/MS spectra74
Table 2.2	Intensities of fragment ions from TMPP ⁺ -Ac-derivatized peptides as a function of amino acid residue
Table 3.1	Abundance ratios for underivatized peptides analyzed by FAB-CAD-MS/MS
Table 3.2	Abundance ratios for underivatized peptides analyzed by MALDI-PSD 124
Table 3.3	Abundance ratios for underivatized peptides analyzed by ESI-CAD-MS/MS
Table 3.4	Branching ratios for derivatized peptides analyzed by FAB-CAD-MS/MS
Table 3.5	Branching ratios for derivatized peptides analyzed by MALDI-PSD 140
Table 3.6	Branching ratios for derivatized peptides analyzed by ESI-CAD-MS/MS . 141

LIST OF FIGURES

Figure 1.1	Diagram of an electrospray source	5
Figure 1.2	Diagram of a quadrupole ion trap analyzer	. 16
Figure 1.3	The effect of charge localization on fragmentation by high-energy CAD.	. 22
Figure 1.4	Proposed structures of peptide fragment ions	. 24
Figure 1.5	Alternative structures of peptide fragment ions	. 25
Figure 1.6	Proposed structures of fragment ions produced from charge-derivatized peptides	. 27
Figure 1.7	Methyl iodide derivatization scheme	. 31
Figure 1.8	Trialkylammonium-acetyl derivatization scheme	. 31
Figure 1.9	Thiocholine iodide derivatization scheme	. 31
Figure 1.10	"C5Q" derivatization scheme	. 31
Figure 1.11	N-terminal triphenylphosphonium derivatization scheme	. 36
Figure 1.12	TMPP ⁺ -Ac derivatization scheme	. 36
Figure 1.13	Derivatization schemes of Renner and Spiteller	. 36
Figure 1.14	N-hydroxysuccinimide-2-(3-pyridyl)acetate (SPA) derivatization scheme	41
Figure 1.15	C-terminal pyridinium derivatization scheme	. 41
Figure 1.16	C-terminal acyl urea derivatization scheme	. 41
Figure 1.17	Carboxypeptidase derivatization scheme	. 41
Figure 1.18	C-terminal N,N-dimethylethanolamine derivatization scheme	. 45
Figure 1.19	C-terminal triphenylphosphonium derivatization scheme	. 45
Figure 1.20	2,4,6-trimethylpyridinium derivatization scheme for lysine side-chains	. 45
Figure 1.21	Conversion of lysine side-chains to homoarginine	. 47

Figure 1.22	Pentafluorobenzoyl fluoride derivatization scheme
Figure 1.23	C-terminal 4-aminonaphthalenesulphonic acid (ANSA) derivatization 47
Figure 2.1	Synthesis of TMPP ⁺ -Ac reagents
Figure 2.2	FAB-MS spectra of TMPP*-Ac-OSu (A) and TMPP*-Ac-SPf (B)
Figure 2.3	TMPP ⁺ -Ac derivatization scheme
Figure 2.4	FAB-CAD-MS/MS spectra of TMPP ⁺ -Ac-OSu (A) and TMPP ⁺ -Ac-SPf (B)
Figure 2.5	Low mass fragments of TMPP*-Ac-derivatized peptides analyzed by FAB-CAD-MS/MS (A) and MALDI-PSD (B)
Figure 2.6	Low mass fragments of TMPP ⁺ -Ac-derivatized peptides analyzed by ESI-CAD-MS/MS on an ion trap (A) and ESI-ISF-MS (B)
Figure 2.7	Formation of $*a_n$ ions involving transfer of hydrogen from the β -carbon 80
Figure 2.8	FAB-CAD-MS/MS spectra of TMPP ⁺ -Ac-osteocalcin fragment (45-49), $C^+ = 1154$, showing * a_n -14, * a_n -30, and * a_n -46 peaks
Figure 2.9	Possible rationalization for losses of 14, 30, and 46 Da from TMPP ⁺ -Ac derivatives
Figure 2.10	HPLC chromatographs of TMPP ⁺ -Ac-OSu + buccalin reaction mixtures performed in unbuffered (A) and buffered (B) solutions
Figure 2.11	HPLC chromatographs of TMPP ⁺ -Ac-OSu + A-γ-EKAA reaction mixtures performed in unbuffered (A) and buffered (B) solutions
Figure 2.12	MALDI-PSD spectra of N-terminal (A), side-chain (B), and doubly-derivatized (C) A-γ-EKAA
Figure 2.13	HPLC chromatographs of TMPP ⁺ -Ac-OSu + γ-ECG reaction mixtures performed in unbuffered (A) and buffered (B) solutions
Figure 2.14	ESI-CAD-MS/MS spectra of N-terminal (A), side-chain (B), and doubly-derivatized (C) γ-ECG
Figure 2.15	HPLC chromatographs of TMPP ⁺ -Ac-OSu + VQAAIDYING-NH ₂ reaction mixtures performed in unbuffered (A) and buffered (B) solutions

Figure 2.16	VQAAIDYING-NH ₂ , and the ESI-CAD-MS/MS spectrum of the doubly-derivatized (C) product
Figure 2.17	MALDI-MS spectra of buccalin (A), TMPP ⁺ -Ac-buccalin (B), and an equimolar mixture of the two (C)
Figure 3.1	Structures of aspartate, β -aspartate, glutamate, and γ -glutamate
Figure 3.2	Formation of β-aspartate in solution
Figure 3.3	ESI-CAD-MS/MS spectra of Glu-Cys-Gly (A) and γ-Glu-Cys-Gly (B) at a relative collision energy of 14.9%
Figure 3.4	ESI-CAD-MS/MS spectra of Asp-Phe-OMe (A) and β-Asp-Phe-OMe (B) at a relative collision energy of 17.4%
Figure 3.5	y ion formation by glutamyl (A) and γ-glutamyl (B) peptides128
Figure 3.6	y ion formation by aspartyl (A) and β-aspartyl (B) peptides130
Figure 3.7	[MH ⁺ -H ₂ O] formation by glutamyl (A) and γ-glutamyl (B) peptides 133
Figure 3.8	[MH ⁺ -H ₂ O] formation by aspartyl (A) and β-aspartyl (B) peptides 134
Figure 3.9	ESI-ISF-MS spectra of AEKAA (A) and A-γ-EKAA (B) at a cone voltage of 55 V
Figure 3.10	MALDI-PSD spectra of TMPP ⁺ -Ac-Asp-Phe-OMe (A) and TMPP ⁺ -Ac-β-Asp-Phe-OMe (B)
Figure 3.11	*b _n formation by derivatized aspartyl (A) and β-aspartyl (B) peptides 144
Figure 3.12	MALDI-PSD spectra of TMPP ⁺ -Ac-Asp-Phe-OMe (A) and methylated TMPP ⁺ -Ac-Asp-Phe-OMe (B)
Figure 3.13	MALDI-PSD spectra of derivatized AEKAA (A) and A-γ-EKAA (B) 148
Figure 3.14	*d _n formation by derivatized aspartyl (A) and β-aspartyl (B) peptides 149
Figure 3.15	*b _{n-1} +H ₂ O formation by derivatized aspartyl (A) and β-aspartyl (B) peptides
Figure 3.16	*c _{n-1} formation by derivatized aspartyl (A) and β-aspartyl (B) peptides 154

Figure 3.17	*c _{n-1} formation by derivatized aspartyl (A) and glutamyl (B) peptides without transfer of the acidic proton	6
Figure 3.18	ESI-CAD-MS/MS spectra of the C ⁺ (A) and [C+H] ²⁺ (B) precursor ions of TMPP ⁺ -Ac-AEKAA at collision energies of 72.5 eV and 32.5 eV,	
	respectively	8

CHAPTER 1

INTRODUCTION

I. Introduction

Mass spectrometry is a powerful analytical technique based on the principle that the motion of charged particles (ions) in a vacuum can be controlled by the use of electric and magnetic fields. The behavior of these ions is also related to the mass-to-charge ratio. Therefore, by subjecting ions to an electric or magnetic field in a vacuum, it is possible to determine the mass-to-charge ratio (m/z) of those particles. If the charge is known, then the mass of the ion can be determined. When fragmentation of the analyte is induced, the m/z values of the fragment ions can provide clues to the structure of the original analyte.

This chapter briefly discusses some of the techniques for forming ions from the condensed phase, some of the commonly used approaches for the determination of m/z, and some methods for inducing fragmentation. In addition, the use of mass spectrometry for the analysis of peptides is introduced, along with a discussion of commonly observed peptide fragment ions. Finally, the use of charge-derivatization to aid the sequence determination of peptides is discussed, and the scientific literature involving charge-derivatization is reviewed.

II. Ionization Techniques

A. Fast Atom Bombardment (FAB) and Liquid Secondary-Ionization Mass Spectrometry (LSIMS)

Although numerous desorption/ionization techniques can be used to generate gasphase ions for analysis by mass spectrometry, only three are discussed here: fast atom bombardment (FAB), matrix-assisted laser desorption/ionization (MALDI), and electrospray ionization (ESI). Fast atom bombardment was introduced by Barber *et al.* (1). During the desorption/ionization process, a beam of Ar or Xe atoms with several keV of translational energy strikes a solution of analyte dissolved in a liquid matrix. Commonly used matrices include glycerol, thioglycerol, and 3-nitrobenzyl alcohol. The translational energy from the primary ion beam is transferred to the analyte and matrix, resulting in desorption of the analyte and the matrix into the gas phase. Ionization of the analyte has been proposed to occur in the solution prior to desorption or by proton transfer in the gas phase as a result of collisions with ionized matrix molecules in the high pressure selvedge region (2, 3).

FAB is closely related to two other desorption/ionization techniques: secondary ionization mass spectrometry (SIMS) and liquid secondary ionization mass spectrometry (LSIMS). LSIMS differs from FAB in that the primary beam is composed of ions (usually Cs⁺) instead of neutral atoms. Desorption/ionization by LSIMS has been reported to give more efficient ionization of analytes and lower detection limits than FAB as a result of better focusing of the primary beam (4). The mass spectra obtained by FAB and LSIMS are very similar (5); as a result, the terms FAB and LSIMS are sometimes used interchangeably. SIMS was developed prior to the development of FAB and differs

from FAB and LSIMS in that the primary beam strikes an analyte in the solid phase without any matrix. The extent of fragmentation during desorption/ionization by SIMS is much greater than that during desorption/ionization by FAB or LSIMS. As a result, SIMS is usually limited to the atomic analysis of surfaces.

In FAB or LSIMS, a primary atom or ion with a kinetic energy in the keV range strikes the matrix, and the energy is dispersed by collisional processes among the matrix and analyte molecules that occupy about the top 80 Å of the matrix surface (6). Some of this energy is transferred into kinetic energy for the matrix and analyte, allowing desorption into the gas phase. Another portion of this energy is transferred into internal energy, producing ions with internal energies in the range of 8-20 eV (7). Once desorption/ionization has occurred, the ions are accelerated toward the analyzer by a strong potential gradient.

B. Matrix-assisted Laser Desorption/Ionization (MALDI)

The use of lasers for desorption/ionization of organic compounds for subsequent analysis by mass spectrometry dates back to the 1970s (8). However, the use of laser desorption was limited by the extensive fragmentation induced during the desorption/ionization process. The introduction of a crystalline matrix to aid the desorption/ionization process resulted in a technique called matrix-assisted laser desorption/ionization (MALDI) (9).

In preparation for analysis by MALDI-MS, the analyte is co-deposited with a large excess of organic matrix. Some of the most commonly used matrices are α-cyano-4-hydroxycinnamic acid, 2,5-dihydroxybenzoic acid, and 3,5-dimethoxy-4-hydroxy-

cinnamic acid (sinapinic acid). These matrices have strong UV absorption in the 320-350 nm range to allow efficient energy transfer from a nitrogen laser (337 nm) or a frequency-doubled Nd-YAG laser (355 nm). These matrices also crystallize readily, have low vapor pressures, low energies of sublimation, and can readily donate protons to the analyte during the desorption/ionization process (10). A fraction of the energy absorbed by the matrix is transferred to the analyte, apparently by the coupling of the lattice vibrations of the matrix to the internal vibrations of the analyte (11). The ionization mechanism is not clearly understood, although several possible mechanisms have been proposed (12).

Although the mechanisms of desorption and ionization are not well understood, the use of MALDI as a desorption/ionization technique has grown tremendously during recent years. This growth is due to the ability to desorb biomolecules with masses of hundreds of kilodaltons and the ability to detect analytes in the picomole range.

C. Electrospray Ionization (ESI)

Fenn and coworkers (13) developed electrospray as an ionization source for mass spectrometry, building on the work of Dole et al. (14). Common features of the electrospray source are shown in Figure 1.1. Electrospray ionization may be a misnomer because the technique primarily involves the transfer of ions in solution to the gas-phase rather than the ionization of neutral species. During the electrospray process, a solution of analyte is passed through the electrospray capillary held at high potential. As the solution exits the electrospray capillary, the high electric field generates a spray of highly-charged droplets at atmospheric pressure. As the droplets pass through a potential and

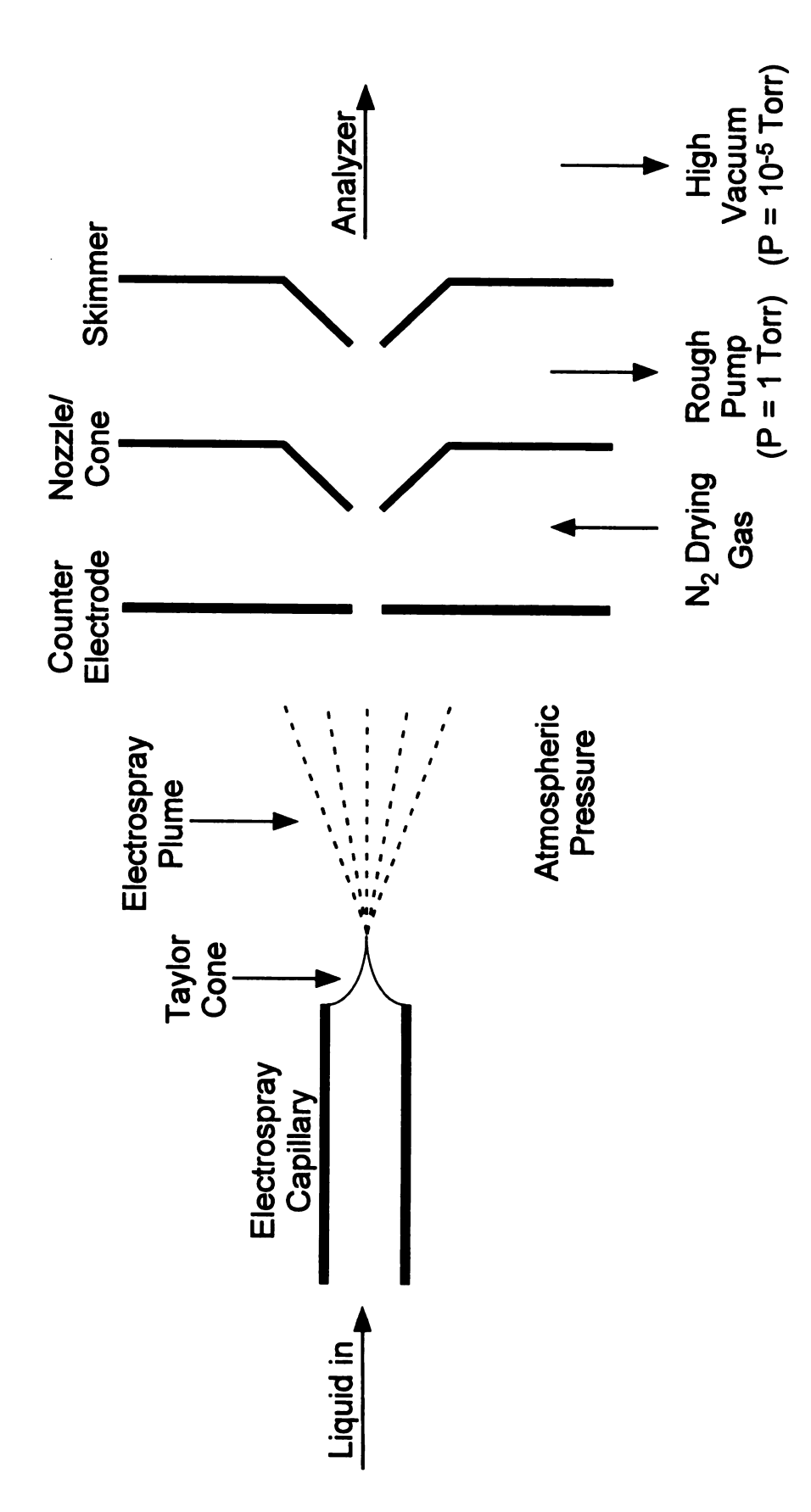


Figure 1.1. Diagram of an Electrospray Source

pressure gradient toward the analyzer, the solvent is removed from the analyte until only individual gas-phase ions remain. One important feature of the electrospray process is that the charge on the ions produced is similar to the charge of the ions in solution. As a result, multiply-charged ions are readily produced by this mechanism.

When the analyte solution reaches the electrospray capillary held at a high positive potential, positive ions in the solution accumulate at the surface of the solution. The electric field draws the charged solution into a cone shape, called a Taylor cone. At the tip of the cone, small droplets (diameter $\approx 1 \mu m$) are drawn into the gas phase to produce the spray (15). Most commercial instruments also use a nebulization gas to assist in the formation of the spray, especially at high flow rates (>50 $\mu L/min$).

After droplets have been sprayed, the size of the droplet decreases by solvent evaporation until the Rayleigh limit is reached. Solvent evaporation is assisted in many instruments by the use of a drying gas or heating of the source. The Rayleigh limit is the point at which the charge repulsion becomes sufficient to overcome the droplet surface tension and is given by the following equation:

$$Q_R^2 = 64\pi^2 \varepsilon_0 \gamma R_R^3$$
 (Equation 1.1)

where Q_R is the charge in coulombs, ϵ_0 is the permittivity of vacuum, γ is the surface tension, and R_R is the radius in meters. When the Rayleigh limit is reached, the droplet undergoes Coulombic explosion resulting in the formation of numerous smaller droplets. The processes of solvent evaporation and Coulombic explosion are repeated until very small droplets (< 10 nm in diameter) are formed. There are two theories that have been proposed to describe the transition from very small droplets to single ions. The single ion droplet theory (16) proposes that Coulombic explosion eventually produces very small

droplets containing only a single ion; and that solvent evaporation of that droplet produces a gas-phase ion. The ion evaporation theory (17, 18) holds that Coulombic explosion produces small droplets containing multiple ions; and that individual ions evaporate from the droplet into the gas phase.

Before reaching the analyzer, the ions pass through a nozzle, also called a cone, and then through a skimmer. In the first differentially-pumped region (pressure ≈ 1 torr), collisional fragmentation can be introduced by raising the voltage gradient in the region and giving the ions enough energy to fragment during collisions. This type of fragmentation is called in-source fragmentation (ISF), nozzle-skimmer dissociation, or cone voltage fragmentation. More detailed information on electrospray ionization can be found in several recently published reviews (19-22).

III. Mass Analyzers

A. Sector Analyzers

Sector analyzers use magnetic fields, electric fields, or both to determine the m/z ratios of ions generated in the source. The kinetic energies of ions leaving the source region are

$$KE = \frac{1}{2} \text{ mv}^2 = \text{zeV}$$
 (Equation 1.2)

where KE is kinetic energy, m is mass, v is velocity, z is the number of elementary charges on the ion, e is the electronic charge, and V is the acceleration potential. When an ion enters a magnetic field, B, the ion follows a circular path that is perpendicular to the direction of the magnetic field. The radius, R_m , of the circular path is given by:

$$R_m = mv/Bze$$
 or $(m/z)v = R_mBe$. (Equation 1.3)

Combining Equations 1.2 and 1.3 gives the equation for separation of ions by a magnetic sector analyzer:

$$m/z = R_m^2 B^2 / 2eV.$$
 (Equation 1.4)

Therefore, by using a fixed value of R_m and scanning B, ions of different m/z values can be made to pass through a detector slit to acquire a mass spectrum. Equation 1.4 assumes that the kinetic energy of the ions is determined only by the m/z value and the acceleration potential. In reality, ions with the same m/z value can have different kinetic energies and velocities as a result of the ionization process and thermal energy. This difference in velocity for ions of the same m/z can alter the flight path of the ions, as shown in Equation 1.3, resulting in a loss of resolution.

An electric sector analyzer with an electric field, E, deflects ions in a circular path with a radius, R_e :

$$R_e = mv^2/zeE = KE/2zeE$$
. (Equation 1.5)

As a result, an electric sector analyzer can be used in conjunction with a magnetic sector analyzer to compensate for the initial kinetic energy spread. Isomass ions with large kinetic energies are deflected by a larger radius and than those with small kinetic energies. By carefully selecting the electric field, the difference in the R_e of isomass ions is used to compensate for the difference in R_m caused by differences in kinetic energy. This allows isomass ions to reach the detector at the same time, resulting in an increase in resolving power.

Sector instruments that utilize both an electric and magnetic sector (double focusing instruments) can be used to generate MS/MS data by a technique called linked scanning. When fragmentation occurs in the field-free region between the source and the

first sector analyzer, the precursor ion with mass m_1 produces a product ion with mass m_2 . The fragment ion will have a velocity that is nearly equal to the velocity of the precursor ion v_1 , but it will have a smaller kinetic energy. Based in Equation 1.5, the conditions that allow the precursor ion and product ion to pass through the electric sector are

$$eE_1 = m_1 v_1^2 / R_e z \qquad (Equation 1.6)$$

$$eE_2 = m_2 v_1^2 / R_e z \qquad (Equation 1.7)$$

where E_1 is the electric field that passes the precursor ion and E_2 is the electric field that passes the product ion. Based on Equation 1.3, the conditions that allow the precursor and product ions to pass through the magnetic sector are

$$eB_1 = m_1 v_1 / R_m z (Equation 1.8)$$

$$eB_2 = m_2 v_1 / R_m z. mtext{(Equation 1.9)}$$

Combining Equations 1.6-1.9 results in the following relationship:

$$B_1/E_1 = B_2/E_2 = R_0/R_m v_1 = constant$$
 (Equation 1.10)

Therefore, by holding the electric and magnetic fields at a constant ratio, only ions arising from the precursor ion (those with a velocity of v_1) will reach the detector. By scanning the electric and magnetic fields at a constant ratio, a product ion mass spectrum can be acquired. Linked scanning can be used to detect metastable ions, or following the introduction of a collision gas into the first field-free region, to detect ions generated by high-energy collisionally-activated dissociation (CAD) from a precursor ion.

B. Time-of-Flight (TOF) Analyzers

Time-of-flight (TOF) analyzers are simple and inexpensive analyzers that are well-suited for pulsed ionization techniques, such as MALDI. A time-of-flight analyzer works by subjecting a group of ions to an accelerating potential, V, in the ion source, allowing the ions to drift down a field-free flight tube of length, L, and measuring the time, t, required to drift down the tube to a detector. Time-of-flight analysis is based on the relationship between kinetic energy, velocity, potential, and mass-to-charge ratio, defined previously in Equation 1.2. Solving Equation 1.2 for velocity yields

$$v = (2eV)^{\frac{1}{2}} (m/z)^{-\frac{1}{2}}$$
. (Equation 1.11)

Equation 1.11 shows that when a group of ions is placed in the same electric field, the velocity of each ion is dependent on the m/z value. Since the time required to traverse the flight tube is L/v, the time-of-flight is:

$$TOF = t = L(2eV)^{-\frac{1}{2}} (m/z)^{\frac{1}{2}}$$
. (Equation 1.12)

By measuring the time-of-flight, the m/z of each ion can be determined. Unlike, scanning analyzers, time-of-flight analyzers allow analysis of all the ions present in the source at a given time. As a result, TOF analyzers usually are more sensitive than scanning analyzers. Also, TOF analyzers have no theoretical upper mass limit.

The resolving power of TOF analyzers is usually lower than that achieved by other analyzers. In the ion source, ions of the same m/z value can have differences in their kinetic energies and they can be moving in different directions. These differences affect the time-of-flight and produce peak broadening. Also, not all ions are the same distance from the analyzer when the accelerating potential is applied. This difference affects the flight distance of the ions, resulting in loss of resolution. The limited

resolving power of TOF analyzers has been addressed by the introduction of reflectron TOF and by the introduction of delayed extraction. Reflectron TOF was introduced by Mamyrin *et al.* (23), and it uses a reflectron or ion mirror to compensate for the initial kinetic energy spread of the analyte. At the end of the flight tube, the ions are reflected by a potential field to a detector located part of the way back down the flight tube. Ions with a higher kinetic energy will travel farther into the ion mirror than ions with lower kinetic energy, allowing ions with smaller kinetic energies to reach the detector at the same time as those with greater kinetic energies. As a result, the peak broadening from differences in kinetic energy is minimized.

Delayed extraction is based on the principle of time-lag focusing developed by Wiley and McLaren (24). Delayed extraction uses a delay between the formation of ions and the extraction of those ions from the source in order to compensate for differences in the initial velocities of the ions. After the ions are formed, they move in a variety directions and speeds. After the delay time has passed, a two-field acceleration potential is applied that gives a greater kinetic energy to the ions farther from the detector than to the ions closer to the detector. As a result, the ions that were moving away from the detector most rapidly receive the biggest increase in velocity and those moving most rapidly toward the detector receive the smallest increase in velocity. Therefore, the ions farther from the detector are able to reach it at about the same time as those closest to the detector at the time of acceleration. The delay time that gives the highest resolving power is mass dependent, so the benefits from delayed extraction decrease as the m/z of the analyte gets farther from the m/z for which the delay time was optimized.

MS/MS analysis is possible for reflectron TOF analyzers by a technique called post-source decay (PSD). PSD was introduced by Spengler *et al.* in 1992 (25) to allow MS/MS analysis of peptides ionized by MALDI. As shown in Equation 1.11, the velocity of an ion leaving the acceleration region is dependent on its m/z value. If the ion fragments in the flight tube, the fragments will have the same velocity as the precursor ion, but they will have smaller kinetic energies than the precursor. In a linear TOF analyzer, the fragment ions will reach the detector at the same time as the intact ions, but if the fragment ions are reflected by an ion mirror, they will be separated on the basis of kinetic energy and therefore on the basis of mass

$$m = 2KE/v^2.$$
 (Equation 1.13)

PSD analysis uses an ion gate to deflect all the ions except those with a velocity equal to that of the desired precursor. The reflectron then separates the fragment ions on the basis of mass and sends them to the detector to be recorded as a PSD spectrum. In practice, PSD spectra are usually collected in several segments so that the reflectron voltages can be adjusted to give the best resolution for the fragment ions. The individual segments are then "stitched" together by computer to give a complete PSD spectrum. PSD spectra have been observed to resemble low-energy CAD spectra, but they have traits of both low-energy and high-energy CAD spectra (26).

C. Quadrupole Analyzers

The quadrupole mass analyzer consists of four parallel rods, ideally of hyperbolic cross-sections that lie along the z-axis. Two rods lie in the x-z plane, and two rods lie in the y-z plane. The radius from the center axis of the quadrupole to the surface of a

hyperbolic rod is r_0 . Most commercial instruments use cylindrical rods instead of hyperbolic rods because cylindrical rods are easier to manufacture. When cylindrical rods are separated by a radius of 1.148* r_0 , they can generate a good approximation of the ideal hyperbolic field (27).

For the analysis of positive ions, the potential applied to the rods in the x-z plane is identical and consists of a positive direct current (dc) component with an amplitude U and an alternating current (ac) component with an amplitude V and a frequency f. The frequency of the ac potential lies within the radiofrequency (rf) range. The rods in the y-z plane have an rf potential with the same amplitude, V, and frequency, f, as that applied to the x-z rods, but the two waveforms are 180° out of phase (opposite in sign). Also, the dc potential on the y-z rods is the negative (-U) of that applied to the x-z rods. The potential distribution (Φ) within the quadrupole at any given time, t, can be described by the expression

$$\Phi = [U + V\cos(\omega t)][(x^2 - y^2) / 2r_0^2]$$
 (Equation 1.14)

where ω is the angular frequency ($2\pi f$). The force, F, exerted on a charged particle along each axis can be determined by taking the partial derivative of Equation 1.14 with respect to each axis and multiplying by the charge on the particle (ze):

$$F_x = -[U + V\cos(\omega t)](zex/r_0^2)$$
 (Equation 1.15)

$$F_y = [U + V\cos(\omega t)](zey/r_0^2)$$
 (Equation 1.16)

$$F_z = 0. mtext{(Equation 1.17)}$$

Equation 1.17 shows that the quadrupole analyzer does not affect the motion of ions in the z direction. Since F = ma, ions with a small mass undergo greater acceleration than ions with a larger mass. As a result, low-mass ions oscillate in response to the changing

rf potential, whereas high-mass ions are relatively unaffected by the rf potential. The force exerted by the dc potential U along the x-axis acts to focus ions toward the center of the quadrupole. However, ions with m/z values below a certain level will collide with the quadrupole rods and be neutralized as a result of the oscillations induced by the rf potential. The dc potential along the y-axis attracts ions to the rods in the y-z plane. Since high-mass ions are relatively unaffected by the rf potential, ions with a m/z value greater than a cutoff value will collide with the rods in the y-z plane. Therefore, the x-z rods act as high-pass filters and the y-z rods act as low-pass filters. Only ions with m/z values that are stable in both the x and the y directions are able to reach the detector. Usually the width of this stability region is less than one dalton. By ramping the potentials U and V at a fixed ratio, the m/z values of ions that are stable in the quadrupole are scanned, producing a mass spectrum after the ions are detected.

Based on the relationship F = ma and the Equations 1.15-1.17, the trajectories of ions in the x and y directions can be described by the following equations:

$$d^2x/dt^2 + (zex/mr_0^2)[U + Vcos(\omega t)] = 0$$
 (Equation 1.18)

$$d^2y/dt^2 - (zey/mr_0^2)[U + Vcos(\omega t)] = 0$$
 (Equation 1.19)

These equations are related to the Mathieu differential equations that describe the motion of ions in a quadrupole field. The Mathieu equations are discussed in more detail in the section on ion trap analyzers.

Tandem mass spectrometric analysis (MS/MS) can be accomplished using a triple quadrupole instrument. The first and third quadrupoles use a combination of dc and rf potentials to allow ions with selected m/z values to pass, as described above. In the second quadrupole, precursor ions selected by the first quadrupole collide with a collision

gas to form product ions by low-energy CAD. The second quadrupole uses only an rf potential to focus the product ions formed and to transmit them to the third quadrupole. The third quadrupole scans the product ions formed to generate a mass spectrum. A product ion scan is accomplished by setting the first quadrupole to pass only ions of a given m/z value, and scanning the product ions formed. A precursor ion scan is accomplished by setting the third quadrupole to pass only product ions of a given m/z value and scanning the first quadrupole to determine which precursor ions fragment to from the desired product. A constant neutral loss scan is accomplished by scanning the first and third quadrupoles with a fixed difference in the m/z values passed by each. In this way, only precursor ions that fragment to form product ions resulting from a given neutral loss can reach the detector.

D. Ion Trap Analyzers

The quadrupole ion trap can function as both an instrument to store gas-phase ions and as a mass (m/z) analyzer. Figure 1.2 shows the major components of one commercial ion trap analyzer. The ion trap has three electrodes that generate the potential wells for storing and analyzing ions. In the center of the instrument is a ring electrode that is shaped like a doughnut with a hyperbolic interior. At the two open ends of the ring electrode are end-cap electrodes, also with hyperbolic faces. The potential well that traps ions is generated when a radio-frequency (rf) potential is applied to the ring electrode and the end-cap electrodes are grounded.

The motion of ions in a quadrupole field can be described mathematically by the

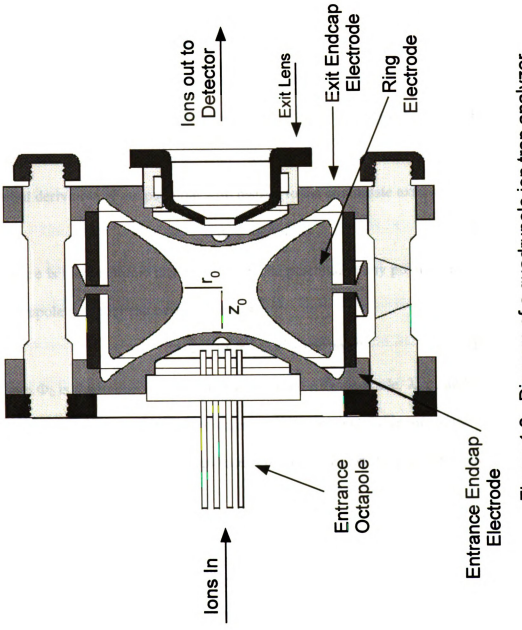


Figure 1.2. Diagram of a quadrupole ion trap analyzer. Reprinted with permission from Thermoquest Corporation.

solutions to the Mathieu equation (28):

$$d^2u/d\xi^2 + (a_u - 2q_u\cos 2\xi)u = 0$$
 (Equation 1.20)

where u represents the coordinate axes (x, y, and z), ξ is a dimensionless parameter equal to $\omega t/2$, ω is the radial frequency (in radians/second) of the rf potential applied to the ring electrode, t is time, and a_u and q_u are additional dimensionless parameters known as trapping parameters. Equation 1.20 can be rearranged to describe the force on an ion:

$$F_u = ma = m(d^2u/dt^2) = -(m\omega^2/4)(a_u - 2q_u\cos\omega t)u$$
 (Equation 1.21)

where m is mass and a is acceleration. The force on an ion can also be expressed as the partial derivative of the potential with respect to the coordinate axis, u:

$$F_{u} = -e(\partial \Phi / \partial u)$$
 (Equation 1.22)

where e is the electronic charge and Φ is the potential at any point within the field. The quadrupole potential can be expressed as:

$$\Phi = \Phi_0/r_0^2 (\lambda x^2 + \sigma y^2 + \gamma z^2)$$
 (Equation 1.23)

where Φ_0 is the applied electric potential on the ring electrode, λ , σ , and γ are weighing constants for the x, y, and z coordinates, and r_0 is the internal radius of the ring electrode, as shown in Figure 1.2. The applied electric potential on the ring electrode is expressed as:

$$\Phi_0 = U + V\cos(\omega t)$$
 (Equation 1.24)

where U is the amplitude of the direct current (dc) potential, and V is the amplitude of the rf potential. For an ion trap, Equations 1.21-1.24 can be simplified to find the trapping parameters, a and q (29):

$$a_r = 8eU / m(r_0^2 + 2z_0^2)\omega^2;$$
 $q_r = -4eV / m(r_0^2 + 2z_0^2)\omega^2$ (Equations 1.25)

 $a_z = -16eU / m(r_0^2 + 2z_0^2)\omega^2;$ $q_z = 8eV / m(r_0^2 + 2z_0^2)\omega^2$ (Equations 1.26)

where a_r and q_r are trapping parameters in the radial direction, a_z and q_z are the trapping parameters in the z direction, r_0 is the internal radius of the ring electrode, and z_0 is ½ the distance between the end-cap electrodes, as shown in Figure 1.2. It should be noted that the trapping parameters a and q are inversely proportional to m/e, however these equations were derived based on the assumption of a charge of 1, see Equation 1.22. Actually, the term e should be replaced by ze where z is the number of charges on an ion. Having made that correction, it can be seen that the trapping parameters are inversely proportional to m/z.

The solutions to Mathieu's equation describe regions in a, q space where ions are stable. Ions in a trap are stable when the values of another trapping parameter, β_u , are between 0 and 1 in both the r and z directions. β_u is approximately equal to $(a_u + q_u^2/2)^{\frac{1}{2}}$. A more detailed discussion of ion motion in an ion trap can be found in the tutorial by March (28). The trapping parameters, a_u and q_u , are functions of U, V, ω , and $(m/z)^{-1}$. Therefore, for given values of U, V, and ω , only m/z values above a certain threshold are stable. Ions with m/z values below that threshold will have β_u values > 1, resulting in ejection from the ion trap (usually in the z direction). By increasing the amplitude of the rf potential V, the m/z threshold increases resulting in the ejection of more ions from the trap. By placing a detector behind a hole in the endcap electrode and gradually raising the rf potential, it is possible to successively eject and detect ions with a series m/z values, producing of a mass spectrum.

Tandem mass spectrometry can be accomplished by a technique called resonant excitation. Equations 1.24 and 1.25 imply a relationship between the frequency of the

potential on the electrodes and the stability of ions of a particular m/z. Resonant excitation uses a small oscillating potential at the end-cap electrodes to excite ions of a particular m/z value along the z axis. This oscillating potential is in addition to the rf potential applied to the ring electrode. Ions with m/z values less than that of the desired precursor ion can be ejected by ramping the rf potential, V, as described above. Ions with m/z values greater than that of the desired precursor ion are ejected by resonant excitation. During resonant excitation, ions with selected m/z values (those greater than the desired precursor) are excited to the extent that they are no longer stable in the ion trap. When only the precursor ions remain in the trap, they are excited by resonant excitation. However, this time resonant excitation is used to increase the kinetic energy of the ions, but not to eject them. The kinetically excited precursor ions collide with the helium buffer gas (pressure ≈ 1 mTorr) present in the trap and fragment by collisionallyactivated dissociation. The kinetic energy of the precursor ions (and therefore the extent of fragmentation) can be adjusted by changing the amplitude of the potential used for resonant excitation. For this reason, the collision energies used in an ion trap are sometimes expressed as a percentage of the maximum potential that can be applied before the precursor ions are ejected from the trap. Once fragmentation occurs, the m/z values of the fragment ions can be determined by scanning the rf voltage as described above. The CAD-MS/MS spectra obtained on an ion trap may differ from those obtained on other instruments because the precursor ions spend more time in the collision region and experience more collisions than the precursor ions analyzed by other techniques.

IV. P

techn segu

app!

seqi

mas

der

spe

pe

pl

ur

a

SI

S

t

IV. Peptide Sequencing by Mass Spectrometry

During the past few decades, mass spectrometry has arisen as a powerful technique for the analysis of peptides and proteins (30) to now complement chemical sequencing (31) and gene sequencing (32, 33). Although mass spectrometry had been applied to the analysis of peptides as early as 1959 (34), analysis by electron ionization mass spectrometry (EI-MS) made only a limited contribution to the area of peptide sequence determination. For the EI methods, micromolar quantities of peptides had to be derivatized prior to analysis by direct probe (35) or gas chromatography mass spectrometry (GC-MS) (36). The direct probe method allowed sequencing of peptides with ten or fewer amino acid residues, and the GC-MS method was typically used for peptides that contain six or fewer residues.

The development of desorption/ionization techniques, e.g., field desorption (37), plasma desorption (38), and fast atom bombardment (FAB) (1), allowed the analysis of underivatized peptides by mass spectrometry. FAB and LSIMS gained widespread use as alternative approaches for peptide analysis. The utility of FAB and LSIMS was strengthened by the development of tandem mass spectrometry (MS/MS), which allows fragmentation to be induced by collisionally activated dissociation (CAD), also called collision-induced dissociation (CID), to produce a variety of structurally significant fragment ions (39-41). In addition, MS/MS allows fragment ions from the analyte to be separated from background ions during analysis of the sample, thereby simplifying the spectra and allowing analyses of simple mixtures.

The introduction of these new ionization techniques and MS/MS revolutionized the mass spectral analysis of peptides; however two problems remained: lack of

sensitivit

develop

contain

analys

increa

desor

V. F

that frag

fraș

loc

loo Pe

a

.

I

.

sensitivity and difficulty in data interpretation. Several types of derivatives were developed to improve the detection limits of peptide analytes. Some of these derivatives contained nonpolar functionalities to increase the surface activities of peptides during analysis by FAB and LSIMS (42-44). Other derivatives generated preformed ions, which increased ionization efficiencies of many analytes during analysis by desorption/ionization techniques (45).

V. Peptide Fragmentation

Peptide mass spectra can be complicated due to the many types of fragment ions that can arise during desorption/ionization and MS/MS (41). The observed peptide fragments can be amino-terminal fragments (\mathbf{a}_n , \mathbf{b}_n , \mathbf{c}_n , and \mathbf{d}_n ions), carboxy-terminal fragments (\mathbf{x}_n , \mathbf{y}_n , \mathbf{z}_n , \mathbf{v}_n , and \mathbf{w}_n ions), or internal fragments. The extent of charge localization influences the types of fragment ions produced (46). The effect of charge localization on fragmentation by high-energy CAD is summarized by Figure 1.3. Peptides with an acetylated amino-terminus (N-terminus) are protonated on one of the amide nitrogens, and fragment primarily by charge-driven mechanisms (40) to produce primarily \mathbf{b}_n and \mathbf{y}_n ions. Peptides with basic sites have some degree of charge-localization, and may produce fragments by a mixture of charge-directed and charge-remote mechanisms, as indicated by the middle region in Figure 1.3. The extent of charge localization and charge-directed fragmentation depend on the basicity of the site, with the arginine (Arg) side-chain being more basic than histidine (His) or lysine (Lys) side-chains, which in turn are more basic than the free N-terminus of the peptide (47).

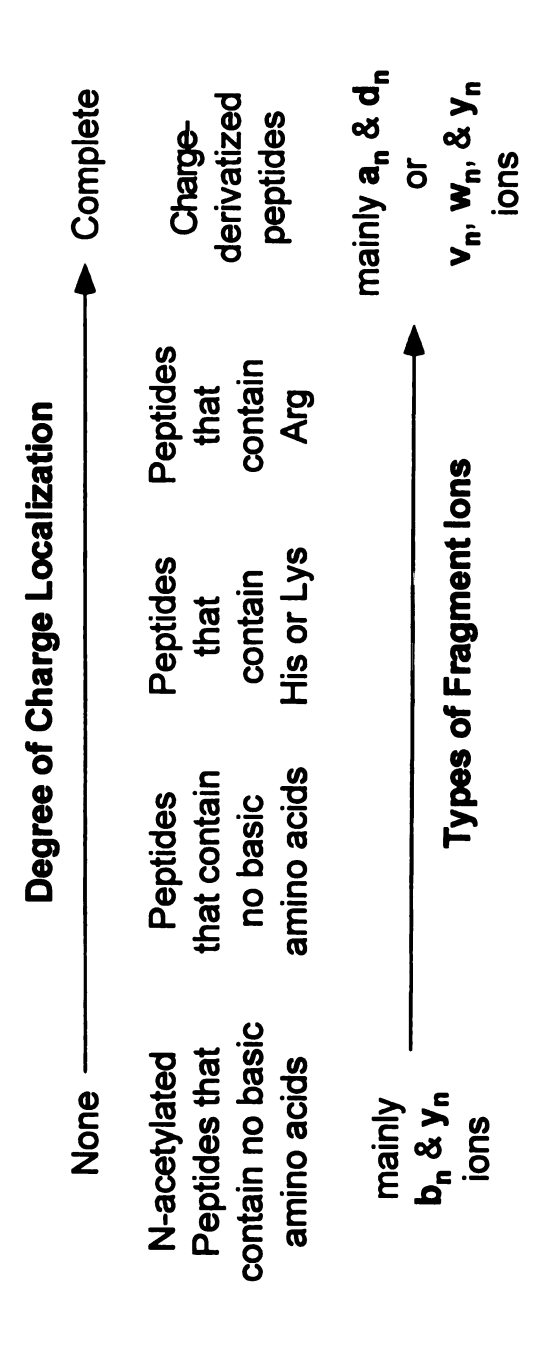


Figure 1.3. The effect of charge localization on fragmentation by high-energy CAD.

Charge

with th

peptid

form

types

grea

mo

the

Ъç

F

15

31

i

re

W

ha

am

Charge-derivatized peptides have complete charge-localization and produce fragments with the charge retained at the site of derivatization.

Charged derivatives were developed to simplify and direct the fragmentation of peptides to facilitate interpretation of their mass spectra. Charged peptide derivatives form fragment ions through charge-remote mechanisms (48, 49). As a result, specific types of fragment ions are observed. Charge-remote fragmentation mechanisms require greater internal energies than charge-directed fragmentation mechanisms (50), and are most readily formed by high-energy CAD. The structures of peptide fragment ions and the mechanisms that produce those ions are the subject of debate (40, 51-59). Figure 1.4 shows the originally proposed structures for the generic fragment ions of underivatized peptides (40). In this review, we use the nomenclature recommended by Johnson et al. (54); this is a refinement of the nomenclature originally suggested by Roepstorff and Fohlman (60). Alternative generic structures for selected peptide fragment ions are shown in Figure 1.5. The alternative a_n (56), c_n (53), and y_n (40) structures were proposed for fragment ions that formed by charge-remote mechanisms. The a_n and y_n ions are proposed to form by charge-driven mechanisms when basic residues (Arg, Lys, or His) are absent and by charge-remote mechanisms when basic residues are present. The c_n ions are proposed to form primarily through charge-remote mechanisms and are related to the presence of certain amino acid residues in the n+1 position (53). The alternative b_n structure (57, 58) was based on ab initio calculations that showed that it was a more stable structure than that originally proposed for b_n ions. The b_n+H_2O ion has a mass that is one dalton higher than that of the c_n ion, and arises from the loss of one amino acid residue from the peptide carboxy-terminus (61-63). Because the mass of the

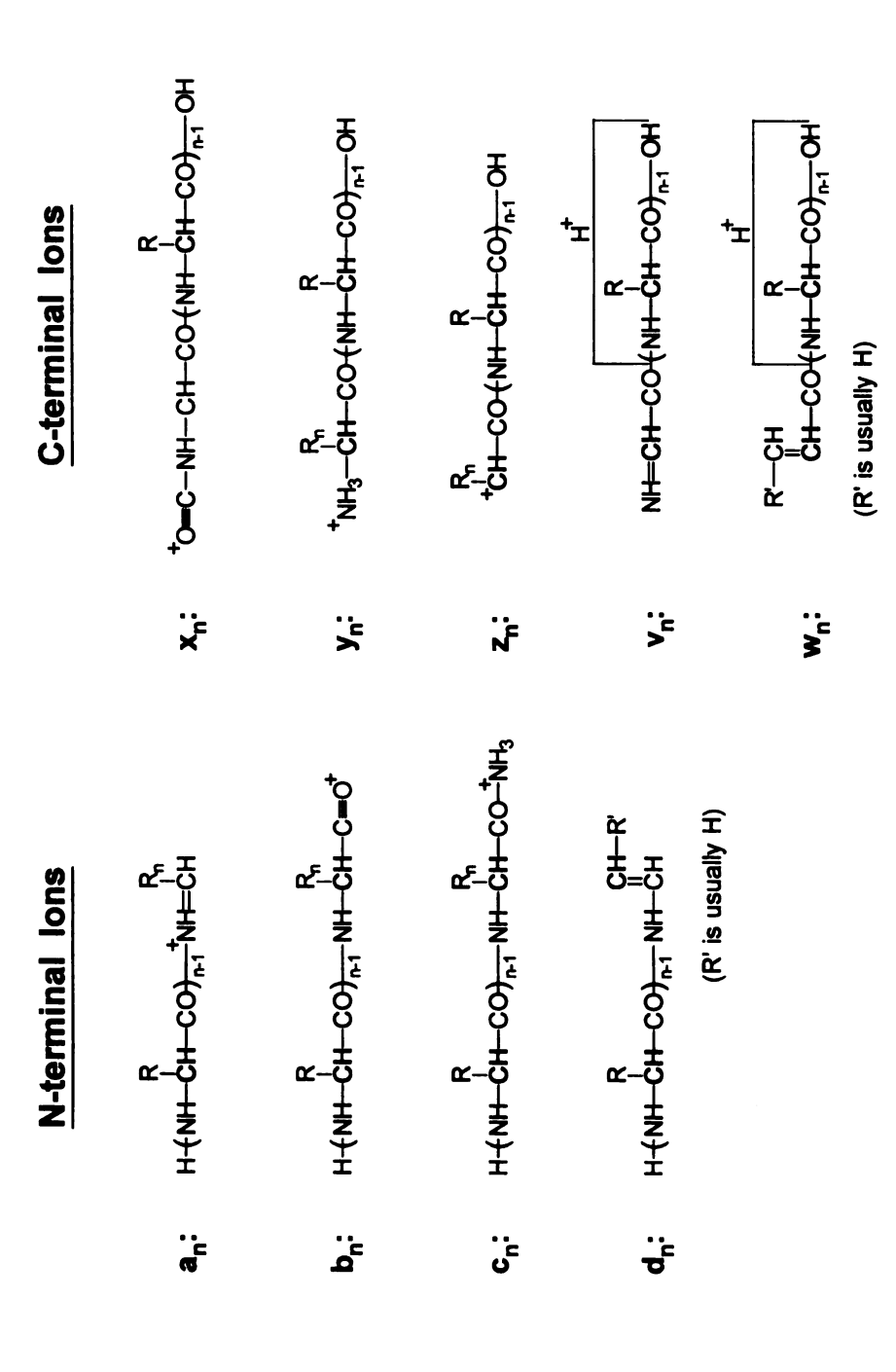


Figure 1.4. Proposed structures of peptide fragment ions

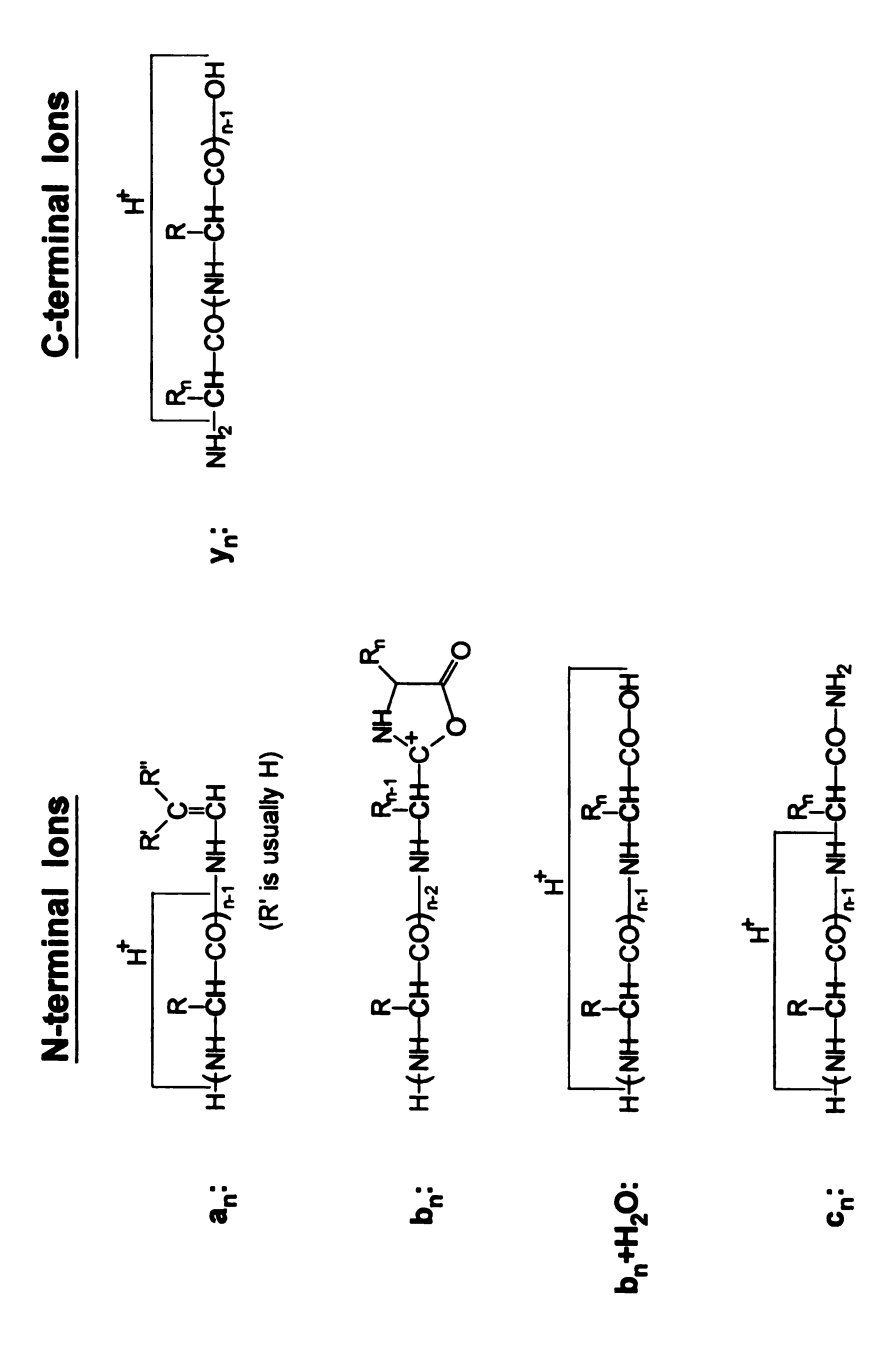


Figure 1.5. Alternative structures of peptide fragment ions.

b_n+H₂

structu

structu

charg

corre

addi

deriv

frag

it ar

der

fra the

dit

hy

67

fo

ar

w th

de

C-

 $\mathbf{b_n} + \mathbf{H_2O}$ ion is so close to that of the $\mathbf{c_n}$ ion, it is frequently misidentified. The $\mathbf{b_n} + \mathbf{H_2O}$ structure shown in Figure 1.4 was proposed by Thorne, Ballard, & Gaskell (63), but other structures have been proposed (55, 62). The $\mathbf{b_n} + \mathbf{H_2O}$ ion is proposed to arise from charge-remote fragmentation (55, 62, 63).

The nomenclature used here for the fragment ions of charge-derivatized peptides corresponds to the nomenclature of protonated peptides when the mass shift (due to derivatization) in (singly-charged) precursor ions is taken into account, but an asterisk is added to denote the presence of the derivative moiety. For example, the N-terminal fragment ion that results from cleavage of the $CH(R_n)$ —CO bond is called an a_n ion when it arises from a protonated peptide, and is called an a_n ion when it arises from a charged derivative.

The structures of fragment ions from charged derivatives and the associated fragmentation mechanisms are also debated (56, 64-67). Proposed structures of some of these fragment ions are shown in Figure 1.6. The two proposed structures for $*a_n$ ions differ on which hydrogen atom is lost. The first structure results from the loss of a hydrogen atom from the β -carbon during analysis by FAB-high-energy CAD-MS/MS (64, 67). The second structure results from the loss of a hydrogen atom from the neighboring amide nitrogen (65) during analysis by MALDI-PSD. The uppermost proposed structure for the $*b_n$ ion in Figure 1.6 (56) was proposed to arise from charged peptide derivatives with any amino acid present at residue n. An alternative structure (65) was proposed for the $*b_n$ ion in the special case when aspartic acid is present at residue n; in this case, derivatized peptides produce abundant $*b_n$ ions that correspond to fragmentation on the C-terminal side of aspartic acid (65, 66). Lin and Glish (68) observed $*b_n+H_2O$ fragment

N-terminal lons

C-terminal lons

Figure 1.6. Proposed structures of fragment ions produced from charge-derivatized peptides.

ions from a charge-derivatized peptide, but referred to them as $\mathbf{b_n}+\mathbf{OH}$ ions. Because no structures have been proposed for $*\mathbf{b_n}+\mathbf{H_2O}$ ions, the $\mathbf{b_n}+\mathbf{H_2O}$ structure proposed for underivatized peptides by Thorne, Ballard, & Gaskell (63) was adapted. The $*\mathbf{c_n}$ and $*\mathbf{d_n}$ structures shown are those proposed by Stults *et al.* (66). The $*\mathbf{x_n}$ structure was proposed by Watson *et al.* (67). The $*\mathbf{y_n}$ and $*\mathbf{y_n}-\mathbf{2}$ structures were proposed by Johnson (64) and by Watson *et al.* (67). Charged derivatives fragmented by high-energy CAD produce a combination of $*\mathbf{y_n}$ and $*\mathbf{y_n}-\mathbf{2}$ ions; the $*\mathbf{y_n}-\mathbf{2}$ ions are the more common (67). The $*\mathbf{z_n}$ and $*\mathbf{z_n}+\mathbf{1}$ ions are both formed from charged derivatives, but a structure has only been proposed for the $*\mathbf{z_n}+\mathbf{1}$ ion (56). The structures of the $*\mathbf{v_n}$ and $*\mathbf{w_n}$ ions were proposed by Johnson (64). The structure of the $*\mathbf{v_n}$ ion was also proposed by Watson *et al.* (67).

Charge derivatization limits the types of fragment ions generated from peptides. Derivatization at the N-terminus causes N-terminal charge-remote fragments to be observed, and derivatization at the carboxy-terminus (C-terminus) causes C-terminal fragment ions to be observed. High-energy CAD of N-terminal-charged derivatives produces primarily $\mathbf{*a_n}$ and $\mathbf{*d_n}$ ions plus a few $\mathbf{*b_n}$ and $\mathbf{*c_n}$ ions (69), whereas C-terminal charged derivatives produce primarily $\mathbf{*y_{n-2}}$, $\mathbf{*y_{n}}$, $\mathbf{*v_{n}}$ and $\mathbf{*w_{n}}$ ions (67, 70). This review will focus on derivatives that localize a charge on the peptide to control its fragmentation during analysis by MS or MS/MS.

The vast majority of charged derivatives were developed for use with FAB or LSIMS desorption/ionization techniques. Most of these papers were published between the mid-1980s and the mid-1990s. Many instruments during this period made use of high-energy CAD, which can provide the internal energies necessary to induce charge-remote fragmentation. Derivatization to increase analyte signal intensity was also more

important when FAB or LSIMS was used, because the response of many peptides could be increased by increasing their relative hydrophobicity (42-44).

The use of charged derivatives with plasma desorption (PD) has been quite limited (71, 72), mainly because PD was never as widely used as FAB or LSIMS. However, the high internal energies of ions generated by PD produce abundant fragment ions without the use of CAD-MS/MS techniques.

The analysis of charged derivatives by electrospray ionization (ESI) has received limited attention (50, 73-77). It is difficult to form charge-remote fragment ions during analysis by ESI because ions are produced with lower internal energies than those formed by LSIMS (50), and because the majority of electrospray instruments use low-energy CAD to form fragment ions for analysis by tandem mass spectrometry. Also, ESI provides peptide detection limits that are orders of magnitude lower than those obtained by FAB or LSIMS, so there has been little need to pursue derivatization approaches to increase signal intensities of the analytes.

Only recently (65, 78-85) have charged derivatives been applied to the analysis of peptides by matrix-assisted laser desorption/ionization (MALDI). MALDI has detection limits for peptides and proteins that are several orders of magnitude better than those obtained with FAB or LSIMS; hence, there was little incentive to develop derivatization approaches to increase signal intensities of the analytes. Before the development of post-source decay (PSD) (25), most MALDI instruments were incapable of generating and observing fragment ions of peptides. Although the spectra of underivatized peptides obtained by MALDI-PSD have been observed to resemble those obtained by LSIMS low-energy CAD (26), PSD is an effective technique to form fragment ions of charged

derivatives, and now charge derivatization to control fragmentation is an attractive option.

In 1984, Kidwell and coworkers reported the development of several

VI. N-Terminal-Charged Derivatives

A. Quaternary Ammonium Derivatives

contain three or fewer residues.

derivatization approaches. The first approach (86, 87) to N-terminal derivatization used methyl iodide to form a trimethylammonium derivative as shown in Figure 1.7.

Because this derivatization approach had low yields, another approach (86, 87) that involved successive derivatization of the peptide N-terminus with chloroacetyl chloride followed by reaction with triethylamine to give a triethylammonium derivative was proposed, as shown in Figure 1.8A. Both of these derivatization approaches will also derivatize unprotected lysine side-chains. The derivatized peptides were randomly cleaved with acid or enzymes to generate a series of derivatives that differ by the number of residues present. The cleavage products were esterified and acetylated to suppress ionization of the underivatized fragments. These mixtures were analyzed by secondary ionization mass spectrometry (SIMS), which was the precursor of FAB and LSIMS. The derivatives had detection limits in the low nanogram (picomole) range; detection limits were not given for the underivatized peptides. Data were presented only for peptides that

Stults, Halualani, & Wetzel presented a selective procedure for attaching a quaternary ammonium group to the peptide N-terminus (88). Peptide (1-30 nmol) was reacted with iodoacetic anhydride followed by thiocholine iodide, each at a controlled pH,

NH₂-

Figu

NH

-

Figure 1.7. Methyl iodide derivatization scheme.

A) Hal = Cl,
$$R_1$$
 = Cl, R_2 = R_3 = R_4 = Et

B) Hal = Cl,
$$R_1$$
 = Cl, R_2 = R_3 = R_4 = CH₃

C) Hal = I,
$$R_1 = OC(O)CH_2I$$
, $R_2 = R_3 = CH_3$, $R_4 = CH_3$, C_6H_{13} , or C_8H_{17}

Figure 1.8. Trialkylammonium-acetyl derivatization scheme.

Figure 1.9. Thiocholine iodide derivatization scheme.

Figure 1.10. "C5Q" derivatization scheme.

as shown in Figure 1.9. The pH control allowed for the selective derivatization of the N-terminus by exploiting differences between the pK_a of the N-terminus and the pK_a of any basic amino acid side-chain. However, protection of free cysteines was required to prevent derivatization (89). Although the reactions were complete in a few hours, the products had to be purified by HPLC prior to analysis. Although analysis by FAB or LSIMS followed by CAD-MS/MS gave typical N-terminal charge-remote fragment ions, the spectrum was complicated by the loss of trimethylamine from several ions.

Vath and Biemann proposed another procedure for attaching a trimethyl-ammonium group to the N-terminus of a peptide (90). The procedure involved reaction of approximately one nmol of peptide with chloroacetyl chloride followed by trimethylamine, as shown in Figure 1.8B. This two-step procedure involved a total reaction time of three hours. The signal intensity of the derivative was approximately one-half that generated from an equal amount of the underivatized peptide during analysis by FAB-MS. The derivative gave common charge-remote fragmentation products when analyzed by FAB-CAD-MS/MS.

Stults *et al.* developed a similar reaction scheme for attaching a dimethylalkylammonium (DMAA) group at the peptide N-terminus (65). The derivatization involved reaction of at least 100 pmol of peptide with iodoacetic anhydride followed by reaction with a dimethylalkylamine, as shown in Figure 1.8C. The derivatization required a total reaction time of about two hours and gave overall yields of 60-80%. Although the pH control of the iodoacetylation gave 70-90% selectivity for the N-terminus over the ε-amino group of lysine, cysteine residues had to be protected to prevent derivatization. The presence of a nonvolatile buffer and excess reagents

necessitated HPLC cleanup prior to analysis by mass spectrometry. The derivatives were analyzed by FAB-high-energy CAD-MS/MS or by LSIMS-high-energy CAD-MS/MS. The dimethylhexylammonium and dimethyloctylammonium derivatives of a hexapeptide yielded signal intensities that were higher by a factor of 2-5 compared to the underivatized peptide. The increase in signal intensity is presumably the result of an increased surface activity; however, such enhancements were not observed during analyses of larger peptides (a 14-mer and a 19-mer). The trimethylammonium derivative gave a slight decrease in signal intensity compared to that for the underivatized peptide. The derivative gives abundant N-terminal charge-remote fragments and a small loss of the hexyl group from the dimethylalkylammonium functionality.

Stults has applied the N-terminal derivatization procedure to prepare peptide derivatives with a dimethylhexylammonium group for analysis by ESI (76). The signal from the derivative was 2-5 times less intense than that from the underivatized peptide when analyzed by ESI-MS. The doubly-charged ions of the underivatized peptide $[M + 2H]^{2+}$ and the derivative $[C + H]^{2+}$ were used as precursors for analysis by ESI-low-energy CAD-MS/MS. In contrast to the product-ion spectrum of the underivatized peptide, the product-ion spectrum of the derivative gave primarily *a_n and *b_n ion peaks; no C-terminal fragment ion peaks were observed. The presence of abundant *b_n ions and the presence of only one *d_n is in contrast to the fragmentation patterns observed by high-energy CAD (65, 68). The mechanism of fragment ion formation is not clear. The precursor ion has a charged quaternary ammonium moiety at the N-terminus and a proton located on the peptide. Fragmentation could occur by charge-remote or charge-directed mechanisms, or a mixture of the two. Charge-directed mechanisms might by expected to

produce doubly-charged fragment ions (when the second charge is retained on the N-terminal fragment) or abundant C-terminal fragments, such as y_n ions (when the second charge is transferred to the C-terminal fragment); however, neither doubly-charged fragment ions, nor C-terminal fragment ions were reported. This derivatization technique was also used by Dongré *et al.* (49) to prepare the trimethylammonium acetyl derivative of leucine enkephalin for analysis by electrospray surface-induced dissociation tandem mass spectrometry (ESI-SID-MS/MS).

Bartlet-Jones et al. (77) developed another derivatization approach (Figure 1.10) to attach a trimethylammonium functionality to the peptide N-terminus. This derivative has been named "C5Q", presumably because it consists of a five-carbon chain and a quaternary ammonium group. The C5Q derivatization reaction was complete in 10 minutes and was performed on 20-50 fmol of peptide; 50 fmol of derivatized peptide was readily observed by MALDI. This derivatization approach was studied in detail in a later paper (83). MALDI-PSD analysis of the derivatized peptide with a C-terminal arginine residue generated several y_n ions. Modification of Lys and Arg side-chains was recommended to reduce their basicity. The chemistry used to modify lysine side-chains also results in cleavage of the N-terminal residue. The modification of lysine, derivatization of the N-terminus, and modification of arginine required four reaction steps, more than four hours, 5-10 pmol of peptide, and HPLC purification. When the peptide was charge-derivatized and basic side-chains were modified, only N-terminal fragment ions were produced, primarily $\mathbf{*a_n}$ and $\mathbf{*b_n}$ ions. Abundant $\mathbf{*b_n}$ fragment ions have not usually been observed for other charge-derivatized peptides analyzed by highenergy CAD (68) or MALDI-PSD (64, 84). However, $*b_n$ ions have been observed in the

MALDI-PSD spectra of charge-derivatized peptides when very high laser powers were used for desorption (64). When Hines *et al.* analyzed peptides derivatized with the C5Q reagent (78), several $*a_n$ fragment ion peaks and one $*b_n$ fragment ion peak were observed in the MALDI-PSD spectrum; however, the most abundant fragments were immonium ions and ions that presumably resulted from a combination of backbone cleavage and the loss of trimethylamine from the derivative ([$*a_n$ -59] and [$*b_n$ -59] ions).

B. Quaternary Phosphonium Derivatives

Wagner et al. presented an approach for attaching a triphenylphosphonium group to either the N-terminus or the C-terminus of a peptide (69). For the N-terminal derivative, approximately one nmol of peptide was reacted with 2-bromoethyl-triphenylphosphonium bromide at pH 9 for 3 hours at 37°C, as shown in Figure 1.11A. The derivatization reactions gave yields greater than 75% (66), but with some difficulty in reproducibility. These derivatives provided charge localization and an enhanced surface activity relative to the underivatized peptides on the FAB matrix. As a result of derivatization, the fragmentation was simplified and the signal intensity increased relative to those obtained from the underivatized peptides during analysis by FAB. The detection limit of some peptide derivatives was less than 5 picomoles. Both the N-terminal and C-terminal derivatives produced abundant charge-remote fragments that arose from the derivatized terminus. However, when a peptide containing a disulfide bond was derivatized at the N-terminus, the mass spectrum provided less structural information than the spectrum of the native peptide (91). The derivatization reaction used pH control to prevent reaction with basic side chains, but it required removal of the buffer salts prior

Figure 1.11. N-terminal triphenylphosphonium derivatization scheme.

Figure 1.12. TMPP+-Ac derivatization scheme.

Figure 1.13. Derivatization schemes of Renner and Spiteller.

to analysis; this procedure was later modified to eliminate the need for nonvolatile buffers (92). With the new procedure, the peptide was reacted with vinyltriphenylphosphonium bromide in a mixture of acetonitrile and pyridine, as shown in Figure 1.11B. Although this new procedure eliminated the need for sample cleanup, the pH control was uncertain and allowed the possibility of reaction with basic side-chains.

Bunk and Macfarlane (70) reported the N-terminal derivatization of bradykinin with vinyltriphenylphosphonium bromide, as shown in Figure 1.11B. The reagents were combined in a pH 9.0 buffer solution and allowed to react at room temperature overnight. The derivatives underwent metastable decay to produce N-terminal fragments, with *a_n ions dominating, when analyzed by plasma desorption mass spectrometry (PD-MS). A peak for the protonated derivative [C + H]²⁺ and a few C-terminal fragments were also observed. Although an increase in N-terminal fragmentation was observed, the data obtained by PD-MS analysis of the derivatives gave unsatisfactory results especially when larger peptides were derivatized and analyzed (71). The triphenylphosphonium group was readily cleaved through a reverse Michael-type reaction; this cleavage led to a decrease in sequence-specific fragment ions. Also, the derivative formed primarily metastable fragments that produced broader peaks than the fragment ions obtained from underivatized peptides.

Liao and Allison reported that charge derivatization of a hexapeptide led to signal enhancement when analyzed by MALDI (81). They used the procedure of Wagner *et al.* (69) to prepare the N- and C-terminal ethyltriphenylphosphonium derivatives. A one-pmol sample of the underivatized peptide gave no signal when analyzed by MALDI, but the N- and C-terminal derivatives both produced strong signals at the one-pmol level.

Huang et al. introduced a derivatization procedure that attaches a tris(2,4,6trimethoxyphenyl)phosphonium (TMPP⁺-Ac) group to the peptide N-terminus (80). At least 10 pmol of peptide were reacted with S-pentafluorothiophenyl [tris(2,4,6trimethoxyphenyl)phosphonium]acetate bromide and 4-(dimethylamino)pyridine (DMAP) for 15 minutes at room temperature, as shown in Figure 1.12. Although, the reaction gave yields in excess of 90% for most peptides, a few peptides have yields as low as 64%. The reaction mixture usually does not require purification prior to analysis by FAB or MALDI. In addition, peptides composed primarily of amino acid residues with nonpolar side-chains show significant signal enhancement upon derivatization and analysis by FAB or MALDI. We have observed recently that lysine, cysteine, and tyrosine will form a TMPP+-Ac derivative along with TMPP+-Ac derivatization of the N-terminus when the reaction is performed in an unbuffered system. The spectra of the derivative obtained by FAB-high-energy CAD-MS/MS show a strong series of chargedirected fragments. A variety of N-terminal and C-terminal fragment ions were observed in the MS/MS spectrum of the underivatized peptide. There was no complete series of ions among the fragment types produced from the underivatized peptide. In contrast, the N-terminal derivative shows a complete series of readily discernable $*a_n$ ions. It is also noteworthy that the signal-to-background ratios of fragment peaks produced from the Nterminal derivative were better than the signal-to-background ratios of fragment peaks produced from the underivatized peptide. When TMPP⁺-Ac derivatized peptides were analyzed by LSIMS-CAD-MSⁿ with a quadrupole ion trap instrument, abundant * b_n+H_2O ions were produced in addition to a series of * a_n ions (67).

The TMPP*-Ac derivative has also been applied to peptide analysis by electrospray with an elevated cone voltage to promote in-source fragmentation (ISF) (75). With the cone set at a typical potential of 37 V, the peptide derivatives did not fragment significantly, and the derivatives were observed as the doubly-charged derivative $[C + H]^{2+}$. When the cone voltage was raised to 100 V, extensive fragmentation occurred and the doubly-charged derivative was not observed. The fragmentation produced primarily \mathbf{a}_n and \mathbf{b}_n ions, with some \mathbf{c}_n and \mathbf{d}_n ions produced. This pattern is similar to the fragmentation of the dimethylalkylammonium acetyl derivative when analyzed by ESI-low-energy CAD-MS/MS (76).

The TMPP*-Ac derivative (Figure 1.12) has been used to direct the fragmentation of peptides during analysis by MALDI-PSD (64, 79, 80). The spectra consist of a strong series of *a_n ions plus a few *b_n, *c_n, and *d_n ions. It is interesting to note that the *d_n ion peaks in the MALDI-PSD spectra are less intense than those in the FAB-high-energy CAD-MS/MS spectra (64). When an aspartic acid residue occurred at residue n, abundant *b_n, *d_n, and *c_{n-1} fragment peaks were observed instead of the *a_n fragment peak. At very high laser powers, derivatized peptides produced a variety of *b_n, *c_n, and *d_n fragments, that were not produced at lower laser powers. The TMPP*-Ac reagent has been used to derivatize protein digest mixtures at the 25 pmol level (80). This reagent was also used to derivatize peptides located in an electrophoresis gel or a transfer membrane (84). The modified peptides were analyzed by MALDI and MALDI-PSD directly from the gel or membrane on a modified sample plate.

VII. N-Terminal Derivatives with High Proton Affinities

In addition to derivatives with a fixed charge, several derivatives with high proton affinities have been developed. Although the basic groups provide some degree of charge localization, there is potential for protonation at other sites or for proton transfer to other sites. These derivatives are analogous to peptides with basic residues (Arg, His, or Lys) at the N-terminus. As a result, the nomenclature used for these derivatives will be the same as that used for underivatized peptides.

Renner and Spiteller (93) reported N-terminal derivatization schemes that use dansyl chloride, as shown in Figure 1.13A, and 2-bromo-5-(dimethylamino)-benzene-sulfonyl chloride, as shown in Figure 1.13B. Although these derivatives did not have a fixed charge, the aromatic amine was preferentially protonated during analysis by FAB. The derivatives had greater signal intensities and an increase in fragmentation (without CAD) compared to the underivatized peptides. Although the FAB-MS analysis of the dansyl derivative produced only N-terminal fragments (a_n and b_n), the second derivative produced a_n, b_n, and y_n ions. The a_n and b_n ions that arise from the second derivative produced two peaks for each ion, as a result of the ⁷⁹Br and ⁸¹Br isotopes. These isotope peaks allowed the N-terminal fragments be distinguished from the C-terminal fragments. The chemistry employed would also likely derivatize basic side-chains as well as the N-terminus of the peptide.

Sherman *et al.* (94) have used N-hydroxysuccinimide-2-(3-pyridyl)acetate (SPA) to derivatize the peptide N-terminus, as shown in Figure 1.14, in preparation for analysis by ESI-MS; this chemistry was optimized by Cárdenas *et al.* (72). Although the N-pyridylacetyl functionality is not charged, it does have a slightly increased proton

Figure 1.14. N-Hydroxysuccinimide-2-(3-pyridyl)acetate (SPA) derivatization scheme.

Figure 1.15. C-terminal pyridinium derivatization scheme.

Figure 1.16. C-terminal acyl urea derivatization scheme.

Reagents: i = Carboxypeptidase, NH₂-N(CH₃)₂, ii = CH₃I

Figure 1.17. Carboxypeptidase derivatization scheme.

affinity compared to that of the peptide N-terminus. The derivatives were analyzed by ESI-MS/MS on a triple quadrupole instrument (93) or by ESI-MSⁿ on a quadrupole ion trap instrument (72). The spectra of the derivative contained N-terminal fragment (\mathbf{b}_n and \mathbf{a}_n) peaks and C-terminal fragment (\mathbf{y}_n) peaks. However, the \mathbf{b}_n fragment ion peaks of the derivative were more intense than the corresponding \mathbf{b}_n fragment ion peaks of the underivatized peptides. The optimized reaction occurs in four minutes, and gives yields in the range of 80-100% for peptides that do not contain lysine or tyrosine. The reagent reacts with the side-chain of lysine and reacts to a lesser extent with the side-chain of tyrosine. Reactions with the side-chains produce derivatives that have multiple N-pyridylacetyl functionalities. This derivatization has been used on peptides with as many as 15 residues.

Naven et al. (82) used MALDI-PSD to study peptides derivatized with SPA (Figure 1.14). The derivatization was performed on-target with as little 50 fmol of peptide. The procedure was also applied to tryptic peptides electroblotted onto a PVDF membrane. The reaction was essentially quantitative at the N-terminus and the lysine side-chains. The PSD spectra contained peaks for a series of abundant \mathbf{b}_n ions and some \mathbf{a}_n and \mathbf{y}_n ions.

VIII. C-Terminal-Charged Derivatives

In addition to the N-terminal derivatives discussed previously, Kidwell and coworkers developed several C-terminal derivatization approaches (86). Coupling of the peptide C-terminus to a charged pyridinium salt with 1-(3-dimethylaminopropyl)-3-ethylcarbodiimide (EDC) was used the generate a derivative with a charged pyridinium

functionality, as shown in Figure 1.15. Alternatively, the peptide C-terminus could be reacted with excess EDC to form a basic acyl urea derivative. This derivative could be analyzed directly or could be reacted further with methyl iodide to quaternize the terminal nitrogen, as shown in Figure 1.16. The reagents from Figures 1.15-1.16 will also derivatize unprotected acidic side-chains. To avoid derivatization of the side-chains, an enzymatic approach to C-terminal derivatization was also reported, as represented in Figure 1.17. The peptide methyl ester was formed and reacted with 1,1-dimethyl-hydrazine, using carboxypeptidase Y to catalyze the reaction. This reaction was followed by reaction with methyl iodide to form a quaternary ammonium functionality. Like the N-terminal derivatives discussed above, these derivatized peptides were randomly cleaved, and the cleavage products were esterified and acetylated to suppress ionization of the underivatized fragments during analysis by SIMS.

Figure 1.18 shows a selective C-terminal derivatization procedure reported by Bennett and Day (95). Peptides were reacted with acetic anhydride and N,N-dimethylethanolamine to generate a C-terminal tertiary amine. The tertiary amine was reacted with methyl iodide to generate a C-terminal quaternary amine. Although the procedure was selective, it was very time-consuming. The procedure was only applied to dipeptides, and required large samples (approximately 100 nmol for the derivatization procedure and 10 nmol for the analysis by FAB). This chemistry was adapted by Vath, Zollinger, & Biemann (96) for gas-phase derivatization. The adapted procedure allowed derivatization and FAB-MS analysis of 360 pmol of a pentapeptide; no signal enhancement was observed as a result of derivatization.

Hirayama *et al.* used a similar approach to generate the tertiary amine derivative (97). The procedure was the same as that shown in Figure 1.18, except that the quaternization with methyl iodide was omitted. The dimethylamine functionality is reportedly preferentially protonated during analysis by FAB-MS. However, the FAB-CAD-MS/MS spectrum of the derivative contained peaks for ions that arise from charge retention at the N-terminus (**b**_n ions) and the C-terminus (**y**_n ions). The precursor-ion spectrum of m/z 72 (a fragment of N,N-dimethylethanolamine) contained only peaks for ions that arise from charge retention at the C-terminus. Although sequence information was generated, this approach was not very effective at localizing the charge, and probably should be avoided for peptide sequencing.

A C-terminal triphenylphosphonium derivatization procedure was reported by Wagner et al. (69). The peptide was combined with 2-aminoethyltriphenylphosphonium bromide and dicyclohexylcarbodiimide (DCC) at pH 5 to form the C-terminal derivative, as shown in Figure 1.19. Like the N-terminal derivative reported previously, the derivative increased signal intensity during analysis by FAB-MS and simplified fragmentation by FAB-CAD-MS/MS. Although the derivatization procedure did not require removal of buffer, it had the potential to derivatize acidic side chains. However, reaction products from acidic side chains were not observed. The MS/MS spectra of C-terminal derivatives contained only C-terminal fragments. Using the same derivatization approach, Liao and Allison (81) observed an increase in signal intensity for a peptide derivative analyzed by MALDI.

Reagents: $i = Ac_2O$, $ii = HOCH_2CH_2N(CH_3)_2$

Figure 1.18. C-terminal N, N-dimethylethanolamine derivatization scheme.

Figure 1.19. C-terminal triphenylphosphonium derivatization scheme.

Figure 1.20. 2,4,6-Trimethylpyridinium derivatization scheme for lysine side-chains.

IX. Side-Chain Derivatives

Johnson (39, 63) reported the conversion of a lysine side-chain to a charged 2,4,6-trimethyl pyridinium group, as shown in Figure 1.20. Peptide (20 nmol) was reacted with 2,4,6-trimethylpyrylium tetrafluoroborate for 18-24 hours at room temperature. Excess reagent and buffer salts were removed by solid phase extraction and HPLC. No underivatized peptide was observed during analysis by FAB-MS. Upon analysis by FAB-CAD-MS/MS, primarily charge-remote fragments were detected. If the derivatized lysine was at the N-terminus, then N-terminal fragments were formed. If the derivatized lysine was at the C-terminus, then C-terminal fragments were formed. If an internal lysine was derivatized, then a mixture of N- and C-terminal fragments was formed.

In response to the unsatisfactory results obtained from plasma desorption analysis of triphenylphosphonium derivatives (70), Bunk and Macfarlane developed another derivatization procedure (71); the conversion of lysine residues to homoarginine used O-methylisourea under basic conditions, as shown in Figure 1.21. The reaction mixture was purified by HPLC prior to analysis. The homoarginine residue does not possess a fixed charge, but has a high proton affinity similar to that for arginine. This derivative localizes the charge on the homoarginine residue. During analysis by plasma desorption, sequence-specific fragmentation was increased for some derivatives. This derivative also provides a means for distinguishing between lysine and glutamine residues. The most obvious limitation of this approach is that it is only useful for peptides that contain lysine. The site of derivatization is not known unless the location of the lysine residue is known. Also, there is potential for the charge to be spread over several sites if either an arginine or additional lysine residues are present in the peptide.

Figure 1.21. Conversion of lysine side-chains to homoarginine.

Figure 1.22. Pentafluorobenzoyl fluoride derivatization scheme.

Figure 1.23. C-terminal 4-aminonaphthalenesulphonic acid (ANSA) derivatization.

X. Negatively-Charged Derivatives

Kiplinger et al. (98) used pentafluorobenzoyl fluoride to derivatize peptides at the N-terminus, as shown in Figure 1.22. The derivatization was useful for analyses by LSIMS in the positive and negative modes. In negative LSIMS, the pentafluorobenzoyl group was preferentially ionized to produce a species with a negative charge at the Nterminus. The derivative produced a peak that was 2-40 times more intense than the peak produced by the underivatized peptide. However, in the negative mode no significant fragmentation was observed. The response of the derivative to negative LSIMS-CAD-MS/MS was not examined. In positive LSIMS, no significant enhancement of the signal intensity was observed, but extensive fragmentation was produced without the use of MS/MS. However, in the positive mode, the location of the charge was not fixed, and Nterminal and C-terminal fragments were both observed. The derivatization reaction occurred rapidly, and the derivative could be analyzed without any sample cleanup. However, the reaction was performed on a large scale (approximately 100 nmol), and the reagent reacted with the side-chains of lysine and tyrosine.

Lindh *et al.* reported a C-terminal derivatization approach for use with negative LSIMS (99). The peptide or acetylated peptide was reacted with 4-amino-naphthalene-sulphonic acid (ANSA) and a carbodiimide coupling agent (EDC) to form the negatively-charged derivative, as shown in Figure 1.23. Three small peptides with 3-5 residues were derivatized and analyzed. The reaction was performed on 10-100 nmol of peptide at 25°C for 2 hours to produce yields of 10%-100%, depending on the peptide. After purification by HPLC, the derivatives were analyzed by negative LSIMS. When the peptides were acetylated and derivatized with ANSA, the detection limits obtained upon

·			

analysis by negative LSIMS were a factor of 10-40 times improved compared to those of the underivatized peptide. Analysis by negative LSIMS-CAD-MS/MS produced a variety of C-terminal charge-remote fragments and a few N-terminal fragments. Derivatization with ANSA can occur at the side-chains of aspartic acid and glutamic acid residues in addition to derivatization at the C-terminus. Other side reactions, such as internal cyclization, have been observed during derivatization.

Griffiths *et al.* analyzed ANSA-derivatized peptides using ESI-MS, ESI-ISF-MS, and ESI-high-energy CAD-MS/MS on a sector instrument equipped with an array detector (73). Detection limits in the range of one fmol were obtained from the derivatized peptides during analysis by negative ESI-MS, a factor of 5-50 better than the detection limits of the underivatized peptides. Negative ESI-ISF-MS data were obtained from 10-30 pmol of derivatized peptide, and negative ESI-high-energy CAD-MS/MS data were obtained from as little as 50 fmol of derivatized peptide. Derivatized peptides analyzed by ESI-ISF-MS and by ESI-high-energy CID produced many of the same fragment ions; however, some unique fragment ions were generated by each fragmentation method. Both fragmentation methods produce multiple types of fragments, complicating interpretation.

In a related study, ANSA-derivatized peptides were analyzed by negative ESI-low-energy CAD-MS/MS on a hybrid magnetic sector-orthogonal time-of-flight instrument (74). MS/MS data could be obtained from a few picomoles of derivatized peptide. Primarily C-terminal charge-remote fragments were observed; however, a few c_n ions were observed. The appearance of the low-energy CAD-MS/MS spectra were dependant on the mass of the collision gas used. When helium was used as the collision

gas, the fragments generated were primarily the result of backbone cleavage. When xenon was used as the collision gas, fragments from side-chain cleavage were observed in addition to those from backbone cleavage. Many of the fragment ion peaks in the ESI-low-energy-CAD-MS/MS spectra were the same as those in the ESI-ISF-MS and ESI-high-energy CAD-MS/MS spectra (73); however, the spectra produced by each of these methods were different.

XI. Concluding Commentary

The ideal charged derivatization approach would have several attributes. The chemistry should occur rapidly with high product yield without any unwanted derivatization of peptide side-chains. The derivatives should not require purification prior to analysis. The derivative should be compatible with all mass spectrometry ionization and fragmentation techniques. The ideal derivative would have a better detection limit than the underivatized peptide. The derivative should have a fixed charge, and produce a series of charge-remote fragments during CAD. The added chemical derivative group should not fragment during analysis by tandem mass spectrometry because that fragmentation might complicate the mass spectrum and reduce the intensity of the other fragment ion peaks.

Three of the derivatization approaches discussed in this review come closer to the ideal than the others. Those derivatization approaches produce the dimethylalkylammonium acetyl (DMAA) derivatives reported by Stults *et al.* (65) (Figure 1.8C), the C5Q derivatives of Spengler *et al.* (83) (Figure 1.10), and the [tris(2,4,6-trimethoxyphenyl)-phosphonium] acetate (TMPP⁺-Ac) derivatives reported by Huang *et al.* (80)

(Figure 1.12). These approaches can be used to attach a fixed charge to the N-terminus of the peptide in high yields.

The DMAA derivatization is performed with commercially available reagents. Although the C5O and TMPP⁺-Ac derivatization reagents must be synthesized, the TMPP⁺-Ac reagent, and possibly the C5O reagent, are stable for months. The TMPP⁺-Ac derivatization occurs in a fifteen-minute step, the DMAA derivatization occurs in two steps that require a total of two hours, and the C5O derivatization requires between twenty minutes (without side-chain derivatization) and four hours (with derivatization of Lys and Arg). The amount of peptide required for the derivatization reactions has been reported as 100 pmol for DMAA and the low pmol range for the TMPP+-Ac and C5Q derivatizations. However, the C5O derivatization procedure can be performed on subpicmole quantities of peptide, if neither Lys nor Arg needs derivatization. All three reactions occur with high yields and are selective for the N-terminus when the pH of the reaction mixture is controlled. The DMAA and C5Q derivatizations usually require purification by HPLC to remove excess reagent. Although such purification usually is not required for the TMPP⁺-Ac derivatization when the reaction mixture is analyzed by FAB or MALDI, it is required in analyses by ESI.

The TMPP⁺-Ac derivative has been analyzed successfully with FAB, ESI, and MALDI techniques. Although the DMAA derivatives have only been analyzed by FAB and ESI, they are probably compatible with MALDI. Likewise, although the C5Q reagent has only been analyzed by MALDI, it should be compatible with FAB and ESI.

DMAA derivatives give a small increase in signal intensity in some conditions and a small decrease under others. No loss of signal intensity was observed for C5Q

derivatization; however, the relative signal intensities of underivatized and derivatized peptides were not reported. For most peptides, the TMPP+-Ac derivative has only a small effect on signal intensity; however, some hydrophobic peptides have shown a significant signal enhancement upon derivatization. All of the derivatives have detection limits in the low picomole to sub-picomole range.

Because the derivative moieties have fixed charges, the fragment ions produced from these derivatives are proposed to form by charge-remote mechanisms. FAB-high-energy CAD-MS/MS analysis of the DMAA and TMPP+-Ac derivatives produces primarily $\mathbf{^*a_n}$ and $\mathbf{^*d_n}$ plus a few $\mathbf{^*b_n}$ and $\mathbf{^*c_n}$ ions. In addition, the DMAA derivative loses the alkyl group to generate a peak that can complicate the high-mass end of the spectrum. When DMAA (76) and TMPP+-Ac (75) derivatives are analyzed by ESI, primarily $\mathbf{^*a_n}$ and $\mathbf{^*b_n}$ ions are generated plus a few $\mathbf{^*c_n}$ and $\mathbf{^*d_n}$ ions. Because the precursor ions have a double-charge, it is not clear whether the fragment ions arise by charge-remote fragmentation, charge-directed fragmentation, or a combination of the two.

When TMPP⁺-Ac derivatives are analyzed by MALDI-PSD (64, 79, 84), a dominant series of $*a_n$ ions is produced and a few $*b_n$, $*c_n$ and $*d_n$ ions are produced. Peptides derivatized with C5Q (including modification of Lys or Arg) are reported to form primarily $*a_n$ and $*b_n$ ions, however $*c_n$ and $*d_n$ ions also form to a lesser extent. In a preliminary study by Hines *et al.* (78), a C5Q derivative was reported to form primarily $*a_n$ -59 and $*b_n$ -59 ions. The differences in these fragmentation patterns are difficult to explain. Perhaps the laser power (or some other experimental parameter) causes the differences in fragmentation, as has been documented in one case of fragmentation of charged derivatives during analysis by MALDI-PSD (64). The C5Q

derivative moiety has a smaller head group than the TMPP+-Ac moiety, and the C5Q moiety has a flexible five-carbon chain. These differences might allow the formation of secondary structures in which the charge can interact with the peptide backbone to influence fragmentation behavior. All three of these derivatization techniques show promise; however they have yet to be proven in applications of peptide sequencing by mass spectrometry of biological samples.

XII. Summary

Major advantages of charged derivatives are that they simplify the fragmentation of peptides and direct the fragmentation to one end of the peptide. Simplification of the mass spectrum is particularly helpful for interpreting data from peptides with a completely unknown sequence. Derivatives with a fixed charge are the more effective in directing fragmentation than derivatives with elevated proton affinities. N-terminal derivatization can be made selective by exploiting the differences in pK_a of the N-terminus and ε-NH₂ group on lysine; however, the pK_a values for the C-terminus and the acidic side chains are too similar to allow selective derivatization. Because N-terminal charged derivatives produce fewer types of fragment ions than C-terminal derivatives, the spectra of N-terminal derivatives are easier to interpret than those of the C-terminal derivatives.

Charged derivatives of peptides are especially useful in analyses based on FAB and LSIMS, because some derivatives can provide signal enhancement and simplify fragmentation. The utility of MALDI-PSD for the analysis of charged derivatives has been demonstrated in recent years, although different derivatives appear to produce

different fragmentation patterns. The analysis of charged derivatives by ESI has been the subject of preliminary studies; however, a careful and extensive study has yet to be published. In addition, it is not clear whether these derivatives fragment by charge-remote mechanisms, charge-driven mechanisms, or some combination of the two.

XIII. References

- Barber, M.; Bordoli, R. S.; Sedgwick, R. D.; Tyler, A. N. J. Chem. Soc., Chem. Commun. 1981, 325-327.
- 2. Rouse, J. C.; Allison, J. J. Am. Soc. Mass Spectrom. 1993, 4, 259-269.
- 3. Sunner, J.; Marales, A.; Kebarle, P. Anal. Chem. 1987, 59, 1378-1383.
- Stoll, R. G.; Harian, D. J.; Hass, J. R. Int. J. Mass Spectrom. Ion Processes 1984, 61, 71-79.
- 5. Aberth, W.; Straub, K. M.; Burlingame, A. L. Anal. Chem. 1982, 54, 2029-2034.
- Standing, K. G.; Chait, B. T.; Ens, W.; McIntosh, G.; Beavis, R. Nucl. Instrum.
 Methods 1982, 198, 33-38.
- 7. Takayama, M. J. Am. Soc. Mass Spectrom. 1995, 6, 114-119.
- Posthumus, M. A.; Kistemaker, P. G.; Meuzelaar, H. L. C.; Ten Noever de Brauw,
 M. C. Anal. Chem. 1978, 50, 985-991.
- 9. Karas, M.; Bachmann, D. B.; Bahr, U.; Hillenkamp, F. Int. J. Mass Spectrom. Ion Processes 1987, 78, 53-68.
- Juhasz, P.; Costello, C. E.; Biemann, K. J. Am. Soc. Mass Spectrom. 1993, 4, 399-409.
- 11. Vertes, A.; Gijbels, R.; Levine, R. D. Rapid Commun. Mass Spectrom. 1990, 4, 228-233.
- 12. Liao, P.-C.; Allison, J. J. Mass Spectrom. 1995, 30, 408-423.
- 13. Whitehouse, C. M.; Dreyer, R. N.; Yamashita, M.; Fenn, J. B. Anal. Chem. 1985, 57, 675-679.

- Dole, M.; Mack, L. L.; Hines, R. L.; Mobley, R. C.; Ferguson, L. D.; Alice, M. B. J. Chem. Phys. 1968, 49, 2240-2249.
- 15. Wilm, M. S.; Mann, M. Int. J. Mass Spectrom. Ion Processes 1994, 136, 167-180.
- Schmelzeisen-Redecker, G.; Buttering, L.; Röllgen, F. W. Int. J. Mass Spectrom. Ion Processes 1989, 90, 139-150.
- 17. Iribarne, J. V.; Thompson, B. A. J. Chem. Phys. 1976, 64, 2287-2294.
- 18. Thompson, B. A.; Iribarne, J. V. J. Chem. Phys. 1979, 71, 4451-4463.
- 19. Fenn, J. B.; Mann, M.; Meng, C. K.; Wong, S. F.; Whitehouse, C. M. Mass Spectrom. Rev. 1990, 9, 37-70.
- 20. Gaskell, S. J. J. Mass Spectrom. 1997, 32, 677-688.
- 21. Kebarle, P.; Tang, L. Anal. Chem. 1993, 65, 972A-986A.
- Smith, R. D.; Loo, J. A.; Loo, O.; Busman, M.; Udseth, H. R. Mass Spectrom. Rev.
 1991, 10, 359-451.
- Mamyrin, B. A.; Karataev, V. I.; Shmikk, D. V.; Zagulin, V. A. Sov. Phys. JEPT
 1973, 37, 45-48.
- 24. Wiley, W. C. and McLaren, I. H. Rev. Sci. Instr. 1955, 26, 1150-1157.
- 25. Spengler, B.; Kirsch, D.; Kaufmann, R.; Jaeger, E. Rapid. Commun. Mass Spectrom. 1992, 6, 105-108.
- 26. Rouse, J. C.; Yu, W.; Martin, S. A. J. Am. Soc. Mass Spectrom. 1995, 6, 822-835.
- 27. Miller, P. E.; Denton, M. B. J. Chem. Ed. 1986, 63, 617-622.
- 28. Mathieu, E. J. Math. Pure Appl. 1868, 13, 137-203.
- 29. March, R. E. J. Mass Spectrom. 1997, 32, 351-369.

- 30. Yates, J. R. J. Mass Spectrom. 1998, 33, 1-19.
- 31. Edman, P. Acta Chem. Scand. 1950, 4, 283-293.
- 32. Maxam, A. M.; Gilbert, W. Proc. Natl. Acad. Sci. U.S.A. 1977, 74, 560-564.
- Sanger, F.; Nicklen, S.; Coulson, A. R. Proc. Natl. Acad. Sci. US.A. 1977, 74, 5463-5467.
- 34. Biemann, K.; Gapp, F.; Siebl, J. J. Am. Chem. Soc. 1959, 81, 2274-2275.
- 35. Vilkas, E.; Lederer, E. Tetrahedron Lett. 1968, 26, 3089-3092.
- 36. Carr, S. A.; Herlihy, W. C.; Biemann, K. Biomed. Mass. Spectrom. 1981, 8, 51-61.
- 37. Beckey, H. D. Principles of Field Ionization and Field Desorption Mass Spectrometry. Pergamon, Oxford, 1977.
- 38. Macfarlane, R. D. Anal. Chem. 1983, 55, 1247A-1264A.
- 39. Biemann, K.; Scoble, H. A. Science 1987, 237, 992-998.
- 40. Johnson, R. S.; Martin, S. A.; Biemann, K. Int. J. Mass Spectrom. Ion Processes.

 1988, 86, 137-154.
- 41. Papayannopoulos, I. A. Mass Spectrom. Rev. 1995, 14, 49-73.
- 42. Falick, A. M.; Maltby, D. A. Anal. Biochem. 1989, 182, 165-169.
- 43. Ligon, W. V. Anal. Chem. 1986, 58, 485-487.
- 44. Naylor, S.; Findeis, A. F., Gibson, B. W.; Williams, D. H. *J. Am. Chem. Soc.* **1986**, 108, 6359-6363.
- Busch, K. L.; Unger, S. E.; Vincze, A.; Cooks, R. G.; Keough, T. J. Am. Chem. Soc.
 1982, 104, 1507-1511.
- 46. Renner, D.; Spiteller, G. Biomed. Environ. Mass Spectrom. 1986, 13, 405-410.

- 47. Harrison, A. G. Mass Spectrom. Rev. 1997, 16, 201-217.
- 48. Jensen, N. J.; Tomer, K. B.; Gross, M. L. J. Am. Chem. Soc. 1985, 107, 1863-1868.
- 49. Gross, M. L. Int. J. Mass Spectrom. Ion Processes 1992, 118/119, 137-165.
- Dongré, A. R.; Jones, J. L.; Somogyi, Á.; Wysocki, V. H. J. Am. Chem. Soc. 1996,
 118, 8365-8374.
- 51. Biemann, K.; Martin, S. A. Mass Spectrom. Rev. 1987, 6, 1-76.
- 52. Cordero, M. M.; Houser, J. J.; Wesdemiotis, C. Anal. Chem. 1993, 65, 1594-1601.
- 53. Downard, K. M.; Biemann, K. J. Am. Soc. Mass Spectrom. 1993, 4, 874-881.
- Johnson, R. S.; Martin, S. A.; Biemann, K.; Stults, J. T.; Watson, J. T. Anal. Chem.
 1987, 59, 2621-2625.
- Rouse, J. C. Ph.D. Dissertation, Michigan State University, East Lansing, MI,
 1993.
- Wagner, D. S. Ph.D. Dissertation, Michigan State University, East Lansing, MI,
 1992.
- Yalcin, T.; Khouw, C.; Csizmadia, I. G.; Peterson, M. R.; Harrison, A. G. J. Am. Soc. Mass Spectrom. 1995, 6, 1165-1174.
- 58. Yalcin, T.; Csizmadia, I. G.; Peterson, M. R.; Harrison, A. G. J. Am. Soc. Mass Spectrom. 1996, 7, 233-242.
- Yu, W.; Vath, J. E.; Huberty, M. C.; Martin, S. A. Anal. Chem. 1993, 65, 3015-3023.
- 60. Roepstorff, P.; Fohlman, J. Biomed. Mass Spectrom. 1984, 11, 601.

- 61. Deery, M. J.; Summerfield, S. G.; Buzy, A.; Jennings, K. R. J. Am. Soc. Mass Spectrom. 1997, 8, 253-261.
- 62. Gonzalez, J.; Besada, V.; Garay, H.; Reyes, O.; Padron, G.; Tambara, Y.; Takao, T.; Shimonishi, Y. J. Mass Spectrom. 1996, 31, 150-158.
- 63. Thorne, G. C.; Ballard, K. D.; Gaskell, S. J. J. Am. Soc. Mass Spectrom. 1990, 1, 249-257.
- 64. Johnson, R. S. *Ph.D. Dissertation*, Massachusetts Institute of Technology, Cambridge, MA, 1988.
- 65. Liao, P.-C.; Huang, Z.-H.; Allison, J. J. Am. Soc. Mass Spectrom. 1997, 8, 501-509.
- 66. Stults, J. T.; Lai, J.; McCune, S.; Wetzel, R. Anal. Chem. 1993, 65, 1703-1708.
- Watson, J. T.; Wagner, D. S.; Chang, Y. S.; Strahler, J. R.; Hanash, S. M.; Gage, D.
 A. Int. J. Mass Spectrom. Ion Processes. 1991, 111, 191-209.
- 68. Lin, T.; Glish, G. L. Proceedings of the 45th ASMS Conference on Mass Spectrometry and Allied Topics, Palm Springs, California, June 1-5, 1997.
- 69. Zaia, J.; Biemann, K. J. Am. Soc. Mass Spectrom. 1995, 6, 428-436.
- Wagner, D. S.; Salari, A.; Gage, D. A.; Leykam, J.; Fetter, J.; Hollingsworth, R.;
 Watson, J. T. Biol. Mass Spectrom. 1991, 20, 419-425.
- 71. Bunk, D. M.; Macfarlane, R. D. Int. J. Mass Spectrom. Ion Processes. 1991, 111, 55-75.
- 72. Bunk, D. M.; Macfarlane, R. D. Int. J. Mass Spectrom. Ion Processes. 1993, 126, 123-136.

- 73. Cárdenas, M. S.; van der Heeft, E.; de Jong, A. P. J. M. Rapid. Commun. Mass Spectrom. 1997, 11, 1271-1278.
- 74. Griffiths, W. J.; Lindh, I.; Bergman, T.; Sjövall, J. Rapid Commun. Mass Spectrom. 1995, 9, 667-676.
- 75. Lindh, I.; Griffiths, W. J.; Bergman, T.; Sjövall, J. Int. J. Mass Spectrom. Ion Processes 1997, 164, 71-79.
- 76. Sadagopan, N.; Wu, J.; Yang, Y.; Huang, Z.-H.; Watson, J. T. Proceedings of the 45th ASMS Conference on Mass Spectrometry and Allied Topics, Palm Springs, California, June 1-5, 1997.
- 77. Stults, J. T. Proceedings of the 40th ASMS Conference on Mass Spectrometry and Allied Topics, Washington, DC, May 31-June 5, **1992**.
- 78. Bartlet-Jones, M.; Jeffery, W. A.; Hansen, H. F.; Pappin, D. J. C. Rapid Commun.

 Mass Spectrom. 1994, 8, 737-742.
- 79. Hines, W.; Peltier, J.; Hsieh, F.; Martin, S.A. Proceedings of the 43rd ASMS Conference on Mass Spectrometry and Allied Topics, Atlanta, Georgia, May 21-26, 1995.
- 80. Huang, Z.-H.; Wu, J.; Gage, D. A.; Watson, J. T. Proceedings of the 45th ASMS

 Conference on Mass Spectrometry and Allied Topics, Palm Springs, California, June
 1-5, 1997.
- 81. Huang, Z.-H.; Wu, J.; Roth, K. D. W.; Yang, Y.; Gage, D. A.; Watson, J. T. Anal. Chem. 1997, 69, 137-144.
- 82. Liao, P.-C.; Allison, J. J. Mass Spectrom. 1995, 30, 511-512.

- 83. Naven, T. J. P.; Jeffery, W. A.; Bartlet-Jones, M.; Rahman, D.; Pappin, D. J. C. Proceedings of the 45th ASMS Conference on Mass Spectrometry and Allied Topics, Palm Springs, California, June 1-5, 1997.
- Spengler, B.; Luetzenkirchen, F.; Metzger, S.; Chaurand, P.; Kaufmann, R.; Jeffery,
 W.; Bartlet-Jones, M.; Pappin, D. J. C. Int. J. Mass Spectrom. Ion Processes. 1997,
 169/170, 127-140.
- 85. Strahler, J. R.; Smelyanskiy, Y.; Lavine, G.; Allison, J. Int. J. Mass Spectrom. Ion Processes 1997, 169/170, 111-126.
- 86. Kidwell, D. A.; Ross, M. M.; Colton, R. J. J. Am. Chem. Soc. 1984, 106, 2219-2220.
- 87. Kidwell, D. A.; Ross, M. M.; Colton, R. J. Springer Ser. Chem. Phys.: SIMS 4, 1984, 36, 412-414.
- 88. Stults, J. T.; Halualani, R.; Wetzel, R. Proceedings of the 37th ASMS Conference on Mass Spectrometry and Allied Topics, Miami Beach, Florida, May 21-26, 1989.
- 89. Wetzel, R.; Halualani, R.; Stults, J. T.; Quan, C. *Bioconjugate Chem.* 1990, 1, 114-122.
- 90. Vath, J. E.; Biemann, K. Int. J. Mass Spectrom. Ion Processes. 1990, 100, 287-299.
- 91. Chang, Y. S.; Gage, D. A.; Watson, J. T. Biol. Mass Spectrom. 1993, 22, 176-180.
- 92. Wagner, D. S.; Nieuwenhuis, T. J.; Chang, Y. S.; Gage, D. A.; Watson, J. T. Proceedings of the 40th ASMS Conference on Mass Spectrometry and Allied Topics, Washington, DC, May 31-June 5, 1992.
- 93. Renner, D.; Spiteller, G. Angew. Chem. Int. Ed. Engl. 1985, 24, 408-409.

- 94. Sherman, N. E.; Yates, N. A.; Shabanowitz, J.; Hunt, D. F.; Jeffery, W.; Bartlet-Jones, M.; Pappin, D. J. C. Proceedings of the 43rd ASMS Conference on Mass Spectrometry and Allied Topics, Atlanta, Georgia, May 21-26, 1995.
- 95. Bennett, B. D.; Day, R. A. Proceedings of the 35th ASMS Conference on Mass Spectrometry and Allied Topics, Denver, Colorado, May 24-29, 1987.
- 96. Vath, J. E.; Zollinger, M.; Biemann, K. Fresenius Z. Anal. Chem. 1988, 331, 248-252.
- 97. Hirayama, K.; Akashi, S.; Yuji, R.; Niitsu, U.; Fujimoto, Y. Organic Mass Spectrom. 1993, 28, 1516-1524.
- 98. Kiplinger, J. P.; Contillo, L.; Hendrick, W. L.; Grodski, A. Rapid Commun. Mass Spectrom. 1992, 6, 747-752.
- 99. Lindh, I.; Griffiths, W. J.; Bergman, T.; Sjövall, J. Rapid Commun. Mass Spectrom. 1994, 8, 797-803.

CHAPTER 2

STUDIES OF TRIS(2,4,6-TRIMETHOXYPHENYL)PHOSPHONIUM-ACETYL (TMPP*-AC) DERIVATIZATION FOR PEPTIDE SEQUENCING BY MASS SPECTROMETRY

I. Introduction

The tris(2,4,6-trimethoxyphenyl)phosphonium (TMPP*-Ac) reagents were developed to overcome some of the limitations of the triphenylphosphonium (TPP) reagents. The structures of the TMPP*-Ac reagents are shown in Figure 2.1B. The TMPP head group is more polar than the TPP head group. As a result, the TMPP*-Ac reagents have a greater water solubility than the TPP reagents. This allows reactions to be performed in aqueous solutions. Generally, peptides have much higher solubility in water than in the nonaqueous solvents sometimes used for TPP derivatization reactions. Derivatization in aqueous solution also allows control of the reaction pH to provide more selective reactions. The general fragmentation characteristics of TMPP*-Ac-derivatized peptides are described in this chapter. Also, this chapter explores the reaction yields and selectivity of the TMPP*-Ac reagents. Finally, the ionization efficiency and signal suppression effects of TMPP*-Ac derivatives are discussed.

II. Experimental

A. Preparation of TMPP⁺-Ac-Succinimide Bromide ([TMPP⁺-Ac-OSu][Br⁻])

The TMPP⁺-Ac-succinimide reagent was prepared using a two-step synthesis as shown in Figure 2.1. Preparation of the bromacetic acid ester is shown in Figure 2.1A.

A) Br-CH₂-C-Br + H-Y
$$Y = S-C_6F_5 \text{ or } O-N$$
Br-CH₂-C-Y + H-Br

B)
$$CH_3O \longrightarrow OCH_3 \longrightarrow O$$

Figure 2.1. Synthesis of TMPP+-Ac reagents.

N-hydroxysuccinimide (3.0 g, 26 mmol) was dissolved in 20 mL warm benzene. Bromoacetyl bromide (2.5 mL, 29 mmol) was added dropwise, and the mixture was refluxed 20 hours in a sand bath at 90 °C with a drying tube attached to exclude moisture. Upon cooling, a white ppt formed. The reaction mixture was filtered and the ppt was recrystallized from benzene. The yield of the bromoacetic acid succinimide ester intermediate was 0.71 g (3.0 mmol, 12%).

Reaction of the intermediate with TMPP to form the TMPP*-Ac reagent is shown in Figure 2.1B. The bromoacetic acid succinimide ester intermediate (1.0 g, 4.4 mmol) was dissolved in 10 mL benzene. A solution of tris(2,4,6-trimethoxyphenyl)phosphine (2.0 g, 3.8 mmol) in 25 mL benzene was added dropwise with stirring. A fine white precipitate formed immediately. A 35 mL aliquot of hexane was added to force remaining product out of solution. The supernatant was removed, and the precipitate was washed twice with 40 mL benzene/hexane (1:3, v:v) and once with 30 mL hexane. After drying overnight in a vacuum dessicator over phosphorous pentoxide and NaOH pellets, the pure product (1.0 g, 34%) was obtained as a fine, white powder. The product was analyzed by positive FAB-MS as shown in Figure 2.2A.

B. Preparation of TMPP+-Ac-S-Pentafluorophenyl Bromide ([TMPP+-Ac-SPf][Br])

TMPP⁺-Ac-S-pentafluorophenyl ([TMPP⁺-Ac-SPf][Br⁻]) was prepared by a twostep synthesis analogous to that described above (1). The FAB-MS spectrum of the TMPP⁺-Ac-SPf reagent is shown in Figure 2.2B.

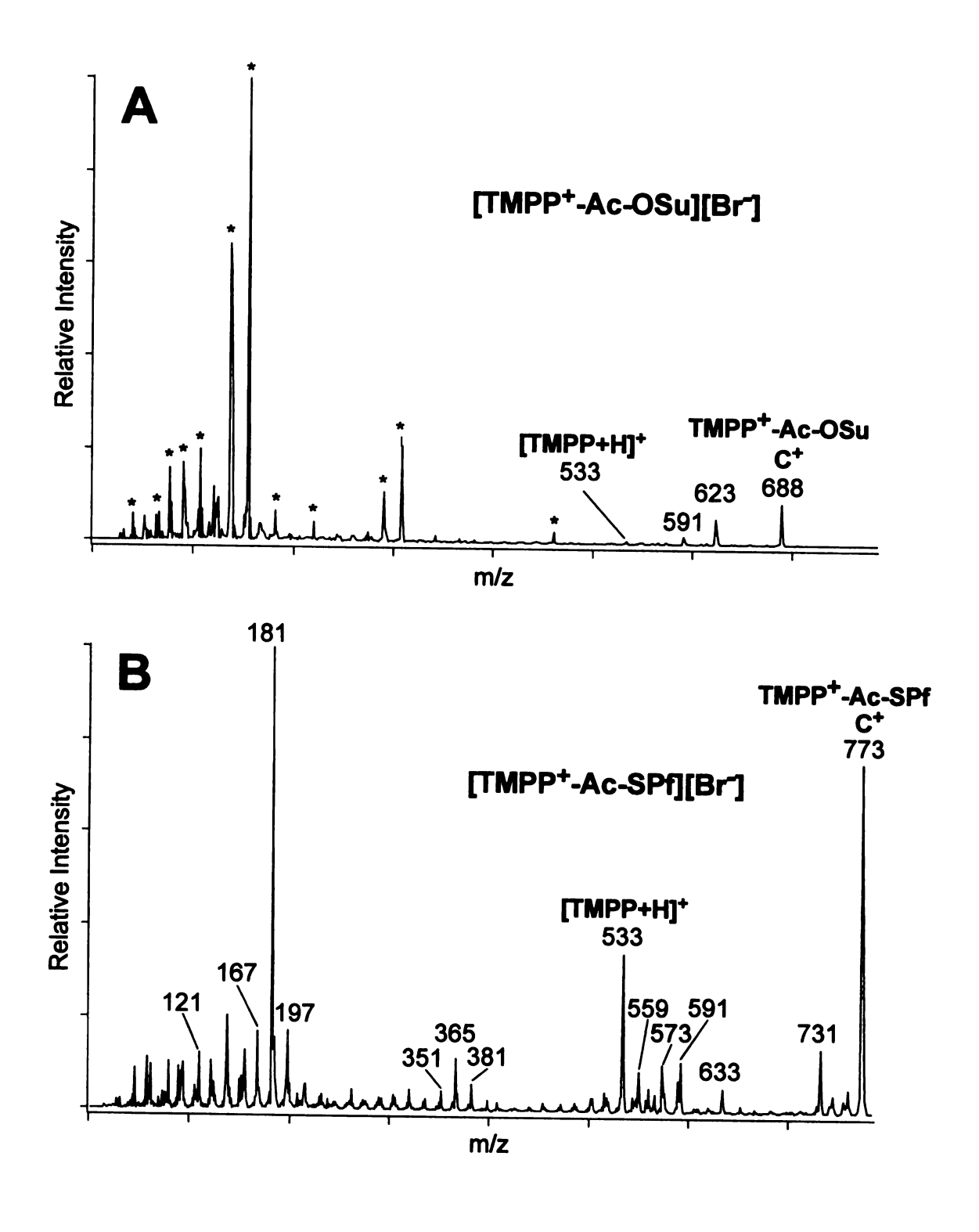


Figure 2.2. FAB-MS spectra of TMPP+-Ac-OSu (A) and TMPP+-Ac-SPf (B).

C. TMPP+-Ac Derivatization of Peptides in Unbuffered Solution

The TMPP⁺-Ac derivatization scheme is shown in Figure 2.3. Peptide derivatives were prepared using the following procedure. 2 nmol of peptide (in 2 μL 10% acetonitrile), 2 μL of 10 mM 4-dimethylaminopyridine in 50% acetonitrile (v/v), and 1 μL of 10 mM [TMPP⁺-Ac-succinimide][Br⁻] in 50% acetonitrile were combined, vortexed for 1 minute, and allowed to stand at room temperature for 30 minutes. For analysis by FAB or MALDI, the reaction mixture was analyzed without any purification. Prior to analysis by ESI, the derivatized peptide was purified by HPLC as described below.

D. TMPP+-Ac Derivatization of Peptides in a Buffered Solution

Peptide derivatives were prepared using the following procedure. Peptide (0.5-10 nmol in 10 μL 10% acetonitrile (v/v)), 2 μL 50 mM TRIZMA (Tris-HCl) buffer (pH 8.3), and 2 μL of 25 mM [TMPP⁺-Ac-succinimide][Br⁻] in 10% acetonitrile were combined. The pH of the reaction mixture was checked and, if necessary, the pH of the reaction mixture was adjusted to pH 8.3 with NaOH solution. The reaction mixture was then vortexed for 1 minute and allowed to stand at room temperature for 30 minutes. No purification was performed prior to analysis by FAB or MALDI. However, purification by HPLC was required prior to analysis by ESI.

E. HPLC Separation

Prior to analysis by ESI-MS or ESI-CAD-MS/MS, the reaction mixture was purified by HPLC. The HPLC system consisted of two Waters Model 6000A pumps

Figure 2.3. TMPP*-Ac derivatization scheme.

controlled by a Waters Millenium data system. Purification was performed on a Phenomenex Jupiter C18 reverse-phase column (5-µm particle size, 4.6 x 250 mm) with the eluant monitored at 215 nm. The mobile phase contained the following: (A) 0.1% TFA, (B) acetonitrile / 0.1% TFA (90:10, v/v). The fraction containing the derivatized peptide was collected and concentrated using a Speed-Vac (Savant Instruments, Farmingdale, NY).

F. Analysis

Fast Atom Bombardment (FAB)

Fast atom bombardment and FAB-CAD-MS/MS spectra were obtained on a double-focusing mass spectrometer (JEOL HX-110, JEOL, Tokyo, Japan). The instrument utilizes a beam of 6-keV xenon atoms and a 10-kV acceleration voltage in the source. The FAB matrix used was thioglycerol/2-hydroxyethyl disulfide (1:1, v/v). One µL of underivatized peptide solution (0.5-2 nmol/µL in 50% acetonitrile) or one µL of derivatized peptide solution (100-500 pmol/µL in 50% acetonitrile) was combined with the matrix for each analysis. For CAD-MS/MS experiments, helium was used as the collision gas, the abundance of the precursor ions was attenuated to 50% for CAD experiments, and 10 scans were averaged to obtain each spectrum. Ions generated by FAB from Ultramark 1621 (PCR Inc., Gainesville, FL) were used for instrument calibration. The data were acquired with a JEOL MS-MP8020D data system.

MALDI

MALDI mass spectra were obtained on a Voyager Elite reflectron time-of-flight mass spectrometer (PerSeptive Biosystems, Inc., Framingham, MA) equipped with a nitrogen laser (337 nm, 3-ns pulse) and delayed extraction. The acceleration voltage used was 20-24 kV and the delay time was 50-100 ns. Data were acquired with the data system provided and based on a transient recorder with 2-ns resolution. The matrix used was α -cyano-4-hydroxycinnamic acid, dissolved in water/acetonitrile (1:1, v/v) to give a saturated solution at room temperature. To prepare the sample, 1 µL of the solution containing the underivatized peptide (at a concentration of 5-10 pmol/uL) or the peptide derivative (at a concentration of 5-10 pmol/μL) was added to 1 μL of the matrix solution and applied to a gold or stainless steel sample plate. The resulting mixture from the derivatization was used directly. The mixture was then allowed to air dry before being introduced into the mass spectrometer. Each spectrum was produced by accumulating data from 256 laser shots. PSD spectra were generated by obtaining several spectra, each optimized for a different range of m/z for the fragment ions. Selected regions of each are stitched together to yield a single PSD mass spectrum. The time-to-mass conversion for PSD was achieved by calibrating with the peak representing the C⁺ cation of the charged derivative to be analyzed and the peak at m/z 379 representing the matrix dimer.

ESI-MS on an Ion Trap Instrument

ESI-CAD-MS/MS analysis was carried out on a quadrupole ion trap instrument (LCQ, Finnigan, San José, CA). Spectra were acquired at a capillary voltage of 4.25 kV, a cone voltage of 28 V, and a capillary temperature of 220 °C. Samples were analyzed by

direct infusion at a flow rate of 3 µL/min, with 20 scans averaged to generate each spectrum. Peptides were diluted to a concentration of 5 pmol/µL in acetonitrile/0.1% formic acid (1:1, v/v). TMPP⁺-Ac-derivatized peptides were diluted to a concentration of 5 pmol/µL in acetonitrile/water (50:50). The singly-charged precursor ions were selected for analysis by MS/MS using a selection window of 3 daltons. Helium was used as the collision gas, and MS/MS spectra were collected over a range of collision energies.

ESI-MS on a Triple Quadrupole Instrument

ESI mass spectra were obtained on a Sciex API 2000 mass spectrometer. Samples were analyzed by direct infusion at a flow rate of 10 μl/min, and 20 scans were averaged to generate each spectrum. Peptides were diluted to a concentration of 50 pmol/μl in acetonitrile/water/formic acid (50:50:0.1). TMPP⁺-Ac-derivatized peptides were diluted to a concentration of approximately 50 pmol/μl in acetonitrile/water (50:50). Nitrogen was used as the collision gas for low-energy CAD experiments.

ESI-In-Source Fragmentation (ISF)-MS

ESI-ISF-MS mass spectra were obtained on a Micromass Platform mass spectrometer. In-source fragmentation, also called nozzle-skimmer dissociation or cone voltage fragmentation, is achieved by raising the cone voltage in order to increase the kinetic energies of analytes. The energetic ions fragment during collisions in the source region. Samples were analyzed by direct infusion at a flow rate of 20 µl/min, and 7 scans were averaged to generate each spectrum. TMPP⁺-Ac-derivatized peptides were diluted

to a concentration of approximately 5 pmol/µl in acetonitrile/water (50:50). Fragmentation was induced by raising the voltage on the cone to the range of 55-100 V.

III. Fragmentation of TMPP+-Ac-derivatized Peptides

A. Fragmentation of the TMPP+-Ac Group

The FAB-CAD-MS/MS spectra of [TMPP⁺-Ac-OSu][Br⁻] (A) and [TMPP⁺-Ac-SPf][Br⁻] (B) are shown in Figure 2.4. The MS/MS spectra contain a number of fragment ions including peaks at m/z 121, 151, 167, 181, 197, 351, 365, 381, 501, 515, 543, 559, 573, and 591. Also, losses of 15, 31, 32, and 46 Da from the molecular cation were observed. Possible assignments of the major peaks in these spectra are shown in Table 2.1. Many of the fragments produced by these reagents are similar to the fragments produced by alkyl triphenylphosphonium salts (2).

TMPP*-Ac-derivatized peptides produce many of the same fragments when analyzed by FAB-CAD-MS/MS, as shown in Figure 2.5A. TMPP*-Ac-derivatized peptides analyzed by MALDI-PSD produce fragments at m/z 181, 351, 365, 381, 501, 559, and 573, as shown in Figure 2.5B. Derivatized peptides analyzed by ESI-CAD-MS/MS in an ion trap produced TMPP*-Ac related peaks at m/z 351, 365, 381, 399, 501, 527, 559, and 573 as shown in Figure 2.6A. Derivatized peptides analyzed by ESI-CAD-MS/MS on a triple quadrupole instrument produced peaks at m/z 559, 570, and 573. The TMPP*-Ac-related peaks produced by derivatized peptides analyzed by ESI-in-source fragmentation-MS were observed at m/z 181, 197, 351, 365, 381, 501, 559, 570, and 573, as shown in Figure 2.6B.

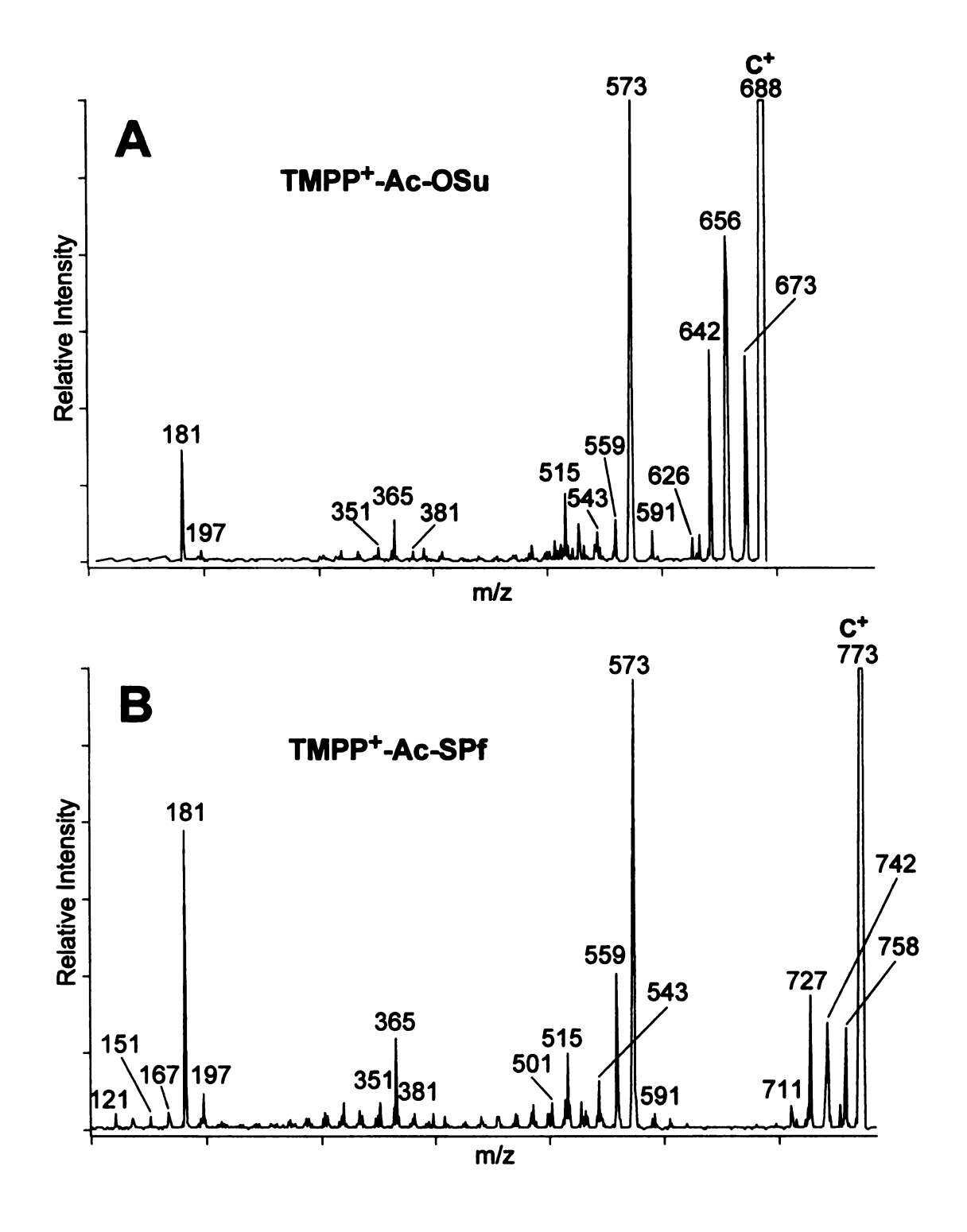


Figure 2.4. FAB-CAD-MS/MS spectra of TMPP*-Ac-OSu (A) and TMPP*-Ac-SPf (B).

Table 2.1. Common TMPP⁺-Ac fragment ions observed in MS/MS spectra.

```
m/z Possible Structure
     121 [(CH<sub>3</sub>O)<sub>2</sub>Ph<sup>+•</sup> -CH<sub>3</sub>]
     136 (CH<sub>3</sub>O)<sub>2</sub>Ph<sup>+</sup>
     151 [(CH<sub>3</sub>O)<sub>3</sub>Ph<sup>+</sup> -O]
167 (CH<sub>3</sub>O)<sub>3</sub>Ph<sup>+</sup>
181 (CH<sub>3</sub>O)<sub>3</sub>Ph-CH<sub>2</sub><sup>+</sup>
    181 (CH<sub>3</sub>O)<sub>3</sub>Ph-CH<sub>2</sub><sup>+</sup>

197 (CH<sub>3</sub>O)<sub>3</sub>Ph-OCH<sub>2</sub><sup>+</sup>

351 [(CH<sub>3</sub>O)<sub>3</sub>Ph]P<sup>+</sup>[(CH<sub>3</sub>O)<sub>2</sub>Ph-OH]

365 [(CH<sub>3</sub>O)<sub>3</sub>Ph]<sub>2</sub>P<sup>+</sup>

381 {[(CH<sub>3</sub>O)<sub>3</sub>Ph]<sub>2</sub>P + O}<sup>+</sup>

501 [TMPP - OCH<sub>3</sub>]<sup>+</sup>•

533 [TMPP + H]<sup>+</sup>
     543 [TMPP<sup>+</sup>-CH=C=O - 2(CH<sub>3</sub>)]
     559 TMPP<sup>+</sup>-CH=CH<sub>2</sub>
     573 TMPP<sup>+</sup>-CH=C=O
     590 TMPP<sup>+</sup>-CH<sub>2</sub>-CO-NH<sub>2</sub>
591 TMPP<sup>+</sup>-CH<sub>2</sub>-CO-OH C<sup>+</sup> - 62 [C - 2(OCH<sub>3</sub>)]<sup>+</sup>
C<sup>+</sup> - 46 [C - OCH<sub>3</sub> -CH<sub>3</sub>]<sup>+</sup>
C<sup>+</sup> - 32 [C - CH<sub>3</sub>OH]<sup>+</sup>
C<sup>+</sup> - 31 [C - OCH<sub>3</sub>]<sup>+</sup>
C<sup>+</sup> - 15 [C - CH<sub>3</sub>]<sup>+</sup>•
```

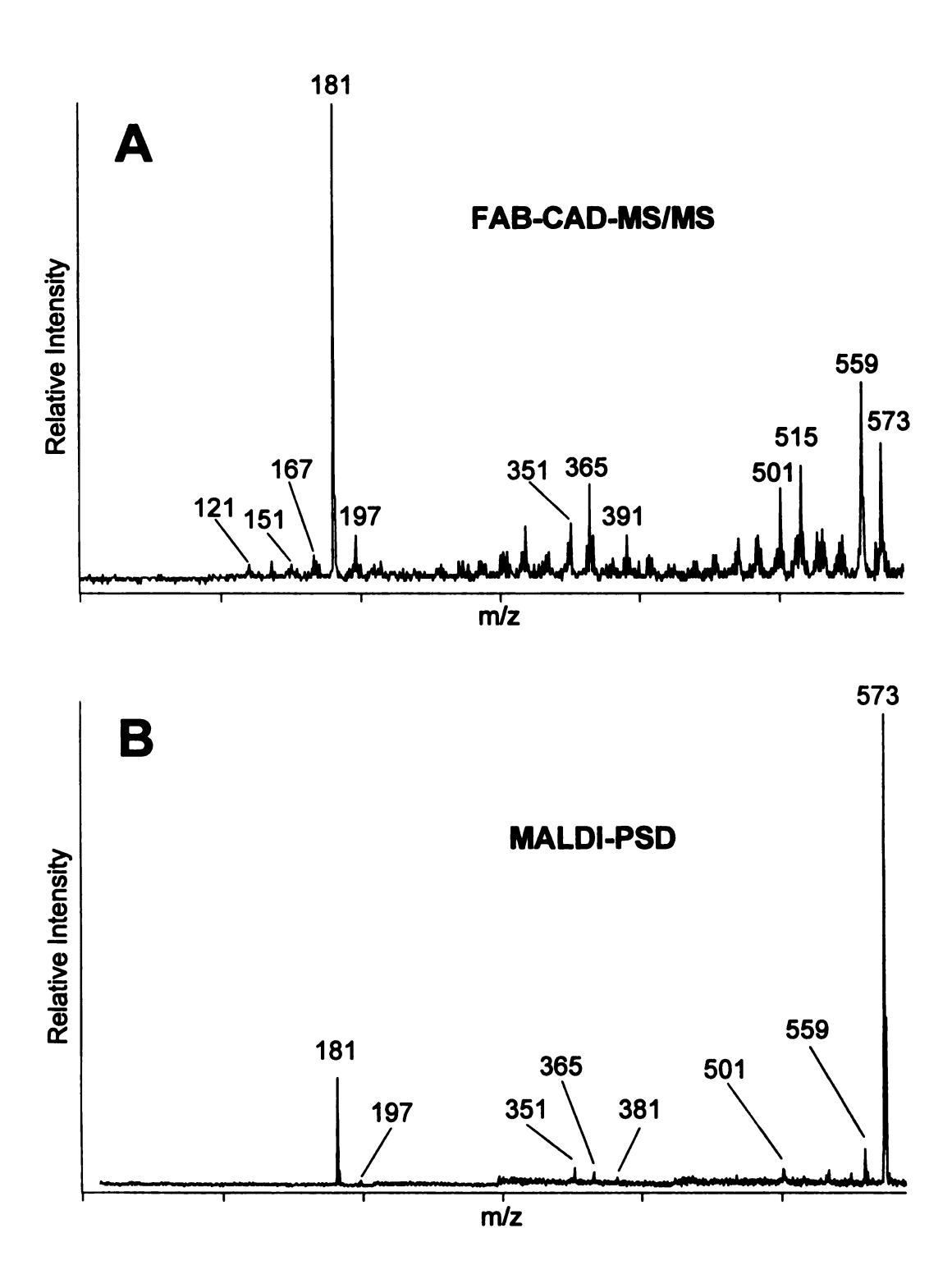


Figure 2.5. Low mass fragments of TMPP⁺-Ac-derivatized peptides analyzed by FAB-CAD-MS/MS (A) and MALDI-PSD (B).

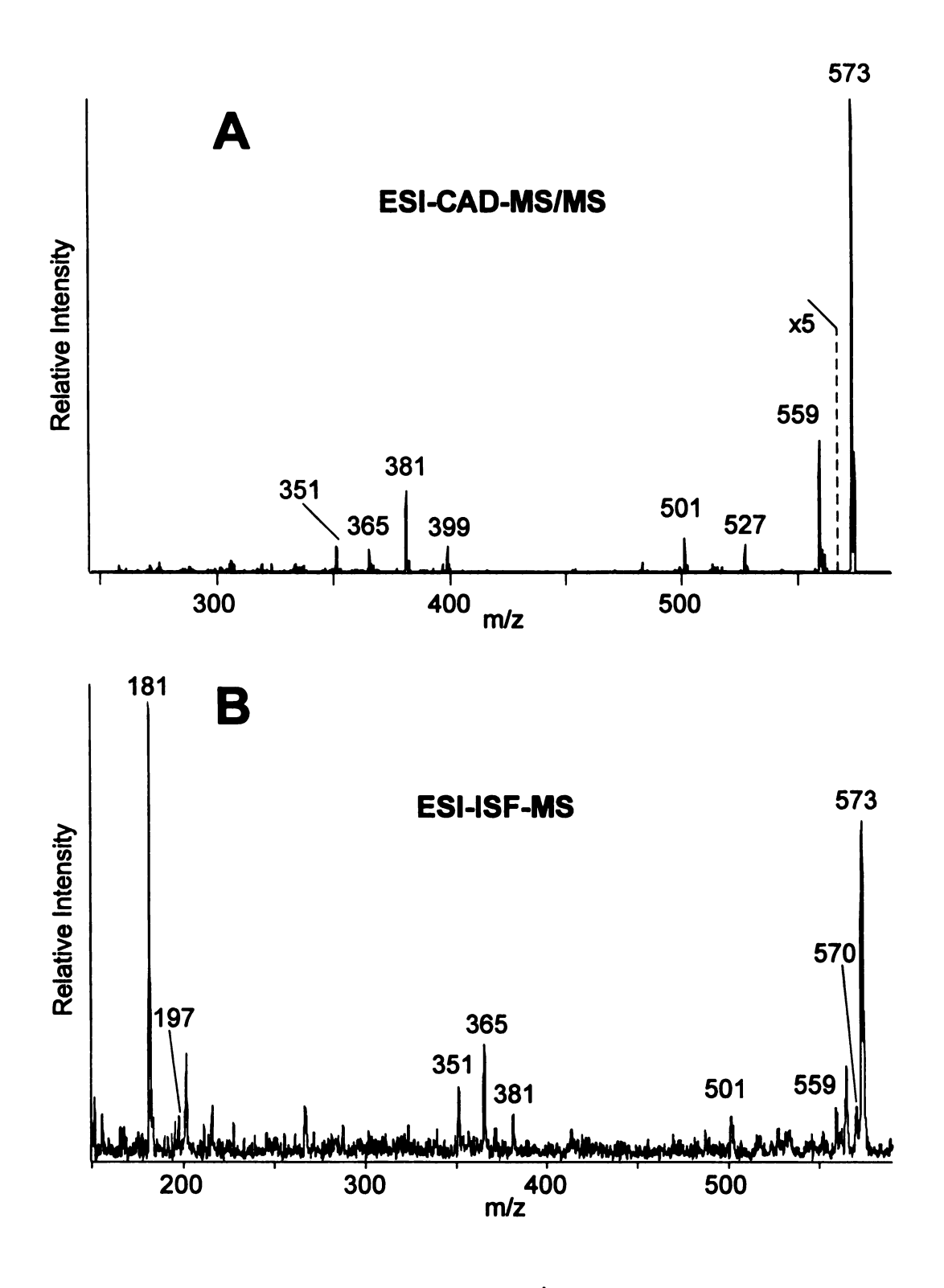


Figure 2.6. Low mass fragments of TMPP⁺-Ac-derivatized peptides analyzed by ESI-CAD-MS/MS on an ion trap (A) and ESI-ISF-MS (B).

B. Se

F

50¦U

ahu

ami

đe:

Ma bu

Sil

[a

•

B. Sequence-specific Fragmentation of TMPP*-Ac-derivatized Peptides by FAB-CAD-MS/MS

Twenty peptides were derivatized using [TMPP+Ac-OSu][Br] in unbuffered solutions and analyzed by FAB-CAD-MS/MS as described above. The effects of the amino acid residue at the n^{th} position on the intensity of the a_n , b_n , c_{n-1} , and d_n ion abundances were studied. The nomenclature used here for the fragment ions of chargederivatized peptides corresponds to the nomenclature of protonated peptides when the mass shift (due to derivatization) in (singly-charged) precursor ions is taken into account, but an asterisk is added to denote the presence of the derivative moiety. The possible structures of these ions are described in Chapter 1. The average signal-to-background ratios (S/B) of the $*a_n$, $*b_n$, $*c_{n-1}$, and $*d_n$ peaks for each type of amino acid residue are shown in Table 2.2. The average S/B ratios are grouped into five different categories. An average S/B of ≤ 1 , was designated with "-" to denote that the ion was not observed. If the ion had an average S/B of > 1 and \leq 2, it was denoted with a "vw" to show that the average abundance was very weak. Although it can be argued that peaks with very weak abundances are the product of random noise, this category was included because the fragment ions were sometimes clearly observed and sometimes not observed. Fragment peaks with an average S/B of > 2 and ≤ 4 were designated "w" for weak; those with an average S/B of > 4 and ≤ 10 were designated "m" for medium; and those with an average S/B of > 10 were designated "s" for strong.

The $*a_n$ ions were observed for every type of amino acid residue. Residues with aromatic side-chains (His, Phe, Trp, and Tyr) produced strong $*a_n$ ions, whereas glycine residues produced weak $*a_n$ ions. The lower abundance of $*a_n$ ions produced from

Table 2.2. Intensities of fragment ions from TMPP⁺-Acderivatized peptides as a function of amino acid residue.

Residue	*a _n	*b _n	*C _{n-1}	*d _n
Ala	m	-	-	-
Arg	m	-	W	m
Asn	m	-	W	m
Asp	m	m	W	m
Cys	m	-	W	m
Gln	m	-	-	m
Glu	m	-	-	m
Gly	W	-	-	-
His	S	-	-	-
lle	m	-	-	m(d), w(d')
Leu	m	-	-	m
Lys	m	-	W	m
Met	m	-	-	m
Phe	S	-	-	vw
Pro	m	-	-	-
Ser	m	-	m	m
Thr	m	-	m	m(d), w(d')
Trp	S	-	-	vw
Tyr	S	-	-	vw
Val	S	-	-	m

(s = S/B > 10, m = S/B 4-10, w = S/B 2-4, vw = S/B 1-2)

glycine residues suggests that $*a_n$ ions may form most readily when there is a hydrogen atom on the β -carbon available for transfer, as shown in Figure 2.7. According to this mechanism, the formation of $*a_n$ fragments at glycine could not occur because glycine has no β -carbon atom on its side-chain. As a result, formation of $*a_n$ ions at glycine would have to go through a less favorable mechanism, resulting in a decrease in the $*a_n$ ion abundance. As a result of deuterium-labeling experiments on charged derivatives, Wagner (3) also concluded that the preferred mechanism for $*a_n$ ion formation during FAB-CAD-MS/MS involves transfer of a hydrogen from the β -carbon. However, TMPP⁺-Ac derivatives analyzed by MALDI-PSD were found to generate abundant $*a_n$ ions for all amino acid residues except for proline, which lacks an amide hydrogen (4). This suggests that different fragmentation mechanisms may predominate for charged derivatives analyzed by FAB-CAD-MS/MS and those analyzed by MALDI-PSD.

The only ${}^*\mathbf{b_n}$ ions observed occurred when an aspartate residue was present at the $\mathbf{n^{th}}$ position. The proposed mechanism for ${}^*\mathbf{b_n}$ formation from derivatized aspartyl peptides is discussed in detail in Chapter 3. The formation of ${}^*\mathbf{c_{n-1}}$ ions was only observed when selected residues were present at the $\mathbf{n^{th}}$ position. The most abundant ${}^*\mathbf{c_{n-1}}$ fragment ions were observed from fragmentation preceeding serine or threonine. Less abundant ${}^*\mathbf{c_{n-1}}$ fragments were observed when arginine, asparagine, aspartatate, cysteine, or lysine were present at the $\mathbf{n^{th}}$ position. These findings agree well with sequence dependence observed by Downard and Biemann (5) for $\mathbf{c_{n-1}}$ fragment ions produced from underivatized peptides.

The formation of $*d_n$ fragment ions was observed for most amino acid residues. However, no $*d_n$ fragments were observed for residues lacking a β -carbon on the

Scheme 2.7. Formation of $*a_n$ ions involving transfer of hydrogen from the β -carbon.

side-chain (alanine, glycine, and proline), and the average S/B ratios for residues with aromatic side-chains (histidine, phenylalanine, tryptophan, and tyrosine) were very weak or not observed at all. Likewise, underivatized peptides generally do not produce \mathbf{d}_n fragment ions resulting from the loss of aromatic side-chains (6, 7). The low abundance of \mathbf{d}_n and \mathbf{d}_n fragment ions probably results from the stability of the β - γ bond for peptides with aromatic side-chains. It is interesting to note that the aromatic residues form \mathbf{a}_n ions with increased S/B ratios and \mathbf{d}_n ions with decreased S/B ratios. Apparently, the reduced ability to form \mathbf{d}_n ions allows the formation of more abundant \mathbf{a}_n ions.

In addition to the fragment ions described above, TMPP*-Ac-derivatized peptides were observed to form fragment ions of 14, 30, and 46 daltons less than the masses of *a_n ions, as shown in Figure 2.8. Note the fragment ions peaks near the *a₁ and *a₂ peaks. For simplicity, these ions will be called *a_n-14, *a_n-30, and *a_n-46 ions. These fragment ions were most commonly observed near *a_n ions produced from cleavage at an aromatic residue. In order to investigate the origin of these fragment ions, the peptide osteocalcin fragment (45-49) (FYGPV) was derivatized and incubated in D₂O overnight to allow deuteration of the exchangeable hydrogen atoms. The FAB-CAD-MS/MS spectrum of the deuterated peptide contained the same *a_n-14, *a_n-30, and *a_n-46 ions, although the masses were shifted by the presence of deuterium atoms. This result demonstrates that the exchangeable hydrogen atoms on the peptide backbone are not lost in the formation of *a_n-14, *a_n-30, and *a_n-46 ions. Osteocalcin fragment (45-49) was then derivatized using vinyltriphenylphosphonium according the procedure of Wagner *et al.* (8) to generate the N-terminal triphenylphosphonium-acetyl (TPP-Ac) derivative. The *a_n-14,

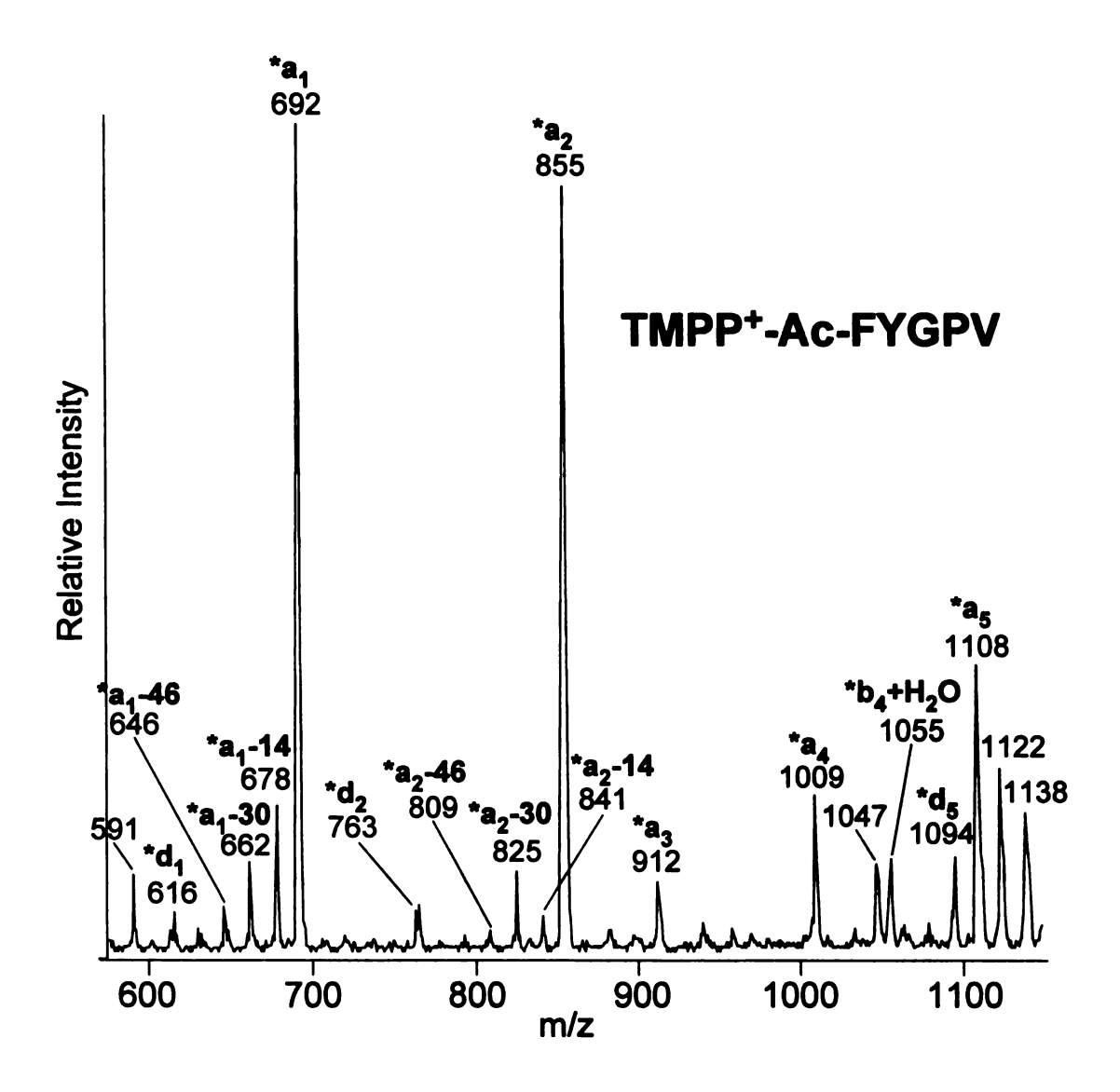


Figure 2.8. FAB-CAD-MS/MS spectra of TMPP⁺-Ac-osteocalcin fragment (45-49), C^+ = 1154, showing * a_n -14, * a_n -30, and * a_n -46 peaks.

* $\mathbf{a_n}$ -30, and * $\mathbf{a_n}$ -46 fragment ions were not observed in the FAB-CAD-MS/MS spectrum of this derivative. This result suggests that the formation of * $\mathbf{a_n}$ -14, * $\mathbf{a_n}$ -30, and * $\mathbf{a_n}$ -46 fragment ions is related to losses from the TMPP⁺ head group. The abundances of these fragment ions are roughly proportional to the abundance of the neighboring * $\mathbf{a_n}$ ion. As a result, they are more readily observed in the vicinity of aromatic * $\mathbf{a_n}$ ions because aromatic residues produce the most abundant * $\mathbf{a_n}$ ions, as discussed above.

Figure 2.9 provides a possible rationalization for the formation of $*a_n-14$, $*a_n-30$, and $*a_n$ -46 ions. The $*a_n$ -14 ion could possibly be formed by the net loss of 14 daltons from the TMPP head group combined with $*a_n$ fragmentation. However, the formation of this fragment must involve a rearrangement of some type, because the loss of a CH₂ neutral is not reasonable. The $*a_n$ -30 ion could possibly be formed by the loss of an O=CH₂ neutral from the TMPP head group combined with *a_n fragmentation. The *a_n-46 ion could be formed by loss of CH₃-O-CH₃ from the head group combined with *a_n fragmentation. FAB-CAD-MS/MS spectra of the *a_n fragment ions produced in the FAB-MS spectrum of TMPP⁺-Ac-osteocalcin fragment (45-49) contain abundant *a_n-46 ions and less abundant $*a_n$ -14 and $*a_n$ -30 ions. This observation suggests that $*a_n$ -46 ions may form directly from $*a_n$ ions, but that $*a_{n-1}4$ and $*a_{n-3}0$ ions may from other precursors. The formation of $*a_n-14$, $*a_n-30$, and $*a_n-46$ ions has not been observed in the spectra of TMPP⁺-Ac-derivatized peptides analyzed by MALDI-PSD, ESI-CAD-MS/MS, or ESI-ISF-MS. The formation of these fragment ions appears to be limited to high-energy CAD.

Loss of 14 Da OCH₃ R

$$CH_3O$$
 OCH_3 R

 CH_3O
 OCH_3 R

 OCH_3 P

 OCH_3 R

 OCH_3 P

 OCH_3 R

 OCH_3 R

Figure 2.9. Possible rationalization for losses of 14, 30, and 46 Da from TMPP*-Ac derivatives.

C. Sequence-specific Fragmentation of TMPP*-Ac-derivatized Peptides by MALDI-PSD, ESI-CAD-MS/MS, and ESI-ISF-MS

Although the sequence-specific fragmentation of TMPP*-Ac-derivatized peptides during analysis by MALDI-PSD, ESI-CAD-MS/MS, and ESI-ISF-MS was not studied as systematically as fragmentation during analysis by FAB-CAD-MS/MS, several trends were observed. Similar to observations in FAB-CAD-MS/MS, the most prominent fragment ions produced during analysis by MALDI-PSD are the *an ions. However, in contrast to FAB-CAD-MS/MS, the *dn and *cn-1 fragments ions are not usually observed during MALDI-PSD analysis. Notable exceptions to these trends occur when the derivatized peptide contains an aspartate residue. When an aspartate residue is present at the nth position, no *an ions are observed. Instead, *cn-1, *dn, and *bn fragment ions are observed. The formation of these fragmentation ions is discussed further in Chapter 3. In addition, *bn+H2O fragment ions arising from the penultimate residue are frequently observed in the MALDI-PSD spectra of TMPP*-Ac-derivatized peptides when the C-terminal residue is basic (arginine or lysine).

Both $*a_n$ and $*b_n$ ion series are observed in the ESI-CAD-MS/MS and ESI-ISF-MS spectra of charge-derivatized peptides. In addition, losses of H_2O and NH_3 from $*a_n$ and $*b_n$ ions are commonly observed. Similar to MALDI-PSD spectra, the presence of aspartate at the n^{th} position of a TMPP⁺-Ac-derivatized peptide produces $*c_{n-1}$, $*d_n$, and more intense $*b_n$ ions. Also, $*d_n$ ions are sometimes observed when glutamate is present at the n^{th} position. The presence of $*b_n+H_2O$ ions at the penultimate position is observed when a basic residue is present at the C-terminal position. In addition, a series of $*b_n+H_2O$ fragment ions is observed in the ESI-CAD-MS/MS spectra of TMPP⁺-Ac-

derivatized peptides analyzed on an ion trap instrument. These fragment ions are proposed to form by sequential loss of the C-terminal residue (9).

IV. Preparation of a Weighable TMPP+-Ac Derivative Standard

In the past, determination of reaction yields of the TMPP*-Ac derivative were based on HPLC peak areas or the intensities of mass spectral peaks because no standard was available for the TMPP*-Ac derivative. As a result, it was necessary to assume that the response of the TMPP*-Ac-derivatized peptide was similar to that of the underivatized peptide in order to estimate yields. In order to avoid this assumption, a weighable amount of purified derivative was prepared. This standard allows the reaction yields to be corrected for differences in the response of the underivatized peptide and the TMPP*-Ac-derivatized peptide. Also, the use of a standard allows the study of ionization efficiency and signal suppression for the underivatized and derivatized peptide.

To prepare the standard, 700 nanomoles of buccalin (GMDSLAFSGGL-NH₂, MW = 1053.3 g/mol) were charge-derivatized in an unbuffered solution by the procedure described above. The reaction mixture was separated by HPLC using the following gradient: 25-40% B in 12 minutes, hold at 40% B for 18 minutes, 40-60% B in 15 minutes, hold at 60% B for 10 minutes. The resulting HPLC chromatogram is shown in Figure 2.10A. Note the buccalin peak at a retention time of 9.9 minutes and the TMPP⁺-Ac-buccalin peak at a retention time of 34.3 minutes. The TMPP⁺-Ac-buccalin fractions were collected, combined, and dried on a Speed-Vac. A total of 0.72 mg of the TMPP⁺-Ac-buccalin standard was obtained. The molecular weight of the TMPP⁺-Ac-buccalin cation is 1626.8 g/mol. Assuming the product is present in the form of the

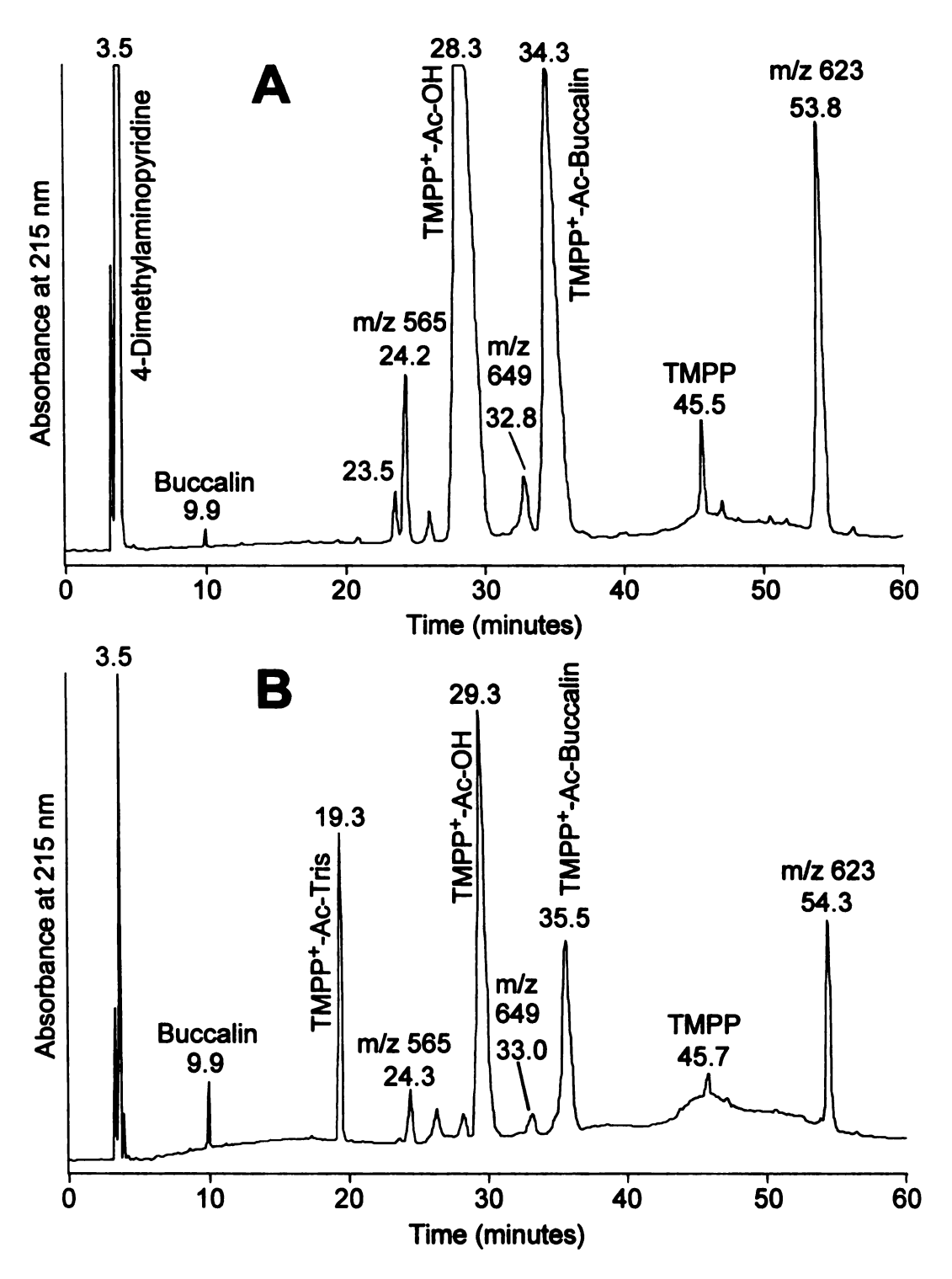


Figure 2.10. HPLC chromatograms of TMPP⁺-Ac-OSu + buccalin reaction mixtures performed in unbuffered (A) and buffered (B) solutions.

trifluoroacetate salt, the formula weight of the salt would be 1739.8 g/mol and the product would correspond to 410 nmoles of the derivative.

V. Reaction Yields and Selectivity

Reaction Yields in Buffered and Unbuffered Solutions

Any chemistry for the derivatization of the peptide N-terminus has the potential to derivatize the side-chains of lysine residues and possibly the side-chains of other residues. The unwanted derivatization of lysine side-chains has been reported by several authors (10-13). The derivatization of cysteine side-chains has been observed by Stults *et al.* (14) and Wetzel *et al.* (15). Tyrosine side-chain derivatization was reported by Cárdenas *et al.* (10) and Kiplinger *et al.* (13). Careful regulation of the pH of the reaction mixture has been reported as a means for selective derivatization of the N-terminus in the presence of lysine (14, 15).

The chemistry originally proposed for the TMPP*-Ac derivatization used 4-dimethylaminopyridine as a basic catalyst (1). This reaction mixture is unbuffered, but measurements with a pH electrode give a reading of approximately 9. The use of pH 8.2 phosphate buffer or Tris-HCl buffer has been reported as a means to selectively derivatize the peptide N-terminus (16). The charge-derivatization of buccalin (GMDSLAFSGGL-NH₂) was studied in an unbuffered reaction mixture and in a reaction mixture buffered to pH 8.3 with a Tris-HCl buffer in order to determine reaction yields. The HPLC separation of the reaction mixtures was performed using the gradient described in the previous section. The HPLC fractions were collected and analyzed by

MALDI-MS. Underivatized buccalin and the TMPP⁺-Ac-buccalin standard were analyzed separately to determine the response of each species at 215 nm.

The HPLC chromatograms for the unbuffered and buffered reaction mixtures are presented in Figure 2.10. Note the peak areas of the buccalin peaks (retention time = 9.9 minutes) and the TMPP+-Ac-buccalin peaks (retention times = 34.3 and 35.5 minutes). Based on peak areas, the unbuffered reaction (A) had a yield of approximately 99.5%. The derivatized peptide had a chromatographic peak area that was approximately 3 times as large as an equal amount of the underivatized peptide. Based on the standards, the unbuffered reaction had a yield of approximately 98.5% of the derivative. The buffered reaction (B) had a yield of approximately 93% based on peak areas and a yield of 80% based on the standards.

B. TMPP+-Ac Derivatization of Lysine

It should be possible to selectively derivatize the peptide N-terminus in the presence of the lysine by exploiting the pK_a differences between the N-terminus (about 8.0) and the lysine side-chain (about 10.5) (17, 18). The extent of charge-derivatization of lysine side-chains was studied using the peptide Ala-D-γ-Glu-Lys-D-Ala-D-Ala. The peptide was derivatized using [TMPP⁺-Ac-OSu][Br⁻] in an unbuffered solution and in a pH 8.3 Tris-HCl buffer. The reaction mixture was separated by HPLC using the following method: 1-25% B in 10 minutes, 25-45% B in 13.3 minutes, hold at 45% B for 6.7 minutes, 45-75% B in 40 minutes. The HPLC fractions were collected and analyzed by MALDI-MS. The chromatograms and peak identities are shown in Figure 2.11. Note the peak areas of the underivatized peptide (RT = 8.9 min), the N-terminal derivative

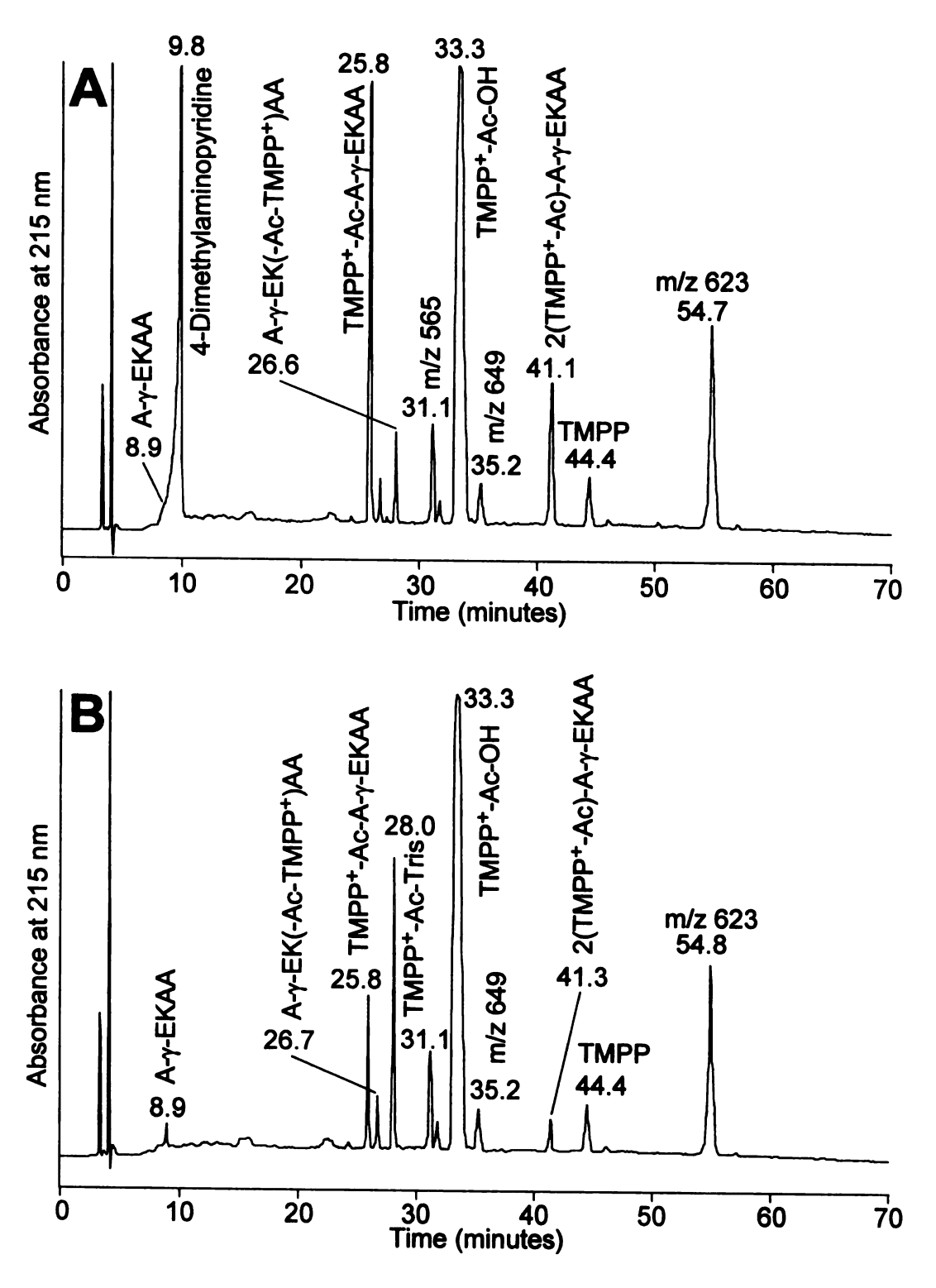


Figure 2.11. HPLC chromatograms of TMPP⁺-Ac-OSu + A-γ-EKAA reaction mixtures performed in unbuffered (A) and buffered (B) solutions.

(RT = 25.8 min), the lysine side-chain derivative (RT \approx 26.6 min), and the doubly-derivatized peak (RT \approx 41.2 min). The 4-dimethylaminopyridine used in the unbuffered solution elutes at a retention time of 9.8 minutes, overlapping with the peak from the underivatized peptide, as shown in Figure 2.11A. This peak was collected and separated with a different gradient to separate the two components. The MALDI-PSD spectra of the purified peptide derivatives are shown in Figure 2.12. Note the absence of $*a_1$, $*b_1$, $*b_1+H_2O$, $*a_2$, $*b_2$, and $*c_2$ peaks in the spectrum of the side-chain derivative (B). Also, there is a $*y_3$ peak in the spectrum representing cleavage at the N-terminal side of the derivatized lysine residue.

Based on the HPLC peak areas of the purified products, the unbuffered reaction mixture contained approximately 1% of the unreacted peptide, 61% of the N-terminal derivative, 5% of the lysine side-chain derivative, and 33% of the doubly-derivatized product, as shown in Figure 2.11A. When the derivatization was performed in a pH 8.3 Tris-HCl buffer, the reaction mixture contained approximately 9% of the unreacted peptide, 54% of the N-terminal derivative, 19% of the lysine side-chain derivative, and 18% of the doubly-derivatized product, as shown in Figure 2.11B. The actual molar percentage of the underivatized peptide should be greater than that determined by HPLC peak areas because the underivatized peptide should have a lower molar absorptivity than the derivatized peptide due to the absence of the TMPP*-Ac group. Based on the peak area of a standard, the molar percentage of the underivatized peptide was 5% for the unbuffered reaction mixture and 37% for the buffered reaction mixture, as shown in Figure 2.11B. Also, the molar percentage of the doubly-derivatized product should be less than that determined by HPLC because the doubly-derivatized product should have a

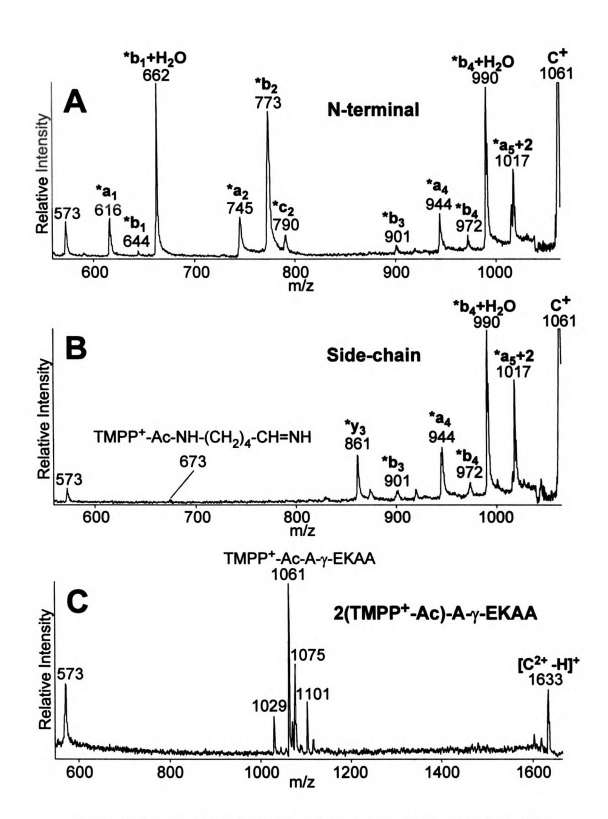


Figure 2.12. MALDI-PSD spectra of N-terminal (A), side-chain (B), and doubly-derivatized (C) A-γ-EKAA.

larger molar absorptivity due to the presence of a second TMPP⁺-Ac group. Based on this data, the only advantage of the buffered solution was a reduction in the amount of the doubly-derivatized product.

C. TMPP⁺-Ac Derivatization of Cysteine

The extent of cysteine side-chain derivatization was studied using the peptide glutathione (γ-Glu-Cys-Gly). The peptide was derivatized using [TMPP⁺-Ac-OSu][Br⁻] in an unbuffered solution and in a pH 8.3 Tris-HCl buffer. The reaction mixture was separated by HPLC using the following gradient: 25-45% B in 13.3 minutes, hold at 45% B for 6.7 minutes, 45-75% B in 40 minutes. The HPLC fractions were collected and analyzed by MALDI-MS and ESI-MS. The chromatogram and peak identities are shown in Figure 2.13A. Note the peak areas of the N-terminal derivative (RT \approx 16.6 min), the cysteine side-chain derivative (RT ≈ 17.8 min), and the doubly-derivatized product (RT ≈ 35.4 min). The peak representing the N-terminal derivative (RT \approx 16.6 min) was broad, presumably as a result of the free cysteine group. Based on the HPLC peak areas, the unbuffered reaction mixture produced approximately 10% of the N-terminal derivative, 24% of the cysteine side-chain derivative, and 66% of the doubly-derivatized product, as shown in Figure 2.13A. The amount of unreacted peptide was not determined because the peptide eluted with the solvent front. The molar percent composition of the doublyderivatized product should be less than that determined by peak areas because it would be expected to have a larger molar absorptivity than the single-derivatized products. When the derivatization was performed in a pH 8.3 Tris-HCl buffer, the product had the following composition based on peak areas: 1% of the N-terminal derivative, 85% of the

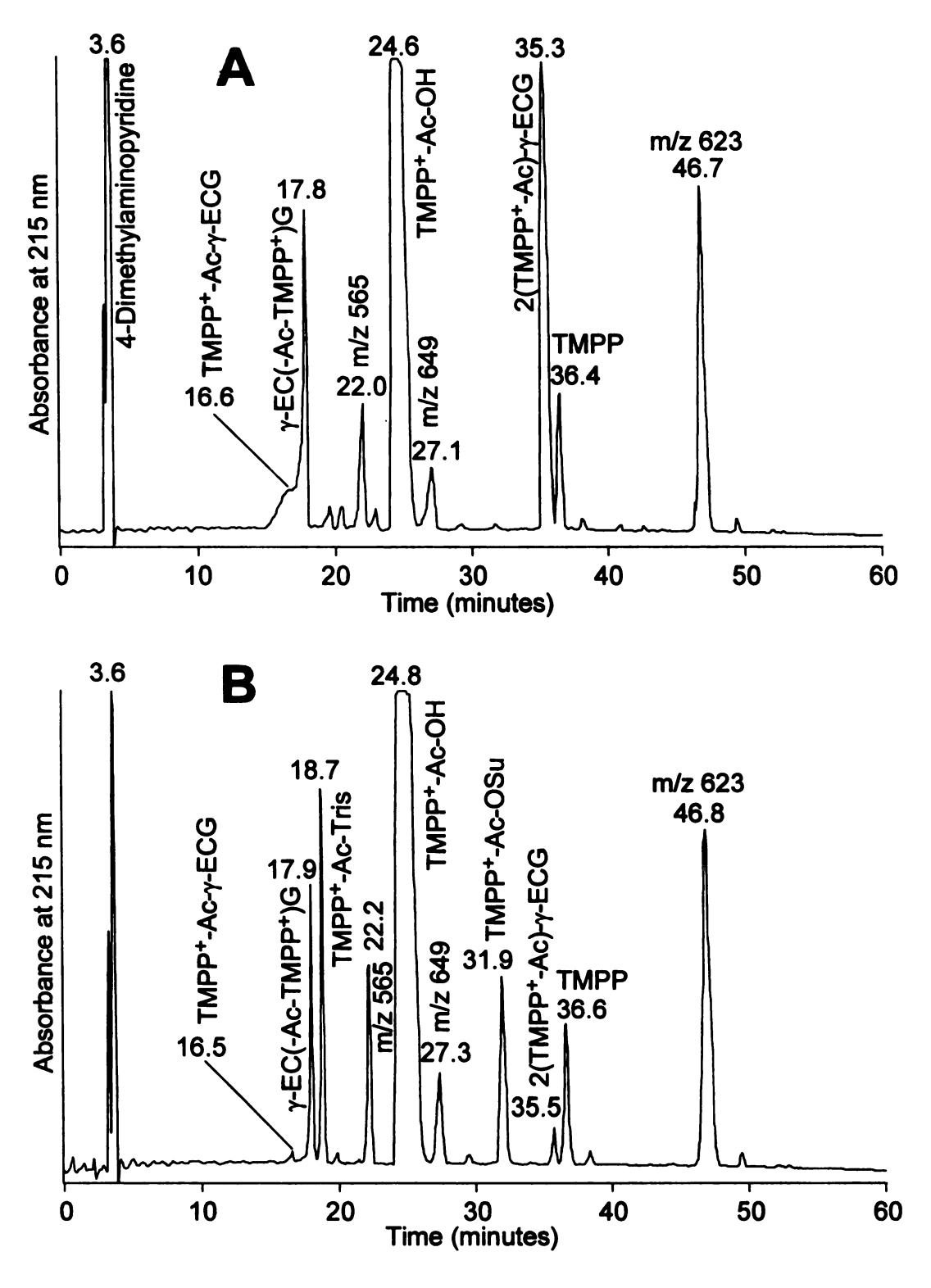


Figure 2.13. HPLC chromatograms of TMPP⁺-Ac-OSu + γ -ECG reaction mixtures performed in unbuffered (A) and buffered (B) solutions.

cysteine side-chain derivative, and 14% of the doubly-derivatized product, as shown in Figure 2.13B. Rather than limit derivatization of the cysteine side-chain, the use of Tris-HCl buffer appears to limit N-terminal derivatization, thereby increasing the relative amount of side-chain derivatization. It appears that blocking of the cysteine side-chain (19) prior to charge-derivatization is necessary to achieve selective derivatization of the N-terminus.

The ESI-CAD-MS/MS spectra of the derivatized products obtained on an ion trap instrument are shown in Figure 2.14. The MS/MS spectra of the N-terminal derivative (A) and the side-chain derivative (B) are surprisingly similar. The MS/MS spectrum of the N-terminal derivative (A) has peaks at m/z 607 (TMPP+-Ac-SH) and m/z 751 (*y₂) that appear to arise from TMPP⁺-Ac derivatization of the cysteine side-chain. These peaks probably result from incomplete separation of the N-terminal derivative from the cysteine side-chain derivative. The major differences in the MS/MS spectra of the Nterminal derivative (A) and the side-chain derivative (B) is the presence of peaks at m/z 591 (* b_0+H_20) and 702 (* b_1) in the spectrum of the N-terminal derivative and the absence of those peaks the in spectrum of the side-chain derivative. Both of these peaks are indicative of γ -glutamate at the n = 1 position of a charge-derivatized peptide, as discussed in Chapter 3. The MS/MS spectrum of the C^{2+} precursor ion of the doublyderivatized product has peaks that are indicative of derivatization at the N-terminus and at the cysteine side-chain, as shown in Figure 2.14C. It is interesting to note that the spectrum produced during analysis of the doubly-derivatized product by MALDI-MS has no discernible C^{2+} peak, a very low intensity $[C^{2+} - H]^+$ peak, and an intense [C²⁺ - TMPP⁺-Ac]⁺ peak (data not shown). Therefore, analysis of the doubly-derivatized

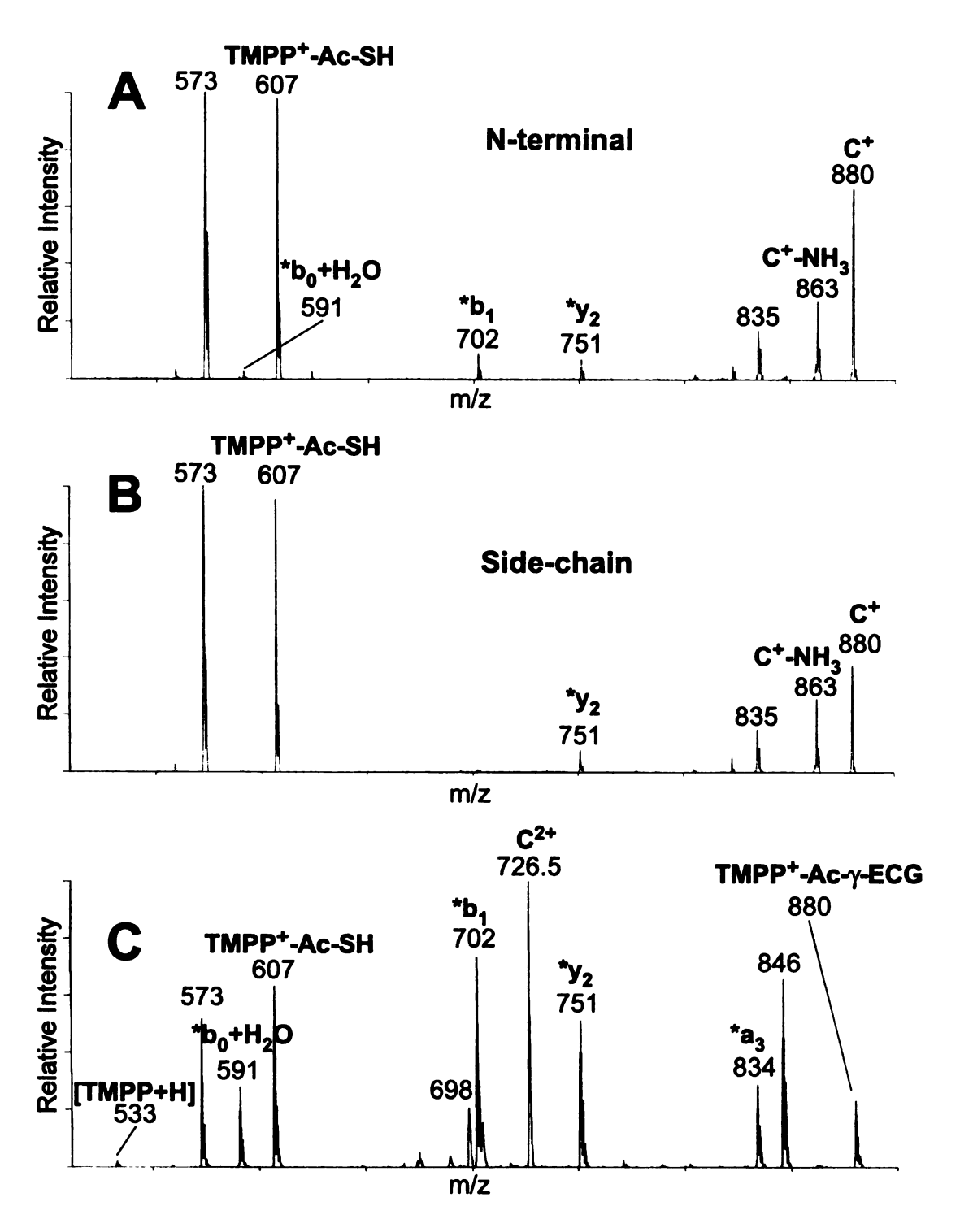


Figure 2.14. ESI-CAD-MS/MS spectra of N-terminal (A), side-chain (B), and doubly-derivatized (C) γ -ECG.

product by MALDI-MS produces a spectrum that is very similar to that produced from the single-derivatized products.

D. TMPP+-Ac Derivatization of Tyrosine

The extent of charge-derivatization of the tyrosine side-chain was studied for the peptide acyl carrier protein fragment (65-74) amide (VQAAIDYING-NH₂). The peptide was derivatized using [TMPP⁺-Ac-OSu][Br⁻] in an unbuffered solution and in a pH 8.3 Tris-HCl buffer. The reaction mixtures were separated by HPLC using the same gradient used to separate the glutathione reaction mixture. The chromatograms and peak identities are shown in Figure 2.15A. Note the peak areas of the tyrosine side-chain derivative (RT \approx 19.8 min) and the doubly-derivatized product (RT \approx 41.5 min). The peak with a retention time of approximately 24 minutes represents a mixture of the N-terminal derivatization product and the TMPP⁺-Ac-OH peak. This peak was collected and separated by HPLC to determine the relative contribution of each component to the total peak area.

The MALDI-PSD and ESI-CAD-MS/MS spectra of the purified peptide derivatives are shown in Figure 2.16. Note that the N-terminal derivative (A) produced only N-terminal fragments. The side-chain derivative (B) produced a mixture of N-terminal and C-terminal fragments. All of the fragments produced include the tyrosine residue. Also, an internal peak representing most of the derivatized tyrosine residue was observed at m/z 708. The ESI-CAD-MS/MS spectrum of the doubly-derivatized product has peaks found in both the N-terminal and C-terminal spectra. In addition, peaks representing doubly-charged fragment ions were present at m/z 953, 1095.5, 1104. The

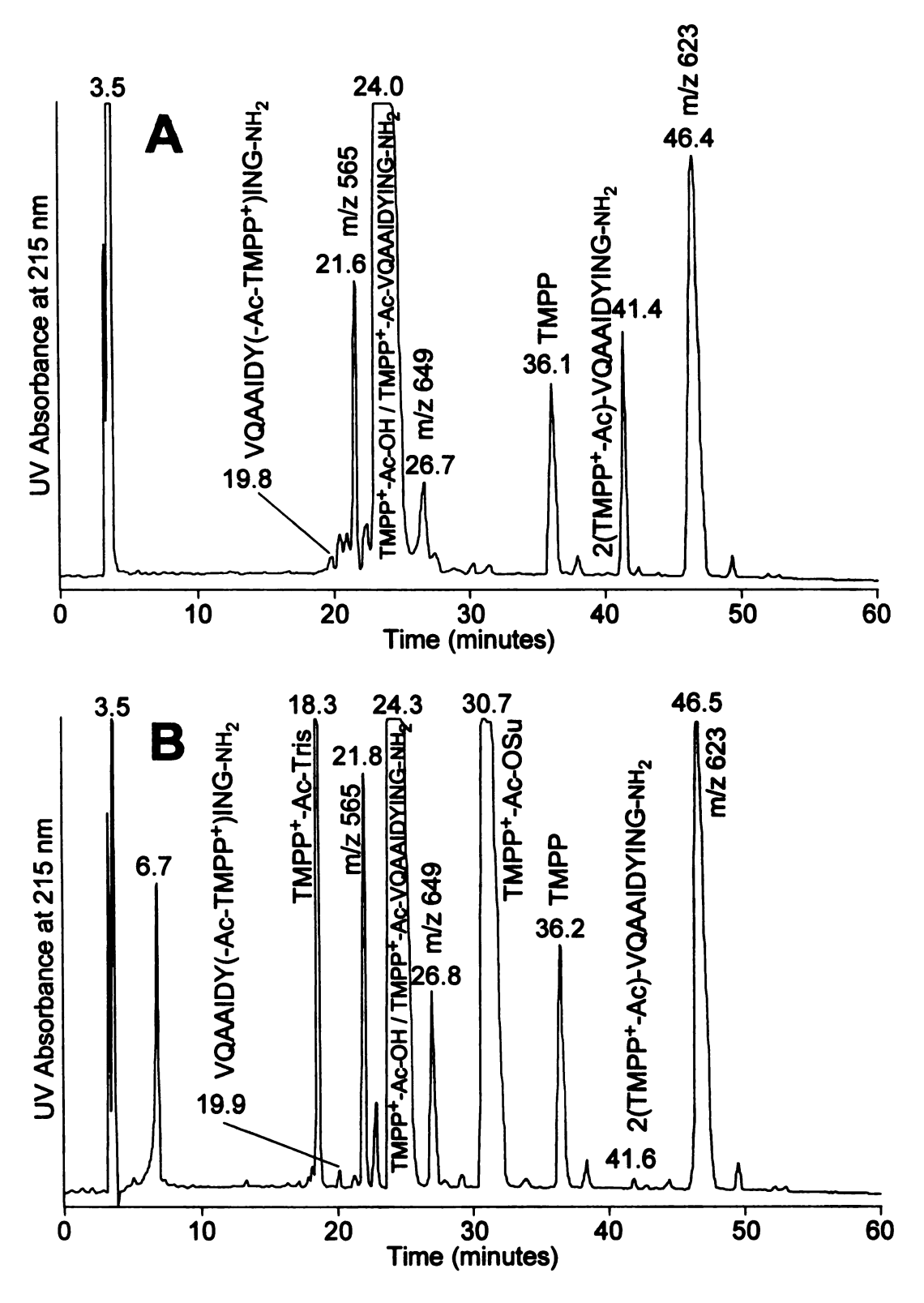


Figure 2.15. HPLC chromatograms of TMPP⁺-Ac-OSu + VQAAIDYING-NH₂ reaction mixtures performed in unbuffered (A) and buffered (B) solutions.

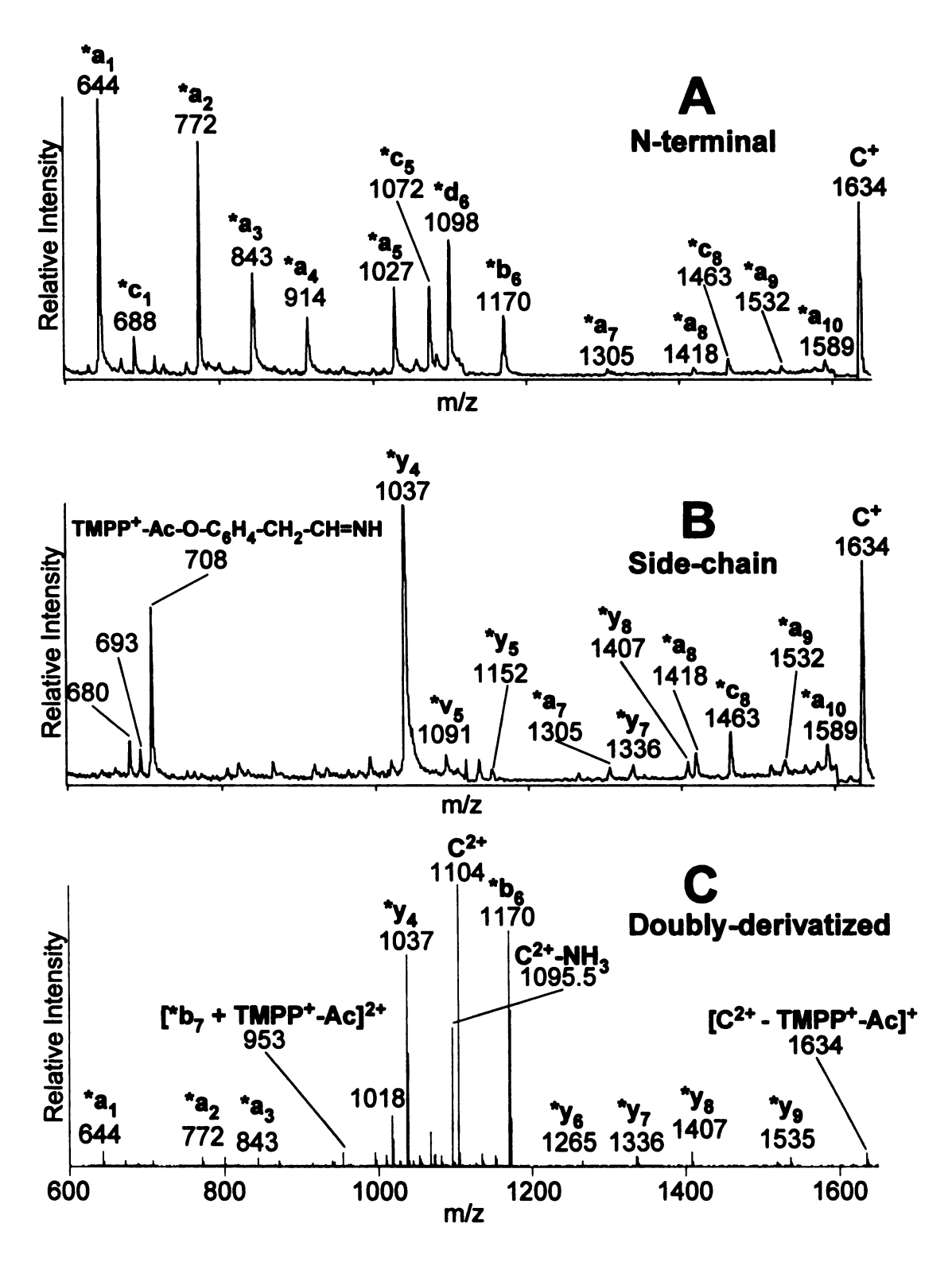


Figure 2.16. MALDI-PSD spectra of N-terminal (A) and side-chain (B) derivatized VQAAIDYING-NH₂, and the ESI-CAD-MS/MS spectrum of the doubly-derivatized (C) product.

MALDI-MS spectrum of the doubly-derivatized product (Figure 2.16C) contains a strong peak resulting from the loss of a TMPP⁺-Ac group (m/z 1634), a very weak peak resulting from loss of a proton (m/z 2207), and no C²⁺ peak (m/z 1104). As a result, it was not possible to obtain a MALDI-PSD spectrum from a doubly-derivatized precursor ion.

Based on the HPLC peak areas of the purified products, the unbuffered reaction produced approximately 87% of the N-terminal derivative, 1% of the tyrosine side-chain derivative, and 12% of the doubly-derivatized product, as shown in Figure 2.15A. The amount of unreacted peptide was not determined because the peptide eluted with the solvent front. When the derivatization was performed in a pH 8.3 Tris-HCl buffer, the reaction mixture contained approximately 75% of the N-terminal derivative, 15% of the tyrosine side-chain derivative, and 10% of the doubly-derivatized product, as shown in Figure 2.15B. Although the amount of underivatized peptide was not determined, the small peak areas for the derivatives are indicative of low yields in the Tris-HCl buffer. Again, no advantage was observed for derivatization in the buffer except for a decrease in the amount of doubly-derivatized product.

In summary, TMPP⁺-Ac-derivatization of peptides in a pH 8.3 Tris-HCl buffer resulted in lower reaction yields than derivatization in an unbuffered solution. Also, no increase in selectivity for the N-terminus was observed for peptides containing lysine, cysteine, or tyrosine when derivatization was performed in a pH 8.3 Tris-HCl buffer.

VI. Ionization Efficiency and Signal Supression

Samples of underivatized and TMPP⁺-Ac-derivatized standards of Buccalin (GMDSLAFSGGL-NH₂) were analyzed by MALDI-MS to study the ionization efficiency and signal supression effects of the underivatized and derivatized peptides. Three spots were prepared containing 5 pmol of the underivatized peptide; three spots were prepared containing 5 pmol of the derivatized peptide; and 3 spots were prepared containing 5 pmol each of the underivatized and derivatized peptide. Each spot was analyzed by MALDI-MS with 256 laser shots. The intensities of the MH⁺, [M+Na]⁺, and [M+K]⁺ peaks were added for the underivatized peptide, and the intensities of the C⁺ and [C-H+Na]⁺ peaks were added for the derivatized peptide. The MALDI-MS spectra produced are shown in Figure 2.17.

The average intensity of the TMPP $^+$ -Ac-buccalin peaks (3700 \pm 1000 counts, Figure 2.17A) was smaller than the average intensity of the underivatized buccalin peaks (5200 \pm 900 counts, Figure 2.17B), but the difference in average intensities was not statistically significant at the 95% confidence level (as determined by a two-sample t-test). However, it is clear that the ionization efficiency of buccalin was not increased by charge-derivatization. In contrast, charge-derivatization of another peptide has been observed to produce a dramatic increase in ionization efficiency (20). Apparently, charge-derivatization provides an increase in ionization efficiency for peptides that normally do not respond well to MALDI-MS, but derivatization does not appear to offer any further increase in ionization efficiency for peptides that respond well without derivatization.

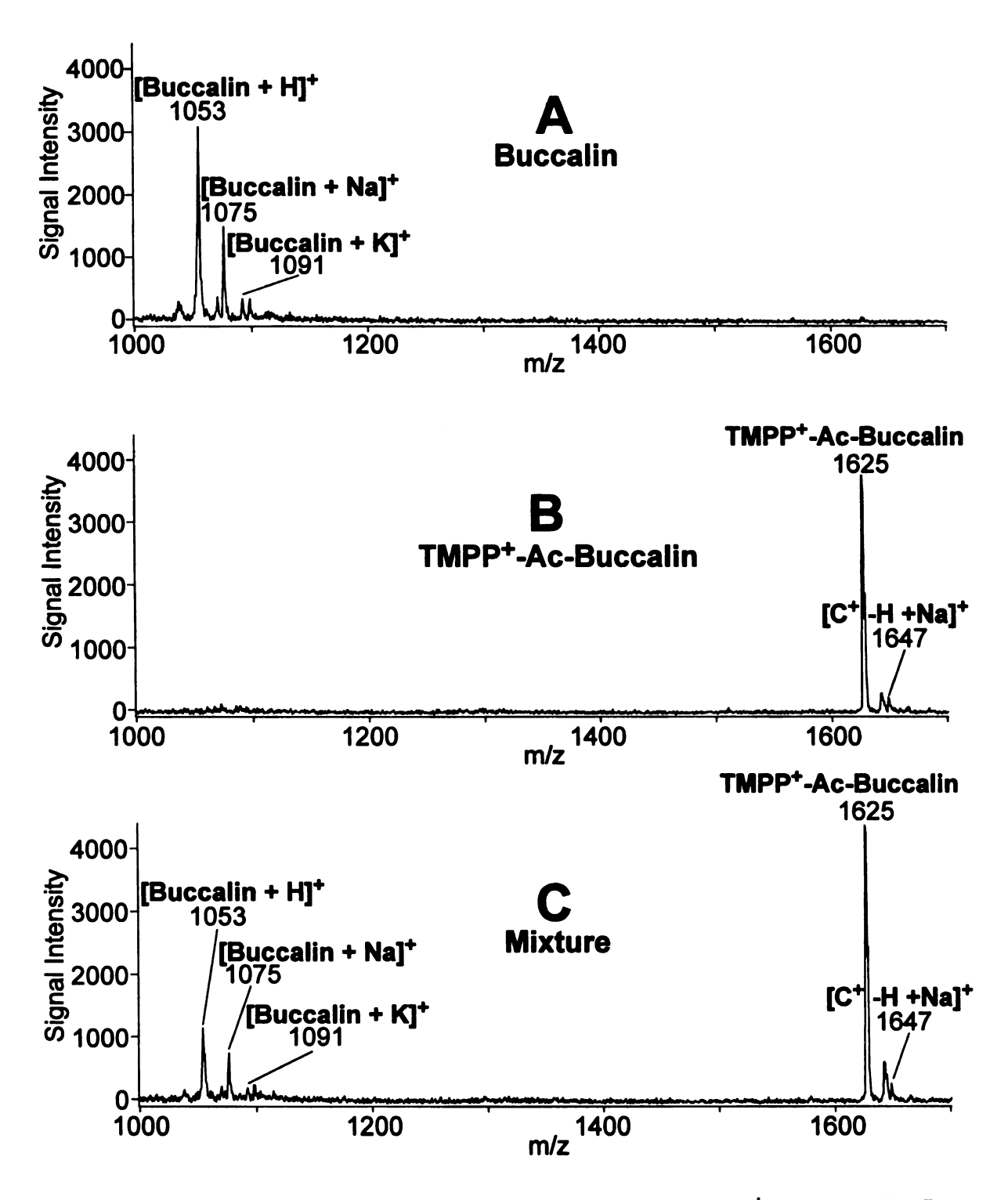


Figure 2.17. MALDI-MS spectra of buccalin (A), TMPP⁺-Ac-buccalin (B), and an equimolar mixture of the two (C).

When an equimolar mixture of buccalin and TMPP⁺-Ac-buccalin was analyzed in three separate spots by MALDI-MS, the signal from the buccalin was suppressed, as shown in Figure 2.17C. The average signal intensity of the buccalin peaks was reduced from 5200 ± 900 to 1680 ± 700 , whereas the average signal intensity of the TMPP⁺-Ac-buccalin (4900 ± 2800) was not reduced. The ratio of the TMPP⁺-Ac-buccalin intensity divided by the buccalin intensity had an average value of 2.8 ± 0.7 . Statistical analysis confirmed that the buccalin intensity was significantly reduced at the 95% confidence level (two-sample *t*-test), and that the ratio of TMPP⁺-Ac-buccalin intensity to the buccalin intensity was significantly greater than 1.0 at the 95% confidence level (one-sample *t*-test).

The signal suppression of the underivatized peptide by the TMPP⁺-Ac-derivatized peptide suggests that MALDI-MS analysis is not a reliable method for estimating reaction yields for TMPP⁺-Ac derivatization reactions. The suppression of underivatized peptide means that the reaction yield estimates of TMPP⁺-Ac derivatization reactions would be overestimated when determined by MALDI-MS.

VII. References

- Huang, Z.-H.; Wu J.; Roth, K. D. W.; Yang, Y.; Gage, D. A.; Watson, J. T. Anal.
 Chem. 1997, 69, 137-144.
- Claereboudt, J.; Baeten, W.; Geise, H.; Claeys, M. Org. Mass Spectrom. 1993, 28, 71-82.
- 3. Wagner, D. S. Ph.D. Dissertation, Michigan State University, East Lansing, MI, 1992.
- 4. Liao, P.-C.; Huang, Z.-H.; Allison, J. J. Am. Soc. Mass Spectrom. 1997, 8, 501-509.
- 5. Downard, K. M.; Biemann, K. J. Am. Soc. Mass Spectrom. 1993, 4, 874-881.
- Johnson, R. S.; Martin, S., A.; Biemann, K. Int. J. Mass Spectrom. Ion Processes 1988, 86, 137-154.
- 7. Papayannopoulos, I. A. Mass Spectrom. Rev. 1995, 14, 49-73.
- 8. Wagner, D. S.; Nieuwenhuis, T. J.; Chang, Y. S.; Gage, D. A.; Watson, J. T. Proceedings of the 40th ASMS Conference on Mass Spectrometry and Allied Topics, Washington, DC, May 31-June 5, 1992.
- 9. Lin, T.; Glish, G. L. Proceedings of the 45th ASMS Conference on Mass Spectrometry and Allied Topics, Palm Springs, California, June 1-5, 1997.
- 10. Cárdenas, M. S.; van der Heeft, E.; de Jong, A. P. J. M. Rapid. Commun. Mass Spectrom. 1997, 11, 1271-1278.
- 11. Kidwell, D. A.; Ross, M. M.; Colton, R. J. J. Am. Chem. Soc. 1984, 106, 2219-2220.
- 12. Kidwell, D. A.; Ross, M. M.; Colton, R. J. Springer Ser. Chem. Phys.: SIMS 4, 1984, 36, 412-414.

13.

1

ı

- 13. Kiplinger, J. P.; Contillo, L.; Hendrick, W. L.; Grodski, A. Rapid Commun. Mass Spectrom. 1992, 6, 747-752.
- 14. Stults, J. T.; Lai, J.; McCune, S.; Wetzel, R. Anal. Chem. 1993, 65, 1703-1708.
- 15. Wetzel, R.; Halualani, R.; Stults, J. T.; Quan, C. *Bioconjugate Chem.* 1990, 1, 114-122.
- 16. Huang, Z.-H.; Shen T.; Wu, J.; Gage, D. A.; Watson, J. T. submitted to Anal. Biochem. 1999.
- 17. Greenstein, J. P.; Winitz, M. Chemistry of the Amino Acids; Wiley: New York, 1961; pp 486-488.
- 18. Means, G. E.; Feeney, R. E. *Chemical Modification of Proteins*; Holden-Day: San Francisco, **1971**; pp 14-15, 68-71.
- 19. Coligan, J. E.; Dunn, B. M.; Ploegh, H. L.; Speicher, D. W.; Wingfield, P. T. Current Protocols in Protein Science, Vols. 1-2; Wiley: New York, 1998; pp 15.1.1-15.1.18.
- 20. Liao, P.-C.; Allison, J. J. Mass Spectrom. 1995, 30, 511-512.

CHAPTER 3

FRAGMENTATION BEHAVIOR OF PEPTIDES AND CHARGE-DERIVATIZED PEPTIDES CONTAINING ISOMERIC ACIDIC RESIDUES

I. Introduction

A. Isomeric Residues

Mass spectrometry is well suited to the determination of the amino acid sequence of peptides. However, distinguishing between amino acid residues that differ in mass by less than one mass unit is difficult. The monoisotopic masses of lysine and glutamine are 128.09496 and 128.05856 mass units, respectively, a difference of 0.0364 mass units. These residues can be distinguished by analysis on a high-resolution mass spectrometer or by reaction with phenylisothiocyanate (1). The glutamine side-chain does not react with phenylisothiocyanate, but the side-chain of lysine reacts to form a phenylthiocarbamoyl derivative that is 135 daltons heavier than the mass of the lysine side chain.

Leucine and isoleucine residues are isomers with a monoisotopic mass of 113.08406 mass units. These residues can be distinguished by the way they fragment under high-energy collisionally-activated dissociation (CAD) conditions (2, 3). The $\mathbf{d_n}$ ion produced by cleavage at the site of leucine is 42 daltons lighter than the corresponding $\mathbf{a_n}$ ion, whereas two different $\mathbf{d_n}$ ions result from similar cleavage at isoleucine; the $\mathbf{d_n}$ ions from isoleucine have masses that are 14 and 28 daltons less than the corresponding $\mathbf{a_n}$ ion. Similarly, the mass of the $\mathbf{w_n}$ ion produced from leucine is 59 daltons less than the corresponding $\mathbf{y_n}$ ion, and the $\mathbf{w_n}$ ions produced from isoleucine are

31 and 45 daltons less than the corresponding y_n ion. Neither the d_n ions nor the w_n ions described are produced during low-energy CAD.

Another challenge for mass spectrometry is identification of the isomeric forms of aspartic acid and glutamic acid residues shown in Figure 3.1. The isomeric form of the aspartic acid residue is called β -aspartate (β -Asp) or isoaspartate. The side-chain of the β -Asp residue is shorter by one methylene unit, but the peptide backbone has an additional methylene unit between the α -carbon and the next amide toward the C-terminus; likewise, the side-chain of the γ -glutamate residue (γ -Glu) is shorter by two methylene units and the backbone is two methylene units longer between the α -carbon and the next amide bond.

The γ -glutamate residue is present in a few naturally-occuring peptides. These γ -glutamyl peptides have been found in brain tissues (4, 5), human urine (6-8), flaxseed (9), the cell walls of *E. coli* (10), in folic acid cofactors of *E. coli* (11), and in the biomolecule glutathione. Glutathione is a very important biopeptide that is involved in the transport of amino acids across cell wells (12, 13), decomposition of hydrogen peroxide (14), DNA and protein synthesis (15), and cellular regulation (16) among other functions.

B. Formation of β -Aspartate and γ -Glutamate

Isoaspartate residues occur naturally in human urine (6, 8), and they can form by the rearrangement of aspartic acid, asparagine, or aspartic acid esters (17). Isoaspartate also forms in tryptic digests of serine proteases (18). The formation of isoaspartate from asparagine, aspartate, or aspartic acid esters at mildly acidic, neutral, or basic pH is shown in Figure 3.2. Aspartic acid, asparagine, or aspartic acid esters can undergo

Figure 3.1. Structures of aspartate, β -aspartate, glutamate, and γ -glutamate.

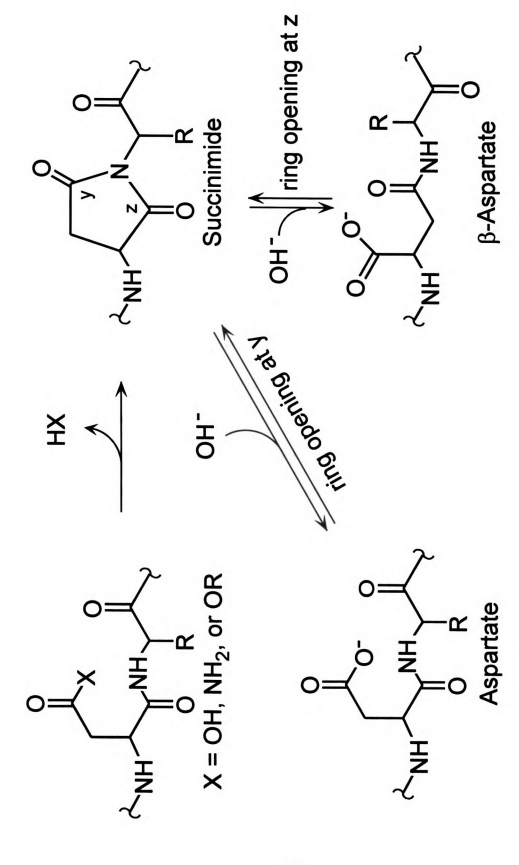


Figure 3.2. Formation of β -aspartate in solution

rearrangement to form a succinimide structure. The formation of the succinimide structure requires the loss of hydrogen from the amide nitrogen to form a reactive anion. The succinimide ring opens to form a mixture of aspartate and β-aspartate at a ratio of approximately (1:3). Opening of the succinimide can be accompanied by a small amount of racemization to form D-aspartate and D-isoaspartate residues (19). Analogous reactions occur for glutamine, glutamate, and glutamic acid esters, but at much slower rates (20).

The formation of the succinimide is the rate-limiting step in isoaspartate formation. Fromation of the succinimide from Asn requires deprotonation of the peptide-bond nitrogen; whereas succinimide formation from Asp requires both deprotonation of the peptide-bond nitrogen and protonation of the side-chain carboxyl to form a hydroxyl leaving group (21, 22). At 37°C and pH 7.4, the half-lives of aspartic acid methyl esters in peptides are on the order of minutes, the half-lives of asparagine residues are on the order of days, and the half-lives of aspartate residues are on the order of weeks (22).

The rate of succinimide formation is affected by the residue following the Asx residue (where Asx denotes Asn, Asp, or aspartic acid ester). Succinimide formation occurs most rapidly in peptides where Asx is followed by glycine or serine (22, 23). Glycine has minimal steric hindrance. The –OH side-chain of serine is relatively small and may stabilize the nitrogen anion intermediate necessary to form the succinimide. Asn-Gly and Asn-Ser sequences are common sites for deamidation in proteins, although the stability of the Asx residues is dependent on the three-dimensional structure of the protein (24). The reaction depicted in Figure 3.2 does not occur when Asx is followed by proline, because the proline nitrogen cannot form a reactive anion (19). In proteins,

isoaspartate most commonly forms from deamidation of asparagine, but isomerization of aspartyl residues also occurs under mild conditions (25-27).

Asparagine residues are most stable in the pH range of 3 to 4 (28). As the pH increases, the rate of succinimide formation increases, presumably because the extent of deprotonation of the peptide-bond nitrogen increases at higher pH. At a pH range of 1 to 2, asparagine undergoes direct hydrolysis to form Asp without formation of β-Asp.

Deamidation and isoaspartate formation are of interest to the biotechnology industry because of the importance of the stability and purity of protein-based pharmaceutical products (29). Deamidation/isoaspartate formation, oxidation of methionine, and oxidation of cysteine are considered the principal pathways of degradation of native protein structures under mild conditions (30). Deamidation of Asn and isomerization of Asp in proteins can cause loss of biological activity in proteins when the change occurs in the region of the active site (25, 31-33). In some cases, more stable variants of the proteins can be produced by replacing the unstable Asx residues with Gln, Glu, or other residues (25, 32).

C. Conventional Analysis of β -Aspartate and γ -Glutamate

A variety of techniques have been used to separate and identify β -Asp containing proteins and peptides. As a general rule, it is easier to detect deamidation (conversion of asparagine to a mixture of aspartate and β -aspartate) products than to distinguish between the two forms of aspartate. Deamidated proteins can be separated from native proteins using polyacrylamide gel electrophoresis (34), isoelectric focusing (35), and ion-exchange chromatography (36, 37). In a few cases, hydrophobic interaction

chromatography (37) and affinity chromatography (38) have been successfully used to separate the isoaspartyl and aspartyl forms of an intact protein; however, separation of β -aspartyl variants from aspartyl variants usually requires preliminary digestion of the protein. Isoaspartyl peptides can be separated from analogous aspartate, asparagine, or succinimide-containing peptides by reverse-phase HPLC (39) or capillary electrophoresis (40). When separated by reverse-phase chromatography, isoaspartyl peptides elute before aspartyl peptides because the isoaspartyl side-chain ionizes to a greater degree than the aspartyl side-chain. The determination of the relative acidities of the Asp and β -Asp side-chains are based on the acid dissociation constants of the α - and β -carboxyl groups of aspartic acid. The pKa of the β -carboxyl (analogous to the Asp side-chain) is 3.65, and the α -carboxyl (analogous to the β -Asp side-chain) pKa is 1.88. Similarly, the pKa of the γ -carboxyl of glutamic acid (analogous to the Glu side-chain) is 4.25, whereas the α -carboxyl pKa (analogous to the γ -Glu side-chain) is 2.19 (41).

Approaches to detecting deamidation include crystallographic methods (42), release of ammonia (43), and cleavage with hydroxylamine (44). The most widely used techniques for the identification of isoaspartate-containing proteins and peptides are Edman degradation (45) and methylation with protein L-isoaspartyl O-methyltransferase (PIMT) (46). Other approaches include 2-D NMR (47), tritium incorporation (48), binding with monoclonal antibodies (49), and changes in the activity of certain proteases (50). However, none of the techniques listed above is without limitations. Edman degradation provides only indirect evidence of isoaspartate in the form of low yields for the expected PTH-amino acids beginning at the site of the isoaspartate residue, and these results can be inconclusive. The low yields are the result of inefficient cleavage of the

extended isoaspartyl backbone. PIMT is not commercially available, and the assay requires micromolar quantities of PIMT for efficient methylation; also, the assay requires the use of radiolabeled reagents for detection.

D. Mass Spectrometric Analysis of β -Aspartate and γ -Glutamate

Mass spectrometry has also been used to detect deamidation and isoaspartate formation. Deamidation of the asparagine residue of a peptide to form the analogous aspartyl or isoaspartyl peptide can be recognized by the addition of one dalton to the mass of the peptide (51). Likewise, the succinimide intermediate can be identified by a loss of NH₃ from the asparaginyl peptide or the loss of H₂O from the aspartyl peptides (52). When fragmentation occurs, mass spectrometry can verify the location of the newly formed Asp or β -Asp residue based on the residue mass (53). However, this only identifies the site of deamidation; it does not distinguish between aspartyl and isoaspartyl residues. Mass spectrometry can also be used as an alternative to radiolabeling to detect methylation of isoaspartyl residues by PIMT (54).

The presence of normal aspartate residues in peptides has been observed to significantly alter fragmentation during analysis by mass spectrometry. Preferential cleavage on the C-terminal side of Asp to form $\mathbf{b_n}$ or $\mathbf{y_n}$ ions has been observed for peptides analyzed by LSIMS (55), ESI (56-58), and MALDI (55, 59). In addition, the presence of aspartate at the $\mathbf{n^{th}}$ residue of a charged-derivatized peptide has been observed to produce abundant $\mathbf{*c_{n-1}}$, $\mathbf{*d_n}$, and $\mathbf{*b_n}$ fragment ions during analysis by MALDI-PSD (60).

Several researchers have attempted to use mass spectrometry to identify isoaspartyl residues. Okada and Kawase (61) found differences in the fragmentation of derivatized dipeptides with an N-terminal Glu or γ -Glu residue when analyzed by EI-MS, but the differences were not significant for larger peptides. Dipeptides with either Glu or γ-Glu at the N-terminus were analyzed by chemical ionization (62). The glutamyl dipeptides produced abundant [MH-H₂O]⁺ and [MH-2(H₂O)]⁺ fragments whereas the y-glutamyl peptides produced abundant fragment ions corresponding to protonated pyroglutamic acid (m/z 130) and y₁ fragment ions. Small peptides (2-4 residues) with an acidic residue (Asp., \(\beta \)-Asp, Glu, or \(\gamma \)-Glu) at the N-terminus were analyzed by LSIMShigh-energy CAD-MS/MS (63, 64). The spectra of the γ-glutamyl peptides had a strong y_n peak corresponding to cleavage at the C-terminal side of the γ -Glu residue; this peak was absent in the spectra of the glutamyl peptides, but a strong peak at [MH-H₂O]⁺ was present instead. The relative intensities of the y_n and $[MH-H_2O]^+$ fragments differed for aspartyl and β-aspartyl peptides, but the differences were not significant enough to allow identification of the peptides unless both forms of the peptide are analyzed. Oin (65) observed a stronger [MH-H₂O]⁺ peak for aspartame (Asp-Phe-OCH₃) than for β -aspartame (β -Asp-Phe-OCH₃) when the samples were analyzed by atmospheric pressure chemical ionization low-energy CAD-MS/MS.

Lloyd and co-workers found differences in the relative intensities of $\mathbf{a_n}$ and $\mathbf{b_n}$ ions generated from aspartyl, β -aspartyl, glutamyl, and γ -glutamyl peptides during analysis by FAB-CAD-MS/MS (66). They found that the ratio of the intensity of the $\mathbf{b_n}$ peak to the intensity of the $\mathbf{a_n}$ peak $[I(\mathbf{b_n})/I(\mathbf{a_n})]$ was ≤ 1 for residues with α -linkages (aspartate and glutamate) and that $I(\mathbf{b_n})/I(\mathbf{a_n})$ was ≥ 10 for residues with β - or γ -linkages.

However, the intensities of the $\mathbf{a_n}$ and $\mathbf{b_n}$ peaks were dependent on the collision gas pressure. Under similar conditions, Papayannopoulos and Biemann (52) observed abundant $\mathbf{a_n}$ and $\mathbf{b_n}$ ions for an aspartyl peptide, but not for the analogous β -aspartyl peptide.

Violand et al. compared the fragmentation of an asparagine-containing peptide (VFTNSLVFGTSD) and the analogous isoaspartyl peptide (VFT β -DSLVFGTSD) during analysis by FAB-CAD-MS/MS (67). They observed that the y_9 peak from the isoaspartyl peptide was much more intense than the y_9 peak from the asparagine containing peptide. Unfortunately, the analogous aspartyl peptide was not analyzed, so it is unclear if the fragmentation of the α - and β -aspartyl peptides would differ.

Carr et al. analyzed aspartyl and isoaspartyl forms of a tryptic peptide by FAB-high-energy CAD-MS/MS (53, 68). The \mathbf{w} ion produced from the aspartyl peptide was more abundant than that produced by the isoaspartyl peptide. When the side chains of Asp and β -Asp were methylated, the β -aspartyl peptide produced an abundant \mathbf{v}_6 fragment, but no \mathbf{w}_6 fragment, whereas the aspartyl peptide produced both \mathbf{v}_6 and \mathbf{w}_6 fragments. However, this approach is limited to high-energy CAD because \mathbf{v}_6 and \mathbf{w}_6 ions are not produced during low-energy CAD.

Isoaspartyl peptides with a basic residue near the N-terminus produced a b_n + H_2O ion corresponding to cleavage at the N-terminal side of the isoaspartate residue (52). No corresponding fragment was produced from analogous aspartyl peptides; instead, a c_n ion was formed. Bean and Carr (69) also observed a b_n + H_2O fragment in the high-energy CAD-MS/MS spectrum of a β -aspartyl peptide, and in the spectra of charge-derivatized β -aspartyl peptides. Schindler *et al.* (70) observed the formation of a b_n +

H₂O fragment ion in the ESI-low-energy CAD-MS/MS spectrum of an isoaspartate-containing peptide.

Although several researchers have investigated the use of mass spectrometry to identify β -aspartyl peptides, the studies have generally examined only a small number of peptides. Also, very little work has been done using matrix-assisted laser desorption/ionization with post-source decay (MALDI-PSD) or electrospray ionization collisionally-activated dissociation tandem mass spectrometry (ESI-CAD-MS/MS) to identify β -aspartate or γ -glutamate residues.

This chapter presents the results of a study of six pairs of peptides, differing only by the presence of a normal or isomeric acidic residue, by fast atom bombardment collisionally-activated dissociation tandem mass spectrometry (FAB-CAD-MS/MS), MALDI-PSD, and ESI-CAD-MS/MS. In addition, the results of parallel experiments with the charged derivatives of each of these peptides are described. The fragmentation of these peptides is evaluated for diagnostic purposes, and possible fragmentation mechanisms are proposed.

II. Experimental

A. Reagents

The peptides Asp-Gly, β-Asp-Gly, aspartame, β-aspartame, reduced glutathione, Ala-D-γ-Glu-Lys-D-Ala-D-Ala, angiotensin II, and [β-Asp]¹-angiotensin II were obtained from Sigma Chemical Co. (St. Louis, MO) and were used without further purification. TRIZMA buffer was also obtained from Sigma. Buccalin and acyl carrier protein fragment (65-47) amide were obtained from Bachem Bioscience Inc. (King of Prussia,

PA) and were used without further purification. Glu-Cys-Gly and Ala-Glu-Lys-Ala-Ala were prepared in house using an Applied Biosystems automated synthesizer and were purified by preparative scale reverse-phase HPLC. [β-Asp]³-buccalin and [β-Asp]⁶-acyl carrier protein fragment (65-74) amide were prepared from buccalin and acyl carrier protein fragment (65-74) amide, respectively, using the method of McFadden and Clarke (71). The [tris-(2,4,6-trimethoxyphenyl)phosphonium] acetyl (TMPP⁺-Ac) derivatives were made with the charged group attached to the peptide N-terminus. The synthetic aspects are discussed in detail elsewhere (72). The reagent used is [TMPP⁺-Acsuccinimide][Br⁻]. It is prepared by first reacting bromoacetyl bromide with N-hydroxysuccinimide and then adding tris-(2,4,6-trimethoxyphenyl)phosphine to generate a salt.

B. Charge Derivatization

Peptide derivatives were prepared using the following procedure. 0.5-2 nmol of peptide (in 2 μL 10% acetonitrile), 2 μL of 10 mM 4-dimethylaminopyridine in 50% acetonitrile (v/v), and 1 μL of 10 mM [TMPP+-Ac-succinimide][Br] in 50% acetonitrile were combined, vortexed for 1 minute, and allowed to stand at room temperature for 30 minutes. FAB-CAD-MS/MS and MALDI-PSD analyses were performed without further purification. Prior to analysis by ESI-CAD-MS/MS, the derivatized peptide was purified by HPLC. The HPLC system consisted of two Waters Model 6000A pumps controlled by a Waters Millenium data system. Purification was performed on a Phenomenex Jupiter C18 reverse-phase column (5-μm particle size, 4.6 x 250 mm) with the eluant monitored at 215 nm. The mobile phase contained the following: (A) 0.1% TFA, (B)

acetonitrile / 0.1% TFA (90:10, v/v). The gradient elution was carried out at a flow rate of 1mL/min with gradient 25-45% B in 13 min, hold at 45% B for 7 min, 45-75% B in 40 min. The fraction containing the derivatized peptide was collected and concentrated using a Speed-Vac (Savant Instruments, Farmingdale, NY).

C. Analysis

Fast atom bombardment-collisionally activated dissociation-tandem mass spectrometry (FAB-CAD-MS/MS) spectra were obtained on a double-focusing mass spectrometer (JEOL HX-110, JEOL, Tokyo, Japan). The instrument utilizes a beam of 6-keV xenon atoms and a 10-kV acceleration voltage in the source. The FAB matrix used was thioglycerol/2-hydroxyethyl disulfide (1:1, v/v). One μ L of underivatized peptide solution (0.5-2 nmol/µL in 50% acetonitrile) or one µL of derivatized peptide solution (100-500 pmol/µL in 50% acetonitrile) was combined with the matrix for each analysis. The pressure of the helium collision gas was adjusted to produce 50% attenuation of the precursor ion abundance. Ten scans were averaged to obtain each spectrum. Although the collision gas pressures used allow for multiple collisions, better signal-to-background ratios were obtained at 50% attenuation (multiple-collision conditions) than at 10% attenuation (single-collision conditions). The differences in the CAD-MS/MS spectra of peptide pairs analyzed at 50% attenuation were similar to those of peptide pairs analyzed at 10% attenuation. Ions generated by FAB from Ultramark 1621 (PCR Inc., Gainesville, FL) were used for instrument calibration. The data were acquired with a JEOL MS-MP8020D data system.

MALDI-PSD mass spectra were obtained on a Voyager Elite reflectron time-offlight mass spectrometer (PerSeptive Biosystems, Inc., Framingham, MA) equipped with a nitrogen laser (337 nm, 3-ns pulse) and delayed extraction. The acceleration voltage used was 20 kV and the delay time was 100 ns. Data were acquired with the data system provided and based on a transient recorder with 2-ns resolution. The matrix used was α -cyano-4-hydroxycinnamic acid, dissolved in water/acetonitrile (1:1, v/v) to give a saturated solution at room temperature. To prepare the sample, 1 µL of the solution containing the underivatized peptide (at a concentration of 50-100 pmol/µL) or the peptide derivative (at a concentration of 10 pmol/µL) was added to 1 µL of the matrix solution and applied to a gold or stainless steel sample plate. The resulting mixture from the derivatization was used directly. The mixture was then allowed to air dry before being introduced into the mass spectrometer. Each spectrum was produced by accumulating data from 256 laser shots. PSD spectra were obtained at a laser power 25% greater than the threshold laser power. The instrument generates PSD data by obtaining several spectra, each optimized for a different range of m/z for the fragment ions. Selected regions of each are stitched together to yield a single PSD mass spectrum. The time-to-mass conversion was achieved by calibrating with the peak representing the C⁺ cation of the charged derivative to be analyzed and the peak at m/z 379 representing the matrix dimer.

ESI-CAD-MS/MS analysis was carried out on a quadrupole ion trap instrument (LCQ, Finnigan, San José, CA). Spectra were acquired at a capillary voltage of 4.25 kV, a cone voltage of 28 V, and a capillary temperature of 220 °C. Samples were analyzed by direct infusion at a flow rate of 3 μL/min, with 20 scans averaged to generate each

spectrum. Peptides were diluted to a concentration of 5 pmol/μL in acetonitrile/0.1% formic acid (1:1, v/v). TMPP⁺- derivatized peptides were diluted to a concentration of 5 pmol/μL in acetonitrile/water (50:50). The singly-charged precursor ions were selected for analysis by MS/MS using a selection window of 3 daltons. Helium was used as the collision gas, and MS/MS spectra were collected over a range of collision energies.

Some ESI-CAD-MS/MS were obtained on a Sciex API 2000 mass spectrometer. Samples were analyzed by direct infusion at a flow rate of 10 µl/min, and 20 scans were averaged to generate each spectrum. Peptides were diluted to a concentration of 50 pmol/µL in acetonitrile/water/formic acid (50:50:0.1). TMPP+-Ac-derivatized peptides were diluted to a concentration of approximately 50 pmol/µL in acetonitrile/water (50:50). Nitrogen was used as the collision gas for low-energy CAD experiments.

ESI mass spectra were also obtained on a Micromass Platform mass spectrometer. Samples were analyzed by direct infusion at a flow rate of 20 µl/min, and 7 scans were averaged to generate each spectrum. Peptides were diluted to a concentration of 50 pmol/µL in acetonitrile/water/formic acid (50:50:0.1). TMPP+-Ac-derivatized peptides were diluted to a concentration of approximately 5 pmol/µL in acetonitrile/water (50:50). Fragmentation was induced by raising the voltage on the cone.

III. Results and Discussion

A. Underivatized Peptides

Previous studies on the fragmentation acidic peptides suggested that the presence of a β -aspartate or γ -glutamate residue at the \mathbf{n}^{th} position may alter the relative abundances of [MH⁺-H₂O], \mathbf{c}_{n-1} , \mathbf{b}_{n-1} +H₂O, \mathbf{a}_n , and \mathbf{b}_n fragments; in addition, the

abundances of y, w, and v fragments resulting from cleavage near the acidic residue may be altered (52, 53, 59, 61-70). Also, the MS/MS spectra collected for this study suggested that the abundances of [MH⁺-NH₃], d_n and internal acyl fragments may be altered. In order to evaluate the relative intensities of these fragment peaks, spectra were collected in triplicate on each instrument and the percent contribution of each fragment peak was calculated using the following equation:

$$A(x) = 100 * I(x) / [I(MH^{+}-H_{2}O) + I(MH^{+}-NH_{3}) + I(\mathbf{c_{n-1}}) + I(\mathbf{b_{n-1}} + \mathbf{H_{2}O}) + I(\mathbf{d_{n}}) + I(\mathbf{a_{n}}) + I(\mathbf{b_{n}}) + I(\mathbf{y}) + I(\mathbf{y}) + I(\mathbf{w}) + I(\mathbf{v}) + I(\mathbf{internal})]$$

where A(x) is the abundance ratio of a particular fragment ion peak, I(x) is the intensity of a particular fragment ion peak, I(y) is the intensity of the y fragment resulting from cleavage at the C-terminal side of the acidic residue, and I(internal) is the total intensity of internal acyl peaks representing fragments with an acidic residue at the N-terminal side of the fragment. This equation has the same form as equations used to determine branching ratios (73); however the A(x) values cannot be considered branching ratios because not all of the fragment ions form from a common precursor. The abundance ratio, A(x), is a number between 0 and 100 that represents the percent contribution of a particular ion to the total ion abundance of the fragment ions considered.

To determine abundance ratios for the ESI-CAD-MS/MS experiments, the relative collision energy was raised until the most intense fragment peak was approximately equal to the intensity of the precursor ion peak. The relative collision energy was in the range of 15-45% (of the maximum collision energy that can be generated by the instrument) and the precursor ion attenuation was between 55% and 83%. Collisionally-activated dissociation in an ion trap occurs under multiple-collision

conditions because of the relatively high collision gas pressure (~1 mTorr) used. The abundance ratios obtained by FAB-CAD-MS/MS, MALDI-PSD, and ESI-CAD-MS/MS are presented in Tables 3.1-3.3. The standard deviations of these abundance ratios are ≤ 5 units.

y Ions

Most of the peptide pairs analyzed had large differences in the relative intensities of the y ion peaks formed by cleavage at the C-terminal side of the acidic residue. Other researchers have observed a similar trend for peptide pairs analyzed by chemical ionization mass spectrometry (CI-MS) (62) and by liquid secondary-ionization-tandem mass spectrometry (LSIMS/MS) (63, 64). The y ion abundance ratios obtained by FAB-CAD-MS/MS and ESI-CAD-MS/MS were larger for β -aspartyl or γ -glutamyl peptides than for the analogous normal peptide for all peptide pairs except for the pair of angiotensin II and $[\beta$ -Asp]¹-angiotensin II. For this pair, the trend was reversed. The differences in y ion abundance ratios were even larger between glutamyl and γ -glutamyl peptides than the differences between pairs of aspartyl and β -aspartyl peptides, as illustrated in Figures 3.3 and 3.4. Note that no y_2 peak is present in Figure 3.3A, but an intense y_2 peak is present in Figure 3.3B. The spectra in Figure 3.4A and 3.4B both have y_1 fragment peaks, but the y_1 peak is more intense in the β -aspartyl spectrum (Figure 3.4B).

Possible mechanisms to rationalize the differences in y-ion abundance ratios are shown in Figure 3.5. Peptides with a normal glutamate residue at the N-terminus (A) form y ions accompanied by the loss of a neutral with a strained aziridinone ring (74). If

Table 3.1. Abundance ratios for underivatized peptides analyzed by FAB-CAD-MS/MS.

Peptide	A(y)	A(MH ⁺ -H ₂ O)	A(MH ⁺ -NH ₃)	A(v)	A(w)	A(c _{n-1})	A(b _{n-1} +H ₂ O)	A(a _n)	A(b _n)	A(d _n)	A(internal)
DF-OMe	51	35	7.6	0.0	0.0	0.0	0.0	5.8	0.7	0.1	0.0
BDF-OMe	82	12	2.4	0.0	0.0	0.0	0.0	2.2	4 .0	0.1	0.0
Diff	-31	23	5.2	0.0	0.0	0.0	0.0	3.6	0.3	6. O	0.0
ECG	Φ	71	-	0.0	0.0	0.0	0.0	7.8	1 .	4 .0	0.0
yECG	41	12	37	0.0	0.0	0.0	0.0	3.0	8.1	0.0	0.0
Diff	-33	29	-26	0.0	0.0	0.0	0.0	4 .8	6.3	4 .	0.0
AEKAA	2	30	4	8.4	9	2.0	5.1	3.0	10.1	6.6	5.6
AyEKAA	19	22	19	4.4	12	0.5	6.0	4.	9.4	4.	10.1
Diff	-14	∞	κ̈́	4.0	φ	1.5	4.2	1.6	0.7	8.5	4.5
DRVYIHPF	23	20	33	9	4	0.0	0.0	0.2	0.0	0.0	0.0
BDRVYIHPF	17	30	16	17	15	0.0	0.0	0.0	2.7	0.0	3.6
Diff	9	-10	17	-1	7	0.0	0.0	0.2	-2.7	0.0	-3.6
GMDSLAFSGGL-NH2	4.	20	8	0.0	0.0	1.5	1.8	1.7	7.4	9.0	0.0
GMBDSLAFSGGL-NH,	6 .	8	49	0.0	0.0	4 .8	3.5	3.2	2.0	2.3	0.0
Diff	4 .0	41-	17	0.0	0.0	-3.3	-1.7	-1.5	5.4	-1.7	0.0
VQAAIDYING-NH2	5.0	16	53	0.0	0.0	8.	1.3	0.0	18.2	1.1	3.5
VQAAIBDYING-NH2	5.5	27	¥	0.0	0.0	2.7	2.2	2.0	21.3	0.5	2.0
Diff	-0.5	-	19	0.0	0.0	6.0	6.0	-5.0	-3.1	9.0	1.5
Mean Diff	-12	O	4.7	4 .0	7.	-0.5	0.3	9.0	-1.0	1.2	7.

Figure 3.2. Abundance Ratios for Underivatized Peptides Analyzed by MALDI-PSD.

Peptide	A(v)	A(MH ⁺ -H ₂ O)	A(MH ⁺ -NH ₃)	Ą	A(W)	A(c _{n-1})	A(b _{n-1} +H ₂ O)	A(a _n)	A(b _n)	A(d _n)	A(internal)
DF-OMe	98	26	8.7	0.0	0.0	0.0	0.0	0.0	0.0	0.0	0.0
BDF-OMe	83	9	6.9	0.0	0.0	0.0	0.0	0.0	0.0	0.0	0.0
Diff	-17	16	1.8	0.0	0.0	0.0	0.0	0.0	0.0	0.0	0.0
ECG	0.0	89	32	0.0	0.0	0.0	0.0	0.0	0.0	0.0	0.0
vECG	0.0	75	56	0.0	0.0	0.0	0.0	0.0	0.0	0.0	0.0
#iO	0.0	-7	9	0.0	0.0	0.0	0.0	0.0	0.0	0.0	0.0
AEKAA	16	4	11.5	0.0	0.0	0.0	0.0	1	5.9	0.0	15
Avekaa	16	25	8.4	0.0	0.0	0.0	0.0	7	5.5	0.0	8
JIIO.	0	15	3.1	0.0	0.0	0.0	0.0	0	0.7	0.0	-19
DRVYIHPF	83	6 .6	27	0.0	0.0	0.0	0.0	0.0	0.0	0.0	0.0
BDRVYIHPF	11	6.8	16	0.0	0.0	0.0	0.0	0.0	0.0	0.0	0.0
	4	3.1	1	0.0	0.0	0.0	0.0	0.0	0.0	0.0	0.0
GMDSLAFSGGL-NH,	15	17	89	0.0	0.0	0.0	0.0	0.0	0.0	0.0	0.0
GMBDSLAFSGGL-NH	53	30	4	0.0	0.0	0.0	0.0	0.0	0.0	0.0	0.0
Diff	4-	-13 6	27	0.0	0.0	0.0	0.0	0.0	0.0	0.0	0.0
VQAAIDYING-NH,	12	5.2	7.5	0.0	0.0	5.1	4.7	2.5	43	3.0	17
VOAAIBDYING-NH,	20	9.9	7.0	0.0	0.0	3.0	3.2	5.9	4	3.4	33
JEO JEO	φ	4.1-	0.5	0.0	0.0	2.1	1.5	-3.4	52	4.0	-16
Mean Diff	ග ි.	2.0	& &	0.0	0.0	4.0	0.3	0.5	4.4	6.1	-5.9

Table 3.3. Abundance ratios for underivatized peptides analyzed by ESI-CAD-MS/MS.

Peptide	A(v)	A(MH*-H,O)	A(MH ⁺ -NH ₃)	A(v)	A(w)	A(c _{n-1})	A(b _{n-1} +H ₂ O)	A(a _n)	A(b _n)	A(d _n)	A(internal)
DF-OMe	က	88	10.8	0.0	0.0	0.0	0.0	0.0	0.0	0.0	0.0
BDF-OMe	37	\$	8.9	0.0	0.0	0.0	0.0	0.0	0.0	0.0	0.0
#IO	ጵ	32	1.9	0.0	0.0	0.0	0.0	0.0	0.0	0.0	0.0
ECG	0	100	0.0	0.0	0.0	0.0	0.0	0.0	0.0	0.0	0.0
YECG	93	Ŋ	1.2	0.0	0.0	0.0	0.0	0.0	6.0	0.0	0.0
J. L.	-93	95	-1.2	0.0	0.0	0.0	0.0	0.0	6. O	0.0	0.0
AEKAA	-	79	13.2	0.0	1.3	0.0	0.0	0.0	5.6	0.0	2.1
AYEKAA	22	32	5.7	0.0	0.0	0.0	0.0	0.0	9.0	0.0	4.2
Diff	\$	47	7.5	0.0	1.3	0.0	0.0	0.0	2.0	0.0	-2.1
DRVYIHPF	22	20	21	2.6	1.3	0.0	0.0	0.0	0.0	0.0	0.3
BORVYIHPF	21	98	4	1.2	1.3	0.0	0.0	0.0	0.0	0.0	4 .0
Diff	श्ल	-16	-19	4.	0.0	0.0	0.0	0.0	0.0	0.0	6
GMDSLAFSGGL-NH,	0.7	0	5	0.0	0.0	0.0	0.0	0.0	0.0	0.0	0.0
GMBDSLAFSGGL-NH	1.2	23	75	0.0	0.0	0.0	0.0	0.0	0.0	0.0	0.0
Diff	7	-23	25	0.0	0.0	0.0	0.0	0.0	0.0	0.0	0:0
VQAAIDYING-NH,	4.0	4	80	0.1	0.1	0.0	0.0	0.0	4.7	0.0	4.0
VOAAIBDYING-NH,	0.8	28	8	0.0	0.0	0.0	0.0	0.2	5.8	0.0	6.0
Diff	6 .4	-14	16	0.1	0.1	0.0	0.0	-0.2	1.	0.0	-0.5
		,		(•	•		0	G G	Ġ	u C
Mean Diff	-52	20	4 .	0.3	0.2	0.0	0.0	0.0	0.0	o O	ر .

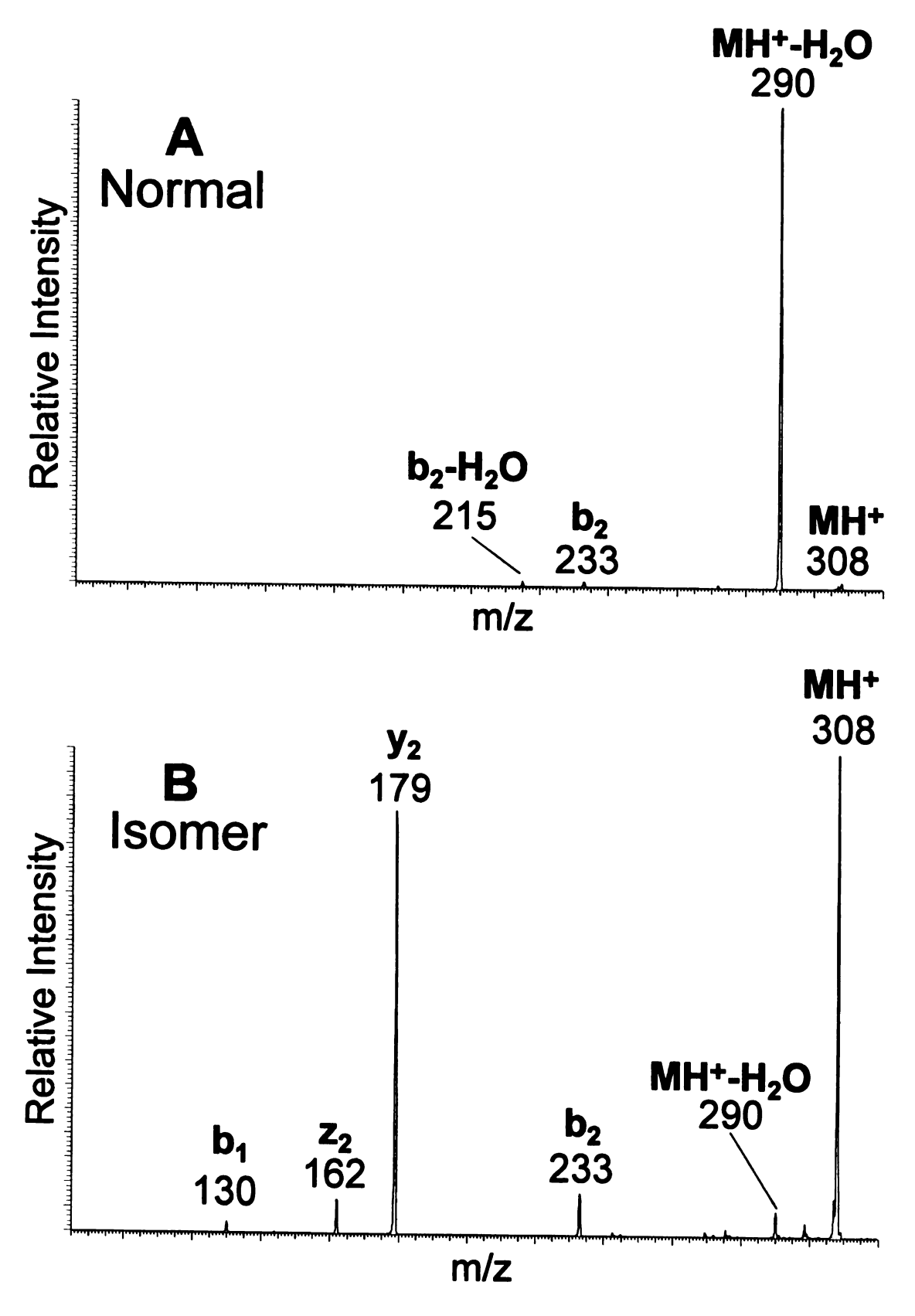


Figure 3.3. ESI-CAD-MS/MS spectra of Glu-Cys-Gly (A) and γ -Glu-Cys-Cly (B) at a relative collision energy of 14.9%.

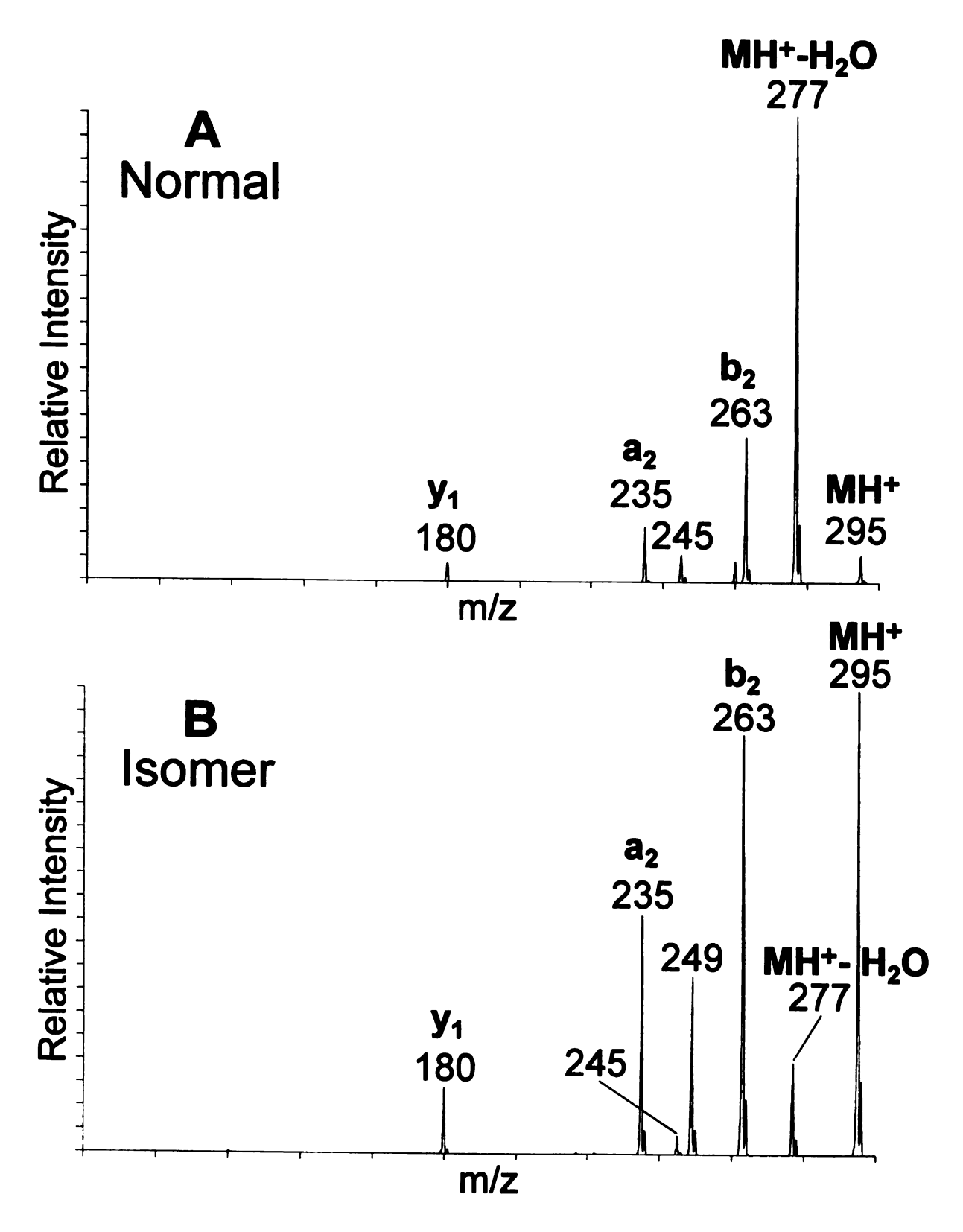


Figure 3.4. ESI-CAD-MS/MS spectra of Asp-Phe-OMe (A) and β -Asp-Phe-OMe (B) at a relative collision energy of 17.4%.

Glu:

COOH

CH₂

C-NH₂-CH-C-NH-S

CH₂-CH

N-H

HOOC-CH₂-CH₂

$$+$$

NH₃-CH-C-NH-S

B)
$$\gamma$$
-Glu:

HOOC-CH CH₂
 \uparrow N-C=O R O
H \uparrow NH₂-CH-C-NH- \uparrow

HOOC
 \uparrow N-R O
+ \uparrow NH₃-CH-C-NH- \uparrow

Figure 3.5. **y** ion formation by glutamyl (A) and γ -glutamyl (B) peptides.

the glutamate residue is not at the N-terminus, a more stable diketopiperazine neutral can be formed. γ -Glutamyl peptides (B) can form \mathbf{y} ions accompanied by a stable 5-membered pyrrolidone ring (64). The pyrrolidone neutral formed by γ -glutamyl peptides is more stable than the aziridinone neutral formed by N-terminal glutamyl peptides, and the MS/MS data suggest that the pyrrolidone neutral may be more stable than the diketopiperazine neutral.

The larger y ion abundance ratios of β-aspartyl peptides can be explained by the mechanisms in Figure 3.6 (55). Both aspartyl (A) and isoaspartyl (B) peptides can possibly transfer a proton from the side-chain to a neighboring amide nitrogen. Although this transfer produces additional charged sites on the ion, the intermediate could be stabilized by ionic interactions (represented by dotted lines on Figure 3.6). The carboxylate oxygen can then attack the amide carboxyl group to form a succinic anhydride neutral and a y fragment ion. Based on these mechanisms, the relative abundances of the y ions would be dependent on the ease of proton transfer from the acidic side-chain.

The β -aspartyl side-chain is more acidic in solution than the aspartyl side-chain. This assertion is based on the acid dissociation constants of the α - and β -carboxyl groups of aspartic acid in solution. The pK_a of the β -carboxyl (analogous to the Asp side-chain) is 3.65, and the α -carboxyl (analogous to the β -Asp side-chain) pK_a is 1.88. Similarly, the pK_a of the γ -carboxyl of glutamic acid (analogous to the Glu side-chain) is 4.25, whereas the α -carboxyl pK_a (analogous to the γ -Glu side-chain) is 2.19 (41). Although losing a proton in solution is quite different than losing a proton in the gas phase, it is possible that the β -aspartyl side-chain loses a proton more readily than the aspartyl

A) Asp:

B) β -Asp:

Figure 3.6. **y** ion formation by aspartyl (A) and β -aspartyl peptides (B).

side-chain in the gas phase. If so, the β -aspartyl peptides would be expected to produce more abundant y ions than the normal aspartyl peptides, as was observed from the abundance ratios. However, the differences in the y-ion abundances from pairs of larger isomeric peptides (10-11 residues) were much smaller than those observed for pairs of small isomeric peptides.

It is not clear why the y ion abundance ratio of angiotensin II was greater than that of $[\beta$ -Asp]¹-angiotensin II. Ionic salt bridges have been proposed to form between aspartate residues and neighboring arginine residues (75). The formation of salt bridges can significantly alter the fragmentation of peptides (76). The formation of this salt bridge may stabilize the ionized β -aspartate side-chain and limit formation of the succinic anhydride.

[MH⁺-H₂O] and [MH⁺-NH₃] Ions

The [MH⁺-H₂O] abundance ratios from pairs of small acidic peptides (2-5 residues) were noticably different for MS/MS spectra generated by FAB or ESI. For these peptide pairs, the [MH⁺-H₂O] abundance ratios were greater for normal peptides than for the isomeric peptides. The differences between glutamyl and γ -glutamyl peptides were greater than the differences observed between aspartyl and β -aspartyl peptides, as demonstrated by Figures 3.3 and 3.4. Similar results have been observed by other researchers using CI-MS (62), LSIMS-CAD-MS/MS (63, 64), and by APCI-CAD-MS/MS (65). For larger peptide pairs (8-11 residues), the abundance ratios did not follow this trend.

The differences in the [MH⁺-H₂O] abundance ratios of glutamyl and γ -glutamyl peptides can be explained by the mechanisms shown in Figure 3.7. The glutamyl peptides can readily lose water through the formation of a pyroglutamate structure (64); a similar reaction can occur in strongly acidic solutions (17). Peptides with an N-terminal γ -glutamate residue cannot lose water easily through the analogous mechanism because the product would have a strained 3-membered ring. When γ -glutamate is present at any position other than the N-terminal position, the carboxy side chain can be attacked by a different amide nitrogen to form a product with a more stable 6-membered ring.

During mass spectral analysis, aspartyl and β -aspartyl peptides probably dehydrate through the formation of a succinimide structure, as shown in Figure 3.8. This mechanism is analogous to the dehydration in solution presented in Figure 3.2. An alternative mechanism for the dehydration of aspartyl and isoaspartyl peptides was proposed by Qin (65) and is based on the high temperature dehydration of dry aspartame (77). It is not clear why dehydration occurred to a greater extent for aspartyl peptides than for β -aspartyl peptides. The mechanisms proposed in Figure 3.8 do not predict significant differences in the [MH⁺-H₂O] peak intensities of aspartyl and β -aspartyl peptides. The most likely explanation is that the competing formation of \mathbf{y} ions limits the dehydration of β -aspartyl peptides. Since the aspartyl and β -aspartyl peptides can fragment by a similar mechanism, it is not surprising that the differences in their dehydration peak intensities would be less significant for larger peptides.

Differences in the [MH⁺-NH₃] abundance ratios were observed for several pairs of peptides. However, these differences do not follow any discernible pattern. Rather,

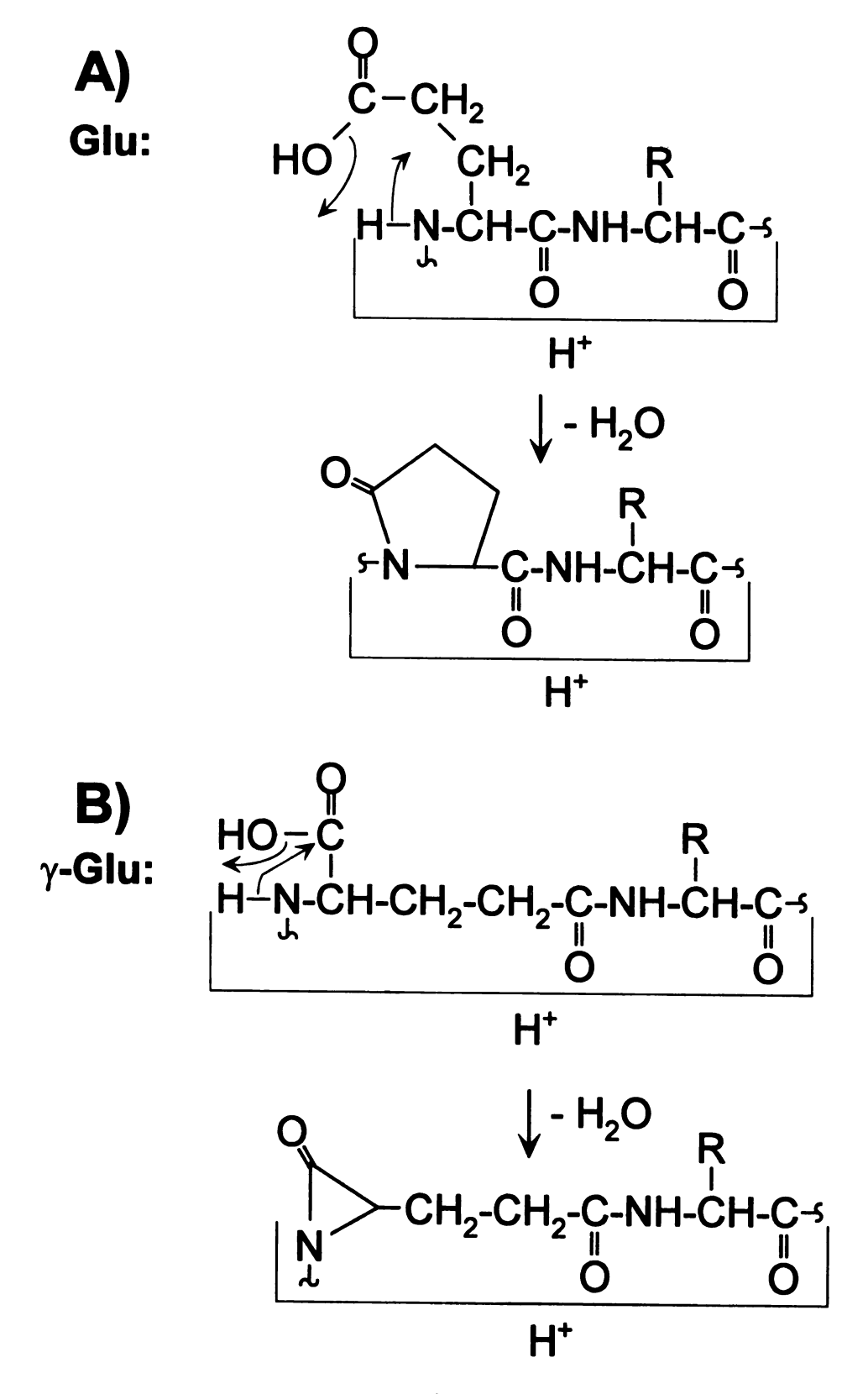


Figure 3.7. [MH $^+$ -H $_2$ 0] formation by glutamyl (A) and γ -glutamyl (B) peptides.

B) β-Asp:

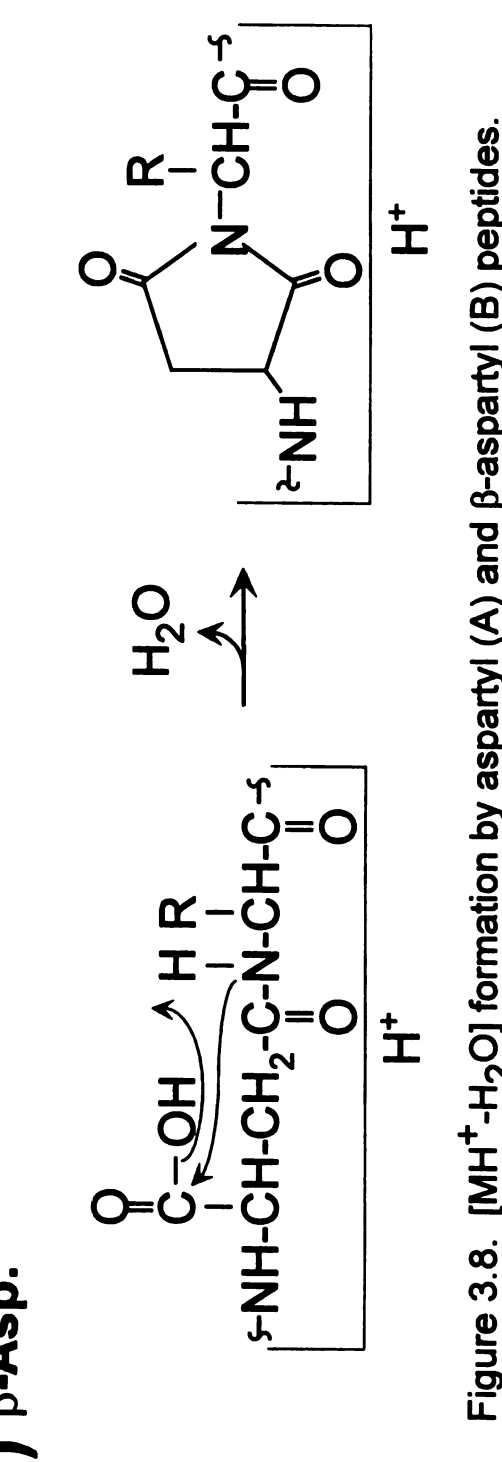


Figure 3.8. [MH⁺-H₂O] formation by aspartyl (A) and β -aspartyl (B) peptides.

the abundance ratio differences seem to be the result of large changes in the intensities of peaks representing [MH⁺-H₂O] and the y ions.

w and v Ions

Differences in the \mathbf{w} and \mathbf{v} ion abundances of aspartyl and β -aspartyl peptides have been reported by Carr *et al.* (53), but no significant differences were observed for the peptides in our study. The peptide pairs analyzed produced only low-intensity \mathbf{w} and \mathbf{v} peaks, most likely because they lacked charge localization near the C-terminus. Although no significant differences in \mathbf{w} and \mathbf{v} abundance ratios were observed for these pairs of peptides, significant differences might be observed for those with a basic residue near the C-terminus (such as tryptic peptides), when fragmented by high-energy CAD.

c_{n-1} , $b_{n-1}+H_2O$, and b_n Ions

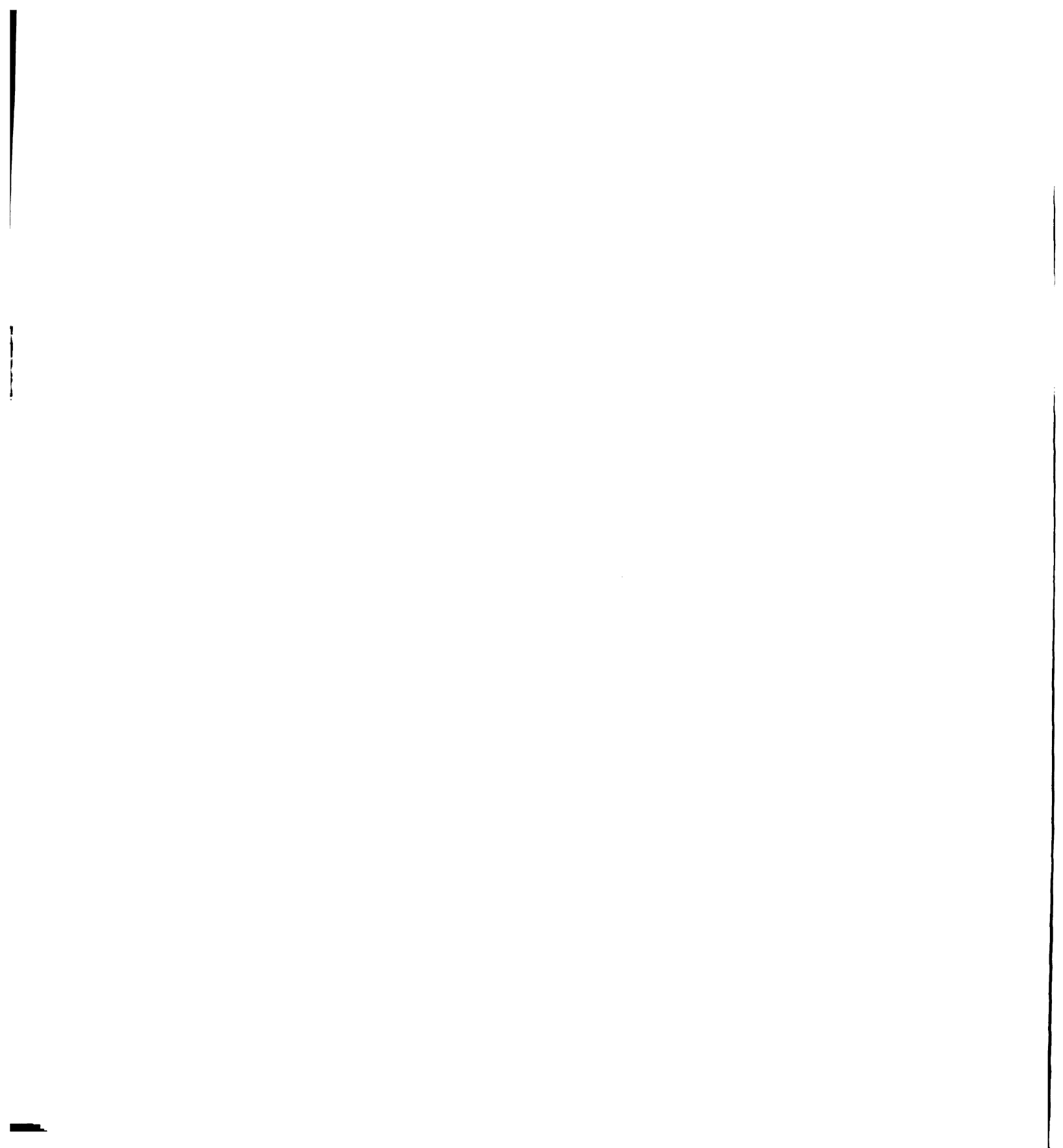
Although differences have been reported in the c_{n-1} (52), $b_{n-1}+H_2O$ (52, 69, 70) and b_n (66) peak intensities of peptide pairs with an acidic residue at the n^{th} position, no significant differences in the c_{n-1} , $b_{n-1}+H_2O$, or b_n abundance ratios were observed for the peptide pairs analyzed here. This may be because the c_{n-1} , $b_{n-1}+H_2O$, and b_n ions arising from the peptides in our study were of low abundance. It is possible that significant differences would be observed for peptide pairs with sequences that allow the formation of abundant c_{n-1} , $b_{n-1}+H_2O$, or b_n ions.

Internal Fragment Ions

Whenever internal acyl fragment ions were produced with the acidic residue at the N-terminus of the fragment, the abundance ratio was greater for the peptide containing β -aspartate or γ -glutamate than for the analogous peptide containing normal aspartate or glutamate, as demonstrated by the ESI-ISF-MS spectra in Figure 3.9. Note that the internal acyl ion at m/z 258 (EK) produced from the aspartyl peptide (A) is less abundant than the corresponding fragment produced from the β -aspartyl peptide (B). Unfortunately, the peak intensities of these fragments were too small for the differences in abundance ratios to be statistically significant, but it is possible that the presence of β -aspartate or γ -glutamate enhances the formation of internal acyl ions.

B. Charge-derivatized Peptides

Charge-derivatization of peptides localizes the charge away from the peptide backbone, and minimizes or eliminates fragmentation by charge-driven mechanisms (60). Charge-derivatization of the peptides in this study produced striking changes in fragmentation patterns during analysis by MS/MS. Examination of the MS/MS spectra of charged derivatives suggested that the presence of a β -aspartate or γ -glutamate residue at the \mathbf{n}^{th} position may alter the relative intensities of $\mathbf{*c_{n-1}}$, $\mathbf{*b_{n-1}} + \mathbf{H_2O}$, $\mathbf{*d_n}$, $\mathbf{*a_n}$, and $\mathbf{*b_n}$ fragment peaks. The nomenclature used here for the fragment ions of charge-derivatized peptides will be presented in a review of charge-derivatization techniques (78) and corresponds to the nomenclature of protonated peptides when the mass shift (due to derivatization) in (singly-charged) precursor ions is taken into account. An asterisk is added to denote the presence of the charged derivative moiety. It is necessary to



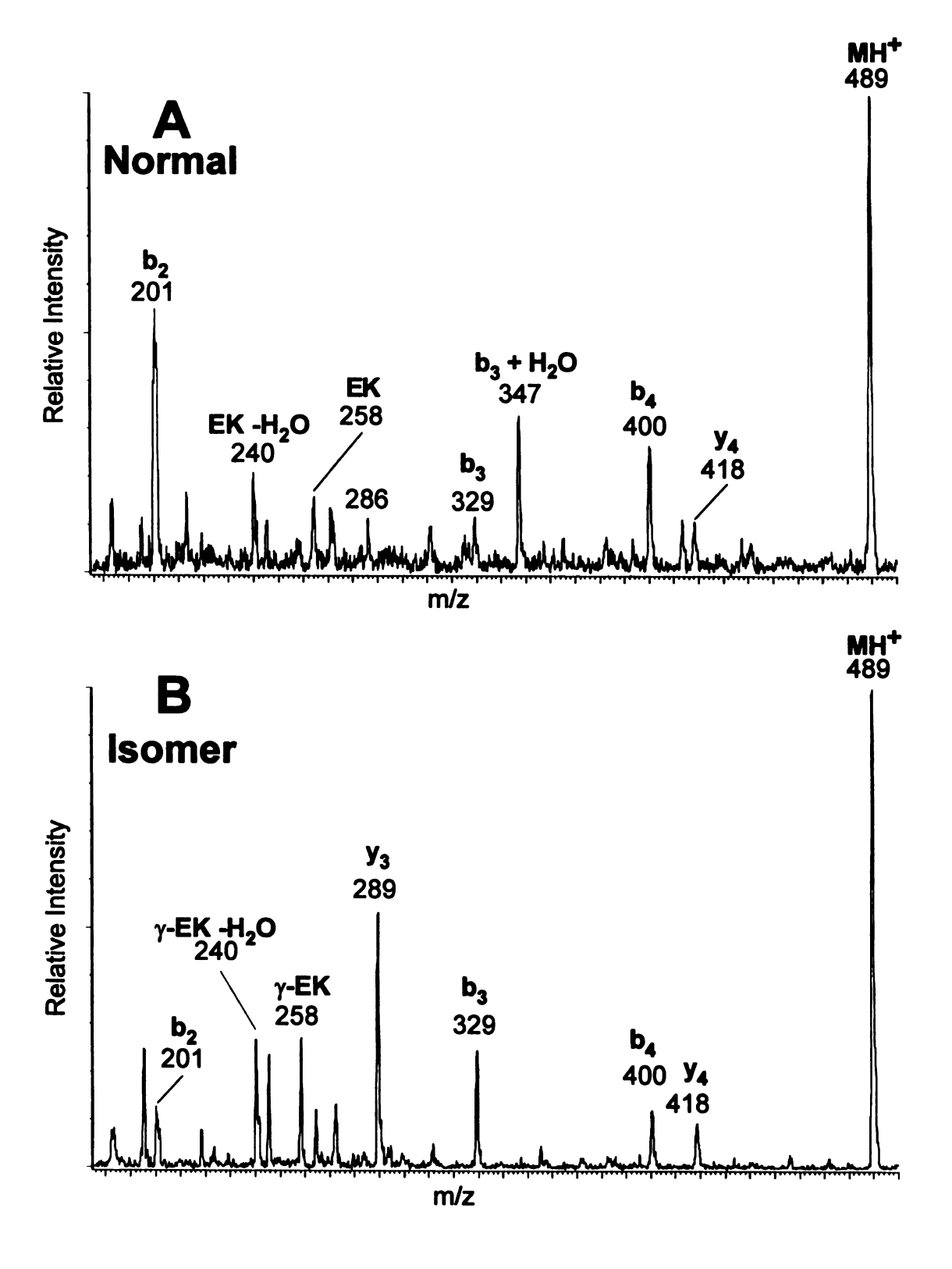


Figure 3.9. ESI-ISF-MS spectra of AEKAA (A) and A- γ -E-KAA (B) at a cone voltage of 55 V.

distinguish between the fragment ions of underivatized and charge-derivatized peptides because the structures and fragmentation mechanisms may be different (78). In order to evaluate the relative intensities of these fragment peaks, MS/MS spectra for the derivatized peptides were obtained in triplicate on each instrument and branching ratios for each of the fragment peaks were calculated using the following equation:

$$B(x) = 100 * I(x) / [I(*c_{n-1}) + I(*b_{n-1}+H_2O) + I(*d_n) + I(*a_n) + I(*b_n)]$$
 where $B(x)$ is the branching ratio of a fragment ion peak and $I(x)$ is the intensity of that particular fragment ion peak. Unlike the similar equation used to compare the relative abundances of fragment ions from underivatized peptides, the values determined by this equation represent true branching ratios because all of the fragment ions are believed to come from the same precursor, an N-terminal derivatized peptide with the charge located

To determine branching ratios for the ESI-CAD-MS/MS experiments, the relative collision energy was raised until the most intense fragment peak was approximately equal to the intensity of the precursor ion peak. For singly-charged precursor ions, the relative collision energy was in the range of 37-60% (of the maximum collision energy that can be generated by the instrument). The branching ratios obtained by FAB-CAD-MS/MS, MALDI-PSD, and ESI-CAD-MS/MS are presented in Tables 3.4-3.6. The standard deviations for these ratios were ≤ 9 units.

*b_n Ions

on the derivative moiety.

The differences in the * $\mathbf{b_n}$ branching ratios of charge-derivatized peptides were quite large. Most derivatized peptides with β -aspartyl or γ -glutamyl residues at the $\mathbf{n^{th}}$

Table 3.4. Branching ratios for derivatized peptides analyzed by FAB-CAD-MS/MS.

Peptide	B(*c _{n-1})	$B(*b_{n-1}+H_2O)$	$B(*d_n)$	B(*a _n)	$B(*b_n)$
DF-OMe	9.9	7.7	36	39	8
βDF-OMe	7.9	13.3	21	24	35
Diff	2.0	-5.6	15	15	-27
ECG	2.0	13	47	34	3
γECG	10.7	31	24	11	24
Diff	-8.7	-18	23	24	-21
AEKAA	14	10	63	7.7	6
ΑγΕΚΑΑ	12	35	22	11.6	20
Diff	2	-25	41	-3.9	-14
DRVYIHPF	11	3	31	23	31
βDRVYIHPF	15	14	14	12	44
Diff	-4	-11	17	11	-13
GMDSLAFSGGL-NH₂	16	10	39	24	10
GMBDSLAFSGGL-NH₂	21	23	19	17	19
Diff	-5	-13	20	7	-9
VQAAIDYING-NH₂	19	10	28	21	23
VQAAIβDYING-NH₂	16	11	21	29	23
Diff	3	-1	7	-8	0
Mean Diff	-1.5	-12	20	8.2	-15

Table 3.5. Branching ratios for derivatized peptides analyzed by MALDI-PSD.

Peptide	B(*c _{n-1})	B(*b _{n-1} +H ₂ O)	B(*d _n)	B(*a _n)	B(*b _n)
DF-OMe	28	14	37	6.5	15
βDF-OMe	16	29	5	1.7	49
Diff	12	-15	32	4.8	-34
ECG	0.0	0.0	32	63	5
γECG	0.0	0.0	5	14	81
Diff	0.0	0.0	27	49	-76
AEKAA	0.0	3	95	1	1
A _Y EKAA	0.0	74	1	11	13
Diff	0.0	-71	94	-10	-12
DRVYIHPF	18	10	16	2.4	53
βDRVYIHPF	24	20	8	1.3	46
Diff	-6	-10	8	1.1	7
GMDSLAFSGGL-NH ₂	18	16	41	1.9	23
GMβDSLAFSGGL-NH ₂	11	36	18	1.6	33
Diff	7	-20	23	0.3	-10
VQAAIDYING-NH2	18	17	34	2.1	29
VQAAIβDYING-NH₂	18	38	15	2.2	26
Diff	0	-21	19	-0.1	3
Mean Diff	2.2	-23	34	7.5	-21

Table 3.6. Branching ratios for derivatized peptides analyzed by ESI-CAD-MS/MS.

Peptide	B(*c _{n-1})	$B(*b_{n-1}+H_2O)$	$B(*d_n)$	$B(*a_n)$	$B(*b_n)$
DF-OMe	11.2	5.3	21	0.4	62
βDF-OMe	2.3	7.8	1	0.0	89
Diff	8.9	-2.5	20	0.4	-27
ECG	0.0	0.0	0.0	0.0	0.0
γECG	0.0	0.0	0.0	0.0	0.0
Diff	0.0	0.0	0.0	0.0	0.0
AEKAA	0.9	13	81	1	4
ΑγΕΚΑΑ	0.8	27	0	22	50
Diff	0.1	-14	81	-21	-46
DRVYIHPF	5.5	0.5	8.1	0.0	86
βDRVYIHPF	10.0	5.7	8.9	1.0	74
Diff	-4.5	-5.2	-0.8	-1.0	12
GMDSLAFSGGL-NH₂	2.8	4.7	18	0.1	75
GMBDSLAFSGGL-NH₂	2.8	5.2	18	0.1	74
Diff	0.0	-0.5	0	0.0	1
VQAAIDYING-NH₂	0.6	1.2	0.6	0.1	97
VQAAIβDYING-NH₂	4.0	2.3	2.6	0.1	91
Diff	-3.4	-1.1	-2.0	0.0	6
Mean Diff	0.2	-4.6	20	-4.3	-11

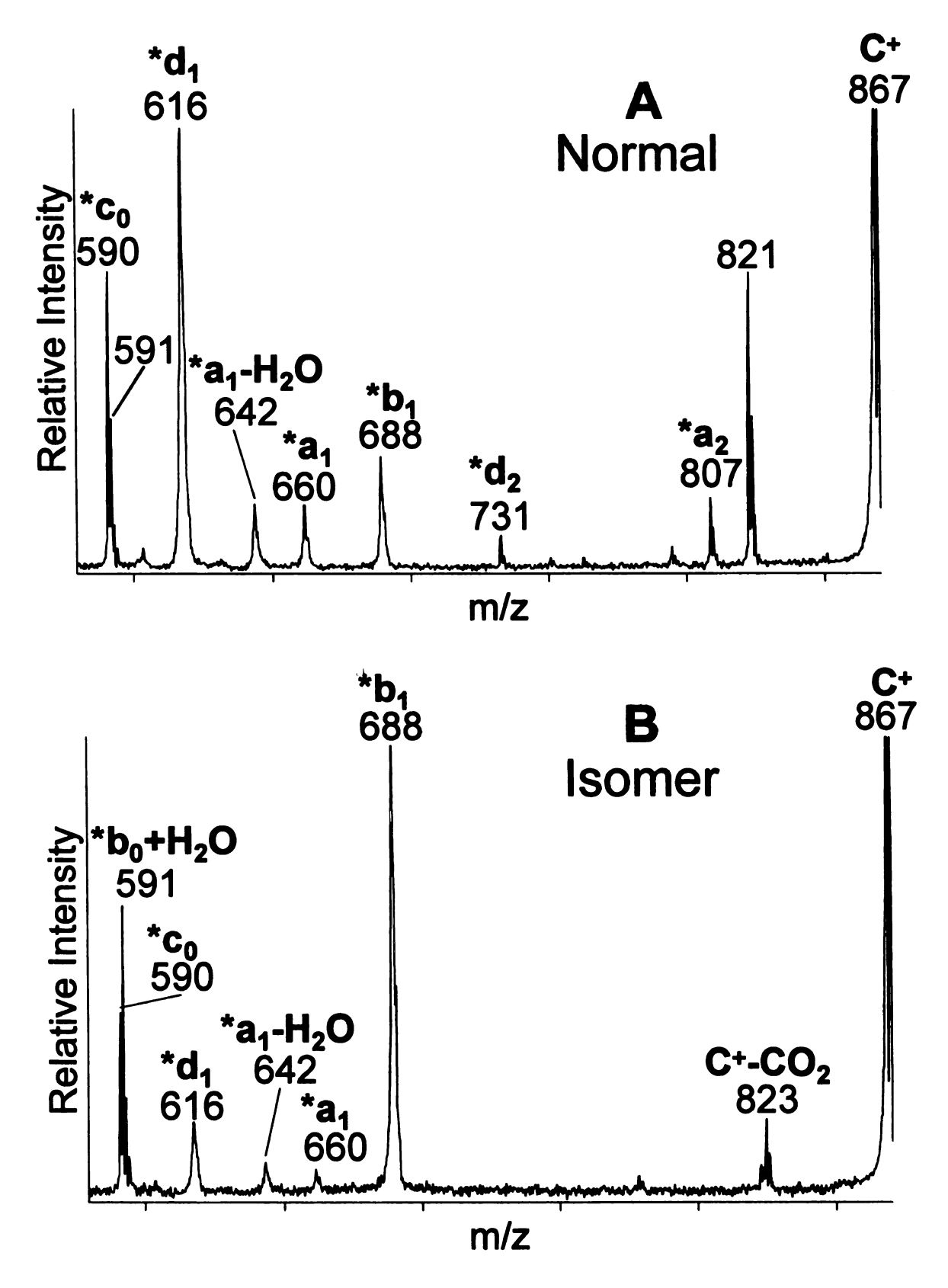


Figure 3.10. MALDI-PSD spectra of TMPP+-Ac-Asp-Phe-OMe (A) and TMPP+-Ac-β-Asp-Phe-OMe (B).

position had larger $B(*b_n)$ ratios than analogous derivatized peptides with normal aspartyl or glutamyl residues. An example of this difference is provided in Figure 3.10. Exceptions to the trend were observed for larger derivatized peptides (8 or more residues) analyzed by MALDI-PSD and ESI-CAD-MS/MS. Also, the ESI-CAD-MS/MS spectra of TMPP*-Ac-Glu-Cys-Gly and TMPP*-Ac- γ -Glu-Cys-Gly were dominated by a rearrangement peak at m/z 607 (TMPP*-Ac-SH). As a result, it was not possible to calculate reliable branching ratios for these derivatives when analyzed by ESI-CAD-MS/MS. For the larger derivatized peptides, the differences in the $B(*b_n)$ ratios were not statistically significant based on a two-sample t-test at a 95% confidence level. Lloyd and coworkers (66) also observed more intense b_n fragment peaks in the FAB-high energy CAD-MS/MS spectra of underivatized peptides with β -Asp or γ -Glu at residue n than for analogous peptides with Asp or Glu at residue n.

The differences in the $B(^*b_n)$ ratios can be rationalized by the mechanisms presented in Figure 3.11. Mechanism A is an adaptation from that presented by Yu et al. (55) to explain the enhanced b_n formation from underivatized peptides with an aspartate residue at position n. A similar mechanism was proposed by Summerfield, Whiting, and Gaskell (75). According to the mechanism, the acidic proton of the aspartate side-chain can be transferred to the neighboring amide nitrogen. The intermediate can be stabilized by ionic interactions (represented by dotted lines in Figure 3.11). The ionized side-chain can then attack the amide carbonyl to form a *b_n ion with a stable succinic anhydride structure. Figure 3.11B shows a similar mechanism for the formation of *b_n ions from derivatized β -aspartyl peptides. The side-chain of the β -aspartate residue is more acidic in solution than the aspartate side-chain (41) and could possibly be more acidic in the gas

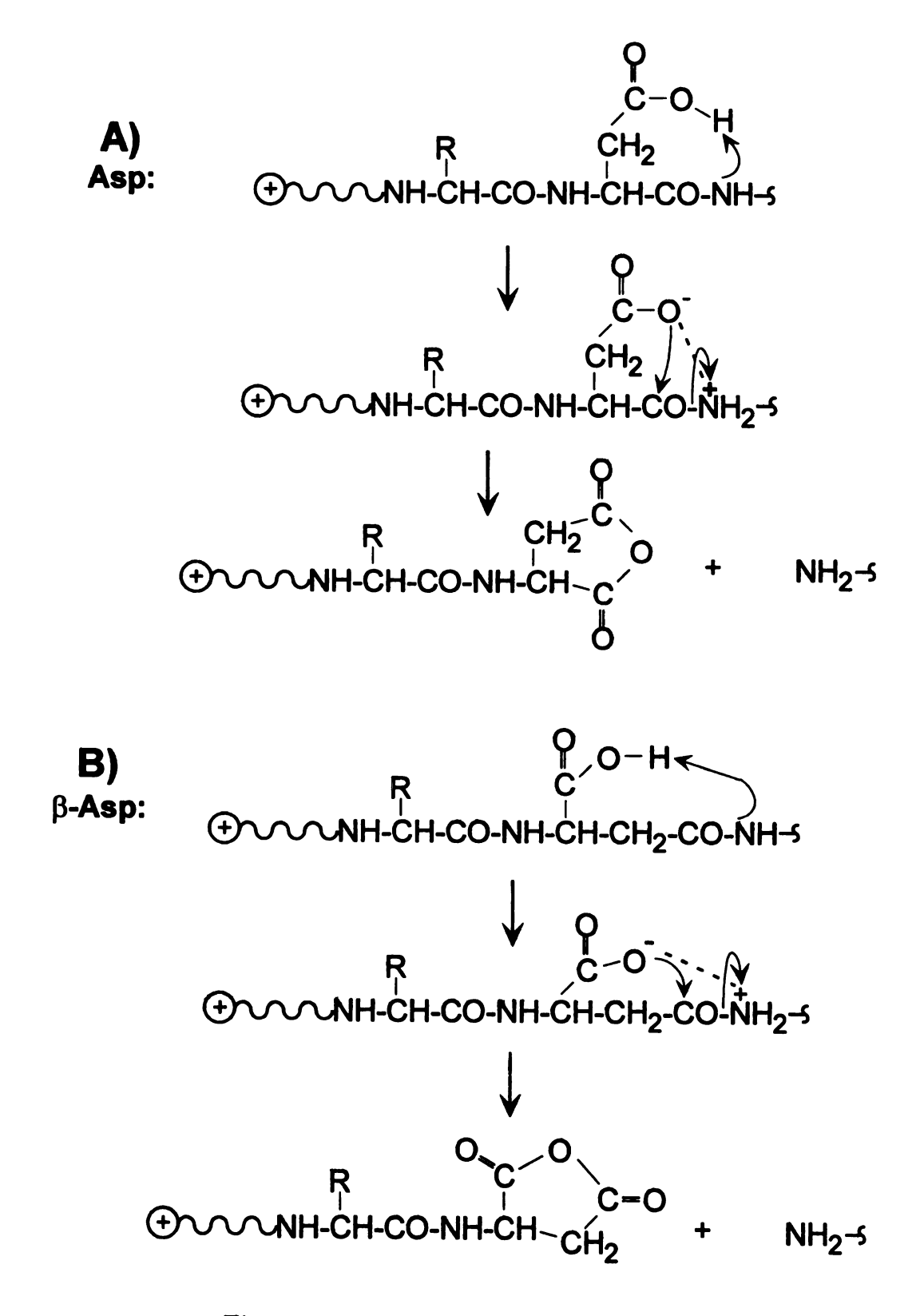


Figure 3.11. * $\mathbf{b_n}$ formation by derivatized aspartyl (A) and β -aspartyl (B) peptides.

phase. If so, the initial proton transfer would proceed more readily for β -aspartyl peptides, resulting in greater $*b_n$ ion formation.

The $*\mathbf{b_n}$ fragmentation mechanisms were investigated further by preparing methyl esters of selected TMPP⁺-Ac-derivatized peptides to eliminate the acidic proton on the side-chains. When the esterified TMPP⁺-Ac-derivatized peptides were analyzed by MALDI-PSD, the $*\mathbf{b_n}$ fragment peaks were absent, as shown in Figure 3.12. This verifies that the transfer of a proton from the acidic side-chain is necessary for the formation of $*\mathbf{b_n}$ fragment ions in agreement with the mechanism shown in Figure 3.11.

Derivatized glutamyl and γ -glutamyl peptides could form $*b_n$ fragments by mechanisms similar to those in Figure 3.11, producing $*b_n$ ions with a six-membered ring instead of the five-membered ring produced by aspartyl and β -aspartyl peptides. If the relative solution phase acidities hold in the gas phase, the derivatized γ -glutamyl peptides would be expected to form more intense $*b_n$ peaks than the derivatized glutamyl peptides because of the difference in the side-chain acidities. This is consistent with the data as summarized by the $*b_n$ branching ratios in Tables 3.4-3.6.

The similarity of the branching ratios for larger acidic peptides analyzed by MALDI-PSD and ESI-CAD-MS/MS is probably the result of competition from the greater number of other fragmentation pathways available.

*d_n Ions

The branching ratios for the $*d_n$ fragment ions also had large differences for analogous pairs of peptides. For purposes of this study, the $*d_n$ fragment of derivatized peptides containing β -Asp or γ -Glu at residue n is defined as the fragment with the same

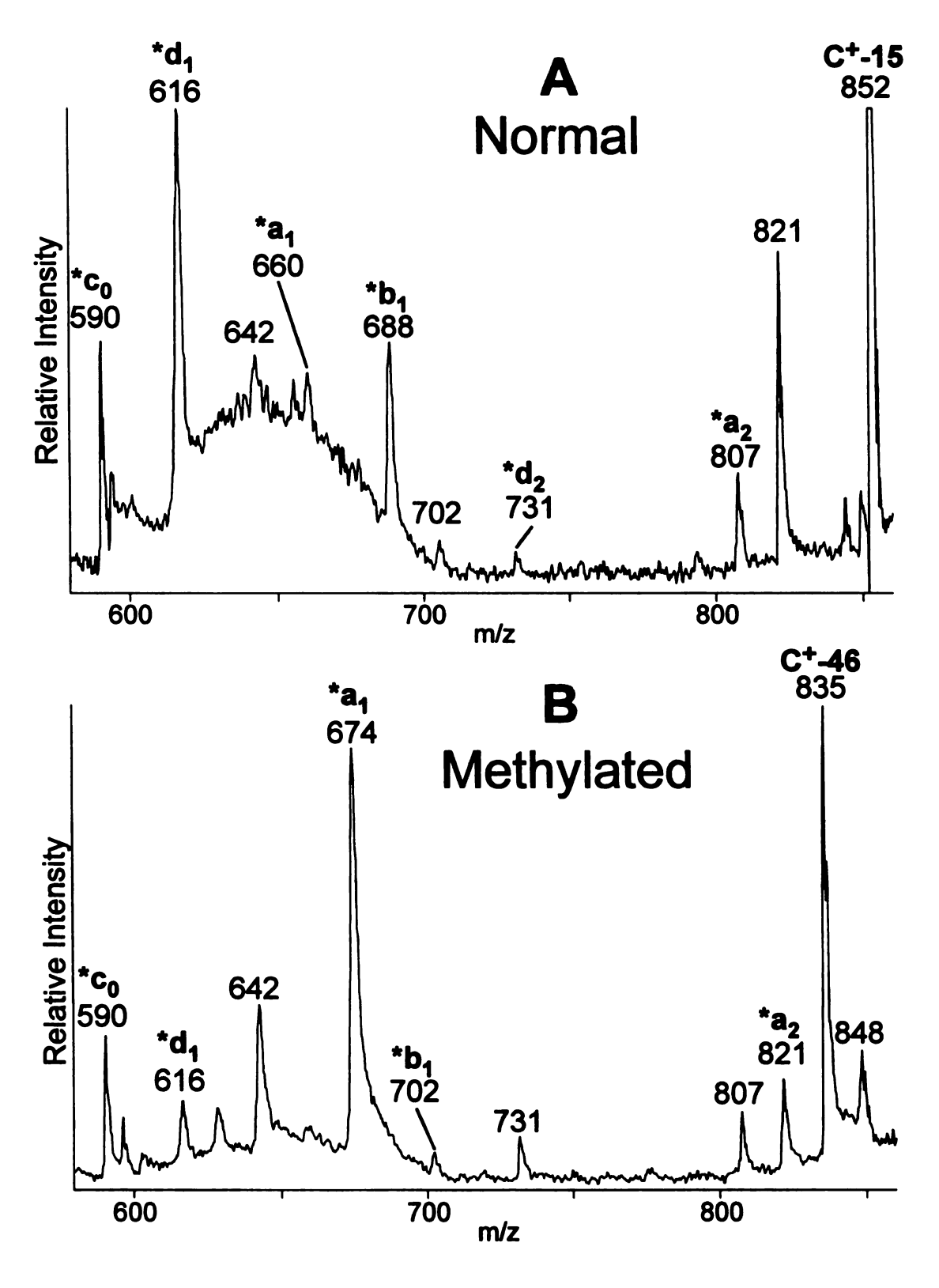


Figure 3.12. MALDI-PSD Spectra of TMPP⁺-Ac-Asp-Phe-OMe (A) and Methylated TMPP⁺-Ac-Asp-Phe-OMe (B).

m/z value as the $*\mathbf{d_n}$ fragment of an analogous derivatized peptide containing normal Asp or Glu. For β -aspartyl or γ -glutamyl peptide derivatives, these $*\mathbf{d_n}$ fragments do not result from cleavage between the β - and γ - carbons of the side-chain, but these fragments may have the same structures as the $*\mathbf{d_n}$ fragments of normal aspartyl or glutamyl peptide derivatives, as illustrated by Figure 3.14.

For all the derivatized peptides analyzed by FAB-CAD-MS/MS and MALDI-PSD, the derivatives containing normal Asp or Glu produced *d_n peaks that were more intense (as determined by branching ratios) than the *d_n peaks produced from the analogous derivatized peptide containing β -Asp or γ -Glu. An example of these differences is shown in Figure 3.13. The same trend was observed for TMPP⁺-Ac-TMPP⁺-Ac-Ala-Glu-Lys-Ala-Ala/ aspartame/TMPP⁺-Ac-β-aspartame and for TMPP⁺-Ac-Ala-D-γ-Glu-Lys-D-Ala-D-Ala as analyzed by ESI-CAD-MS/MS. The ESI-CAD-MS/MS spectra of TMPP+-Ac-Glu-Cys-Gly and TMPP+-Ac-γ-Glu-Cys-Gly were dominated by a rearrangement peak at m/z 607 (TMPP+-Ac-SH), so none of the expected peaks was observed. For larger derivatized peptides (8 or more residues), no significant differences in the $*d_n$ branching ratios, $B(*d_n)$, were observed. These fragmentation differences provide clues to the fragmentation mechanisms for the formation of *d_n fragment ions. These fragments probably do not form by the same mechanism as the d_n ions of underivatized peptides (3) because \mathbf{d}_n fragments are generally not observed during low-energy CAD (79).

Possible mechanisms for the formation of $*d_n$ fragment ions are shown in Figure 3.14. The top mechanism was proposed by Liao, Huang, and Allison (60) and the lower mechanism is an adaptation of it. Both mechanisms involve a proton transfer from the

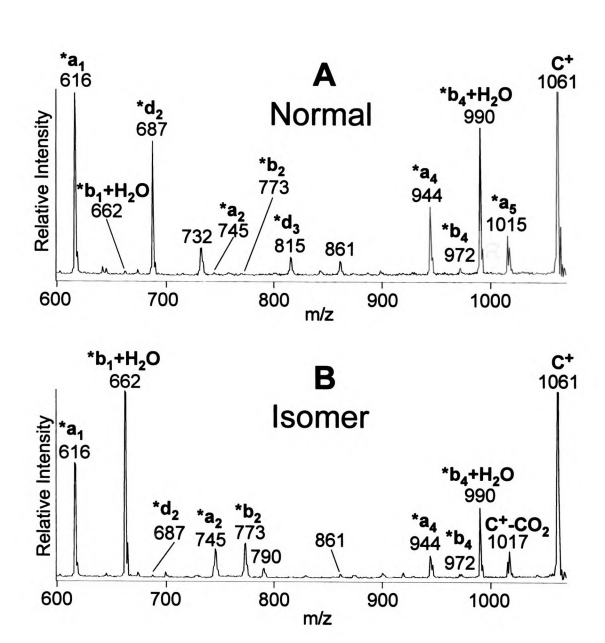


Figure 3.13. MALDI-PSD spectra of derivatized AEKAA (A) and A-γ-EKAA (B).

B) β-Asp:
$$C = O - H$$
 R R $C = O - H$ R C

Scheme 3.14. * $\mathbf{d_n}$ formation by derivatized aspartyl (A) and β -aspartyl (B) peptides.

acidic side-chain to the C-terminal fragment. It is likely that the side-chain is involved in fragmentation because $*\mathbf{d_n}$ fragments are not observed for most residues during analysis by MALDI-PSD or low-energy CAD. The formation of $\mathbf{d_n}$ fragment ions from underivatized peptides during analysis by low-energy CAD has been observed by other researchers (75, 80) for peptides with an acidic residue at the $\mathbf{n^{th}}$ position and a basic residue near the N-terminus. Selected peptide derivatives were methylated to eliminate the acidic proton. After methylation, the $*\mathbf{d_n}$ peaks were less intense, but were still present, as shown in Figure 3.12. This result suggests that transfer of an acidic proton is involved in the preferred fragmentation mechanism, but $*\mathbf{d_n}$ fragments can also form through other mechanisms.

It is not clear why the $*d_n$ branching ratios are larger for derivatized aspartyl and glutamyl peptides than for the analogous derivatized β -aspartyl and γ -glutamyl peptides. The mechanisms in Figure 3.14 suggest that both aspartyl and β -aspartyl peptide derivatives should be able to form $*d_n$ fragment ions with comparable efficiency. The difference in $*d_n$ branching ratios may be the result of competition from $*b_n$ and $*b_{n-1}+H_2O$ formation which are favored by β -aspartyl and γ -glutamyl peptide derivatives.

*b_{n-1}+H₂O Ions

For the derivatized peptides analyzed with an acidic residue at the n^{th} position, the $^*b_{n-1}+H_2O$ branching ratio was larger for the derivatized β -aspartyl or γ -glutamyl peptide of a given pair than the branching ratio for the corresponding derivatized aspartyl or glutamyl peptide. However, not all of the differences in the branching ratios were statistically significant as determined by a two-sample t-test. When the derivatized

peptides studied had the acidic residue at the N-terminal position, a $*b_0+H_2O$ ion (TMPP⁺-Ac-OH) was formed with an m/z value of 591. The formation of $*b_{n-1}+H_2O$ ions from charge-derivatized β -aspartyl peptides was observed by Bean and Carr (69) during analysis by FAB-CAD-MS/MS. Similarly, the formation of $b_{n-1}+H_2O$ fragments from underivatized β -aspartyl peptides has been observed by several researchers (52, 69, 70). The formation of analogous fragments from underivatized and charge-derivatized peptides suggests that the both $b_{n-1}+H_2O$ and $*b_{n-1}+H_2O$ fragments may form by charge-remote mechanisms.

The differences in $*b_{n-1}+H_2O$ branching ratios can be explained by the mechanisms presented in Figure 3.15. The bottom mechanism is adapted from that proposed by Papayannopoulos and Biemann (52) to explain the formation of $b_{n-1}+H_2O$ ions from underivatized peptides with β -aspartate at the n^{th} position. Aspartyl peptides cannot form

* $\mathbf{b_{n-1}}$ + $\mathbf{H_2O}$ fragment ions by this mechanism (A) because one of the neutral fragments produced would be unstable. Derivatized γ -glutamyl peptides could form * $\mathbf{b_{n-1}}$ + $\mathbf{H_2O}$ fragments by a mechanism similar to the lower mechanism in Figure 3.15. Derivatized peptides with a normal glutamyl residue cannot readily form * $\mathbf{b_{n-1}}$ + $\mathbf{H_2O}$ fragments by the same mechanism because one of the neutral fragments formed would be unstable, just as for the derivatized aspartyl peptides.

The intensity of the $\mathbf{*b_{n-1}} + \mathbf{H_2O}$ peak produced from a charge-derivatized β -aspartyl peptide with an esterified side-chain was much lower than the intensity of the same derivatized peptide with an unmodified side-chain (the $\mathbf{*b_{n-1}} + \mathbf{H_2O}$ branching ratio decreased from 24 to 6 as a result of esterification). This indicates that a proton transfer

Figure 3.15. * $\mathbf{b_{n-1}}$ + $\mathbf{H_2O}$ formation by derivatized aspartyl (A) and β -aspartyl (B) peptides.

is involved in the formation of $*b_{n-1}+H_2O$ fragments by derivatized β -aspartyl peptides, and it is consistent with the mechanism presented in Figure 3.15.

*c_{n-1} Ions

The differences in the *c_{n-1} branching ratios of normal derivatized peptides and isomeric derivatized peptides were small and did not follow any clear trend. However, for many of the derivatized aspartyl peptides, the *c_{n-1} peak was more intense than the adjacent *b_{n-1}+H₂O peak as shown in the top portion of Figure 3.10 (see peaks at m/z 590 and 591). Papayannopoulos and Biemann (52) reported a similar observation for underivatized peptides. The greater intensity of the *c_{n-1} peaks than the *b_{n-1}+H₂O peaks of derivatized aspartyl peptides is probably a result of a less favorable pathway for derivatized aspartyl peptides to form *b_{n-1}+H₂O fragment ions, as depicted in Figure 3.15A. At least some of the intensity attributed to the *b_{n-1}+H₂O peaks actually arises from the isotope peak of the *c_{n-1} ions, so the differences between the *c_{n-1} and *b_{n-1}+H₂O peak intensities should be greater than that shown in the branching ratios. It is interesting that for many of the derivatized glutamyl peptides, the *b_{n-1}+H₂O peak is more intense than the *c_{n-1} peak.

Liao, Huang, and Allison (60) proposed a mechanism for the formation of $\mathbf{*c_{n-1}}$ fragments from charge-derivatized peptides with an aspartate at residue \mathbf{n} . This mechanism is shown at the top of Figure 3.16. The bottom of Figure 3.16 shows that derivatized β -aspartyl peptides are less likely to form $\mathbf{*c_{n-1}}$ fragment ions by this mechanism because the neutral fragment produced would be unstable. However, when

Figure 3.16. ${}^*c_{n-1}$ formation by derivatized aspartyl (A) and β -aspartyl (B) peptides.

the aspartyl side-chain of a derivatized peptide was converted to a methyl ester, $*c_{n-1}$ fragment ions were still readily formed, as shown in Figure 3.12. This result contradicts the mechanism of Figure 3.16, because it involves the transfer of an acidic proton from the aspartyl side-chain for $*c_{n-1}$ ion formation. The mechanism of Downard and Biemann (81) can be adapted to describe the formation of $*c_{n-1}$ fragment ions from charge-derivatized aspartyl and glutamyl peptides without the transfer of a proton from the carboxylic acid group, as shown in Figure 3.17. In the top mechanism, the hydrogen atom on the methylene group is activated because it is adjacent to a carbonyl. β -Aspartyl peptides cannot form $*c_{n-1}$ fragment ions by this mechanism because there is no methylene group on the β -aspartyl side-chain. The formation of $*c_{n-1}$ ions from derivatized glutamyl peptides is not favored because the neutral formed would be unstable. It is not clear whether $*c_{n-1}$ fragment ions form exclusively through the mechanisms in Figure 3.17 or whether they form by a combination of the mechanisms shown in Figure 3.16 and 3.17.

*a_n Ions

The differences in the $*a_n$ branching ratios are small. For many derivatized peptide pairs, the $*a_n$ branching ratio was larger for the derivatized peptide containing a normal aspartyl or glutamyl residue than for the derivatized peptide containing a β -aspartyl or γ -glutamyl residue. This difference in branching ratios is probably a default result of significant changes in the branching ratios of some of the other fragmentation products as described earlier. Since the differences in the $*a_n$ branching ratios are minor,

Figure 3.17. *c_{n-1} formation by derivatized aspartyl (A) and glutamyl (B) peptides without tranfer of the acidic proton.

it is likely that the $*a_n$ fragmentation mechanism does not involve the acidic side-chain. A reasonable fragmentation mechanism was proposed by Liao, Huang and Allison (60).

$[C-H_2O]^+$ and $[C+H-H_2O]^{2+}$ Ions

In contrast to the spectra of underivatized peptides, derivatized peptides analyzed by FAB-CAD-MS/MS, MALDI-PSD, ESI-triple quadrupole-MS/MS, or ESI-ISF-MS produced extremely weak [C-H₂O]⁺ peaks. However, ESI-triple quadrupole-MS/MS spectra acquired from the doubly-charged precursor, [C+H]²⁺, of TMPP⁺-Ac-AEKAA produced a significant [C+H-H₂O]²⁺ fragment ion peak, as shown in Figure 3.18. The low intensities of the [C-H₂O]⁺ peaks suggests that a mobile proton may be necessary to produce intense dehydration peaks from acidic peptides during analysis by these techniques. When dehydration did occur, no difference in the relative intensities of the [C+H-H₂O]²⁺ peaks of the normal or isomeric peptide were observed.

IV. Conclusions

There are differences in the fragmentation patterns of pairs of underivatized aspartyl or glutamyl peptides and their analogous β -aspartyl or γ -glutamyl peptides; the relative abundances of fragment ions are compared on the basis of branching ratios. For the peptides in this study, β -aspartyl or γ -glutamyl peptides produced more abundant y ions and less abundant [MH⁺-H₂O] ions than those produced by the corresponding normal aspartyl or glutamyl peptides. However, these differences are less apparent for larger peptides (8-11 residues). Fragmentation mechanisms are proposed that rationalize the differences observed. Differences in the abundances of internal acyl ions were

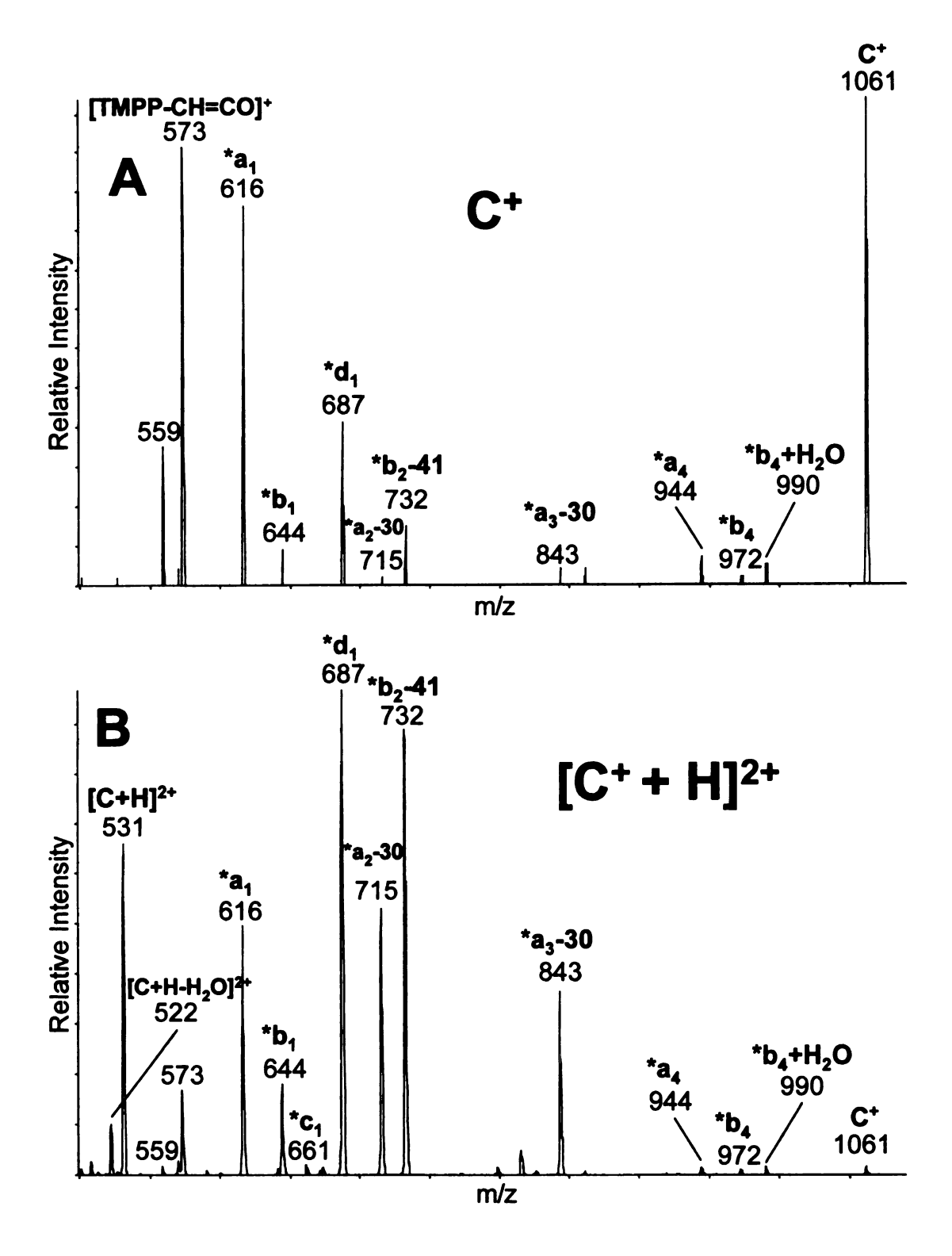


Figure 3.18. ESI-CAD-MS/MS spectra of the C⁺ (A) and [C+H]²⁺ (B) precursor ions of TMPP⁺-Ac-AEKAA at collision energies of 72.5 eV and 32.5 eV, respectively.

observed, but the intensities of the corresponding peaks were too small for the differences to be statistically significant. No differences in the abundances of \mathbf{v} , \mathbf{w} , \mathbf{c}_{n-1} , $\mathbf{b}_{n-1} + \mathbf{H}_2\mathbf{O}$, or \mathbf{b}_n ions were observed for the peptide pairs in this study, but differences might be observed for peptides that produce these fragment ions in large abundance.

The fragmentation patterns of pairs of charge-derivatized peptides also had several differences. Charge-derivatized β -aspartyl or γ -glutamyl peptides produced more abundant * \mathbf{b}_n and * \mathbf{b}_{n-1} + $\mathbf{H}_2\mathbf{O}$ ions, and less abundant * \mathbf{d}_n ions than the analogous charge-derivatized aspartyl or glutamyl peptides. Mechanisms are presented that rationalize the greater abundance of * \mathbf{b}_n and * \mathbf{b}_{n-1} + $\mathbf{H}_2\mathbf{O}$ ions for derivatized β -aspartyl and γ -glutamyl peptides. The decrease in the * \mathbf{d}_n branching ratios could not be rationalized mechanistically, and it appears to be a default result of competition by the * \mathbf{b}_n and * \mathbf{b}_{n-1} + $\mathbf{H}_2\mathbf{O}$ fragmentation pathways. Methylation of the acidic side-chains showed that transfer of an acidic proton from the side-chain plays a role in the formation of * \mathbf{b}_n , * \mathbf{d}_n , and * \mathbf{b}_{n-1} + $\mathbf{H}_2\mathbf{O}$ ions. As with the underivatized peptides, the differences in the branching ratios were smaller for pairs of larger (8-11 residues) charge-derivatized peptides.

Although differences in the fragmentation patterns of pairs of underivatized peptides and pairs of charge-derivatized peptides were observed, these differences appear to be analytically useful only for small peptides (2-5 residues). For larger peptides (8-11 residues), these differences become smaller as a result of competition from the greater number of available fragmentation pathways.

V. References

- 1. Edman, P. Acta Chem. Scand. 1950, 4, 238-293.
- Johnson, R. S.; Martin, S. A.; Biemann, K.; Stults, J. T.; Watson, J. T. Anal. Chem.
 1987, 59, 2621-2625.
- Johnson, R. S.; Martin, S. A.; Biemann, K. Int. J. Mass Spectrom. Ion Processes.
 1988, 86, 137-154.
- 4. Nakamura, K.; Higashiura, K.; Nishimura, N.; Yamamoto, A.; Tooyama, I.; Kimura, H.; Ienaga, K. J. Neurochem. 1990, 55, 1064-1066.
- 5. Reichelt, K. L. J. Neurochem. 1970, 17, 19-25.
- 6. Buchanan, D. L.; Haley, E. E.; Markiw, R. T. Biochemistry 1962, 1, 612-620.
- Martin, S. A.; Karnovsky, M. L.; Krueger, J. M.; Pappenheimer, J. R.; Biemann, K. J. Biol. Chem. 1984, 20, 12652-12658.
- 8. Lou, M. F. Biochemistry 1975, 14, 3503-3508.
- 9. Klosterman, H. J.; Lamoureux, G. L.; Parsons, J. L. Biochemistry, 1967, 6, 170-177.
- 10. Van Heijenoort, J.; Elbaz, L.; Dezélée, P.; Petit, J.-F.; Bricas, E.; Ghuysen, J.-M. Biochemistry 1969, 8, 207-213.
- Ferone, R.; Hanlon, M. H.; Singer, S. C.; Hunt, D. F. J. Biol. Chem. 1986, 261, 16356-16362.
- 12. Meister, A. In Functions of Glutathione: Biochemical, Physiological, Toxicological, and Clinical Aspects; Larsson, A., Orrenius, S., Holmgren, A., Mannervik, B., Eds.; Raven Press: New York, 1983; pp 1-22.

- 13. Viña, J.; Viña, J. R. In Functions of Glutathione: Biochemical, Physiological, Toxicological, and Clinical Aspects; Larsson, A., Orrenius, S., Holmgren, A., Mannervik, B., Eds.; Raven Press: New York, 1983; pp 23-30.
- 14. Jones, D. P.; Kennedy, F. G. In Functions of Glutathione: Biochemical, Physiological, Toxicological, and Clinical Aspects; Larsson, A., Orrenius, S., Holmgren, A., Mannervik, B., Eds.; Raven Press: New York, 1983; pp 109-116.
- 15. Holmgren, A. In Functions of Glutathione: Biochemical, Physiological, Toxicological, and Clinical Aspects; Larsson, A., Orrenius, S., Holmgren, A., Mannervik, B., Eds.; Raven Press: New York, 1983; pp 199-204.
- Orrenius, S; Jewell, S. A.; Bellomo, G.; Thor, H.; Jones, D. P.; Smith, M. T. In Functions of Glutathione: Biochemical, Physiological, Toxicological, and Clinical Aspects; Larsson, A., Orrenius, S., Holmgren, A., Mannervik, B., Eds.; Raven Press: New York, 1983; pp 261-272.
- 17. Barany, G.; Merrifield, R. B. In *The Peptides*, Volume 2; Gross, E.; Meinhofer, J., Eds.; Academic Press: New York, 1979; pp 1-284.
- 18. Naughton, M. A.; Sanger, F.; Hartley, B. S.; Shaw, D. C. *Biochem. J.* 1960, 77, 149-163.
- 19. Geiger, T.; Clarke, S. J. Biol. Chem. 1987, 262, 785-794.
- Clarke, S.; Stephenson, R. C.; Lowenson, J. L. In Stability of Protein Pharmaceuticals, Part A, Chemical and Physical Pathways of Protein Degradation;
 Ahern, T. J., Manning, M. C., Eds.; Plenum Press: New York, 1992; pp 1-29.
- 21. Brennan, T. V.; Clarke, S. Protein Sci. 1993, 2, 331-338.
- 22. Stephenson, R. C.; Clarke, S. J. Biol. Chem. 1989, 264, 6164-6170.

- 23. Tyler-Cross, R.; Schirch, V. J. Biol. Chem. 1991, 266, 22549-22556.
- 24. Clarke, S. Int. J. Peptide Protein Res. 1987, 30, 808-821.
- 25. George-Nascimento, C.; Lowenson, J.; Borissenko, M.; Calderon, M.; Medina-Selby, A.; Kuo, J.; Clarke, S.; Randolph, A. *Biochemistry* **1990**, *29*, 9584-9591.
- 26. Potter, S. M.; Henzel, W. J.; Aswad, D. W. Protein Sci. 1993, 2, 1648-1663.
- 27. Shahrokh, Z.; Eberlein, G.; Buckley, D.; Paranandi, M. V.; Aswad, D. W.; Stratton, P.; Mischak, R.; Wang, Y. J. *Pharmaceut. Res.* 1994, 11, 936-944.
- 28. Patel, K.; Borchardt, R. T. Pharmaceut. Res. 1990, 7, 703-711.
- 29. Liu, D. T. Trends Biotechnol. 1992, 10, 364-369.
- 30. Aswad, D. W. In *Deamidation and Isoaspartate Formation in Peptides and Proteins*; Aswad, D. W, Ed.; CRC Press: Boca Raton, **1995**; pp 1-6.
- Daumy, G. O.; Wilder, C. L.; Merenda, J. M.; McColl, A. S.; Georghegan, K. F.;
 Otterness, I. G. FEBS Lett. 1991, 278, 98-102.
- 32. Friedman, A. R.; Ichhpurani, A. K.; Brown, D. M.; Hillman, R. M.; Krabill, L. F.; Martin, R. A.; Aurcher-Neely, H. A.; Guido, D. M. Int. J. Peptide Protein Res. 1991, 37, 14-20.
- 33. Johnson, B. A.; Langmack, E. L.; Aswad, D. W. J. Biol. Chem. 1987, 262, 12283-12287.
- 34. Sun, A.-Q.; Yüksel, K. Ü.; Gracy, R. W. Arch. Biochem. Biophys. 1992, 293, 382-390.
- 35. Zale, S. E.; Klibanov, A. M. Biochemistry, 1986, 25, 5432-5444.
- 36. Artigues, A.; Birkett, A.; Schirch, V. J. Biol. Chem. 1990, 265, 4853-4858.

- Di Donato, A.; Ciardiello, M. A.; de Nigris, M.; Piccoli, R.; Mazzarella, L.;
 D'Alessio, G. J. Biol. Chem. 1993, 268, 4745-4751.
- 38. Cacia, J.; Quan, C. P.; Vasser, M.; Sliwkowski, M. B.; Frenz, J. *J. Chromatogr.* 1993, 634, 229-239.
- 39. Purcell, A. W.; Aguilar, M. I.; Hearn, M. T. W. J. Chromatogr. 1989, 476, 113-123.
- 40. Stevenson, C. L.; Anderegg, R. J.; Borchardt, R. T. J. Pharm. Biomed. Anal. 1993, 11, 367-373.
- 41. Lide, D. R., Ed. *CRC Handbook of Chemistry and Physics*, 76th Edition; CRC Press: Boca Raton, **1995**; p 7-1.
- 42. Kossiakoff, A. A. Science 1988, 240, 191-194.
- 43. Galletti, P.; Jardino, P.; Ingrosso, D.; Manna, C.; Zappia, V. Int. J. Peptide Protein Res. 1989, 33, 397-402.
- 44. Blodgett, J. K.; Loudon, G. M.; Collins, K. D. J. Am. Chem. Soc. 1985, 107, 4305-4313.
- 45. Smyth, D. G.; Stein, W. H.; Moore, S. J. Biol. Chem. 1963, 238, 227-234.
- 46. Lowenson, J. D.; Clarke, S. In *Deamidation and Isoaspartate Formation in Peptides* and *Proteins*; Aswad, D. W, Ed.; CRC Press: Boca Raton, 1995; pp 47-64.
- 47. Chazin, W. J.; Kordel, J.; Thulin, E.; Hofmann, T.; Drakenberg, T.; Forsen, S. *Biochemistry* 1989, 28, 8646-8653.
- 48. Di Donato, A.; Galletti, P.; D'Alessio, G. Biochemistry, 1986, 25, 8361-8368.
- 49. Lehrman, S. R.; Hamlin, D. M.; Lund, M. E.; Walker, G. A. J. Protein Chem. 1992, 11, 657-663.

- 50. Aswad, D. W.; Guzzetta, A. W. In Deamidation and Isoaspartate Formation in Peptides and Proteins; Aswad, D. W, Ed.; CRC Press: Boca Raton, 1995; p 18.
- Hassell, A. M.; Johanson, K. O.; Goodhart, P.; Young, P. R.; Holskin, B. P.; Carr, S. A.; Roberts, G. D.; Simon, P. L.; Chen, M.-J.; Lewis, M. J. Biol. Chem. 1989, 264, 4948-4952.
- 52. Papayannopoulos, I. A.; Biemann, K. Peptide Research 1992, 5, 83-90.
- 53. Carr, S. A.; Bean, M. F.; Hemling, M. E.; Roberts, G. D. In *Biological Mass Spectrometry*; Burlingame, A. L., McCloskey J. A., Eds.; Elsevier: Amsterdam, 1990, pp 621-652.
- 54. Galletti, P.; Ingrosso, D.; Manna, C.; Sica, F.; Capasso, S.; Pucci, P.; Marino, G. Eur. J. Biochem. 1988, 177, 233-239.
- 55. Yu, W.; Vath, J. E.; Huberty, M. C.; Martin, S. A. Anal. Chem. 1993, 65, 3015-3023.
- 56. Goodlett, D. R. Proceedings of the 45th ASMS Conference on Mass Spectrometry and Allied Topics, Palm Springs, CA, June 1-5, 1997.
- 57. Katta, V.; Chow, D. T. Proceedings of the 45th ASMS Conference on Mass Spectrometry and Allied Topics, Palm Springs, CA, June 1-5, 1997.
- 58. Tsaprailis, G.; Nair, H.; Somogyi, Á.; Wysocki, V. H.; Zhong, W.; Futrell, J. H.; Summerfield, S. G.; Gaskell, S. J. Proceedings of the 46th ASMS Conference on Mass Spectrometry and Allied Topics, Orlando, FL, May 31-June 4, 1998.
- 59. Qin, J.; Chait, B. T. J. Am. Chem. Soc. 1995, 117, 5411-5412.
- 60. Liao, P.-C.; Huang, Z.-H.; Allison, J. J. Am. Soc. Mass Spectrom. 1997, 8, 501-509.
- 61. Okada, K.; Kawase, M. Chem. Pharm. Bull. 1977, 25, 1497-1508.

- 62. Nagasawa, H. T.; Magnan, S. D. J.; Foltz, R. L. Biomed Mass Spectrom., 1982, 9, 252-256.
- 63. Ienaga, K.; Nakamura, K.; Higashiura, K.; Toyomaki, Y.; Kimura, H. *Chem. Pharm.*Bull. 1988, 36, 2796-2801.
- 64. Nakamura, K.; Higashiura, K.; Ienaga, K. Chem. Pharm. Bull. 1989, 37, 73-76.
- 65. Qin, X.-Z. J. Mass Spectrom. 1997, 33, 55-63.
- Lloyd, J. R.; Cotter, M. L.; Ohori, D.; Doyle, D. L. Biomed. Env. Mass Spectrom.
 1988, 15, 399-402.
- Violand, B. N.; Schlittler, M. R.; Toren, P. C.; Siegel, N. R. J. Protein Chem. 1990,
 9, 109-117.
- 68. Carr, S. A.; Hemling, M. E.; Bean, M. F.; Roberts, G. D. Anal. Chem. 1991, 63, 2802-2824.
- 69. Bean, M. F.; Carr, S. A. Proceedings of the 40th ASMS Conference on Mass Spectrometry and Allied Topics, Washington, DC, May 31-June 5, 1992.
- 70. Schindler, P.; Muller, D.; Märki, W.; Grossenbacher, H.; Richter, W. J. J. Mass Spectrom. 1996, 24, 967-974.
- 71. McFadden, P. N.; Clarke, S. J. Biol. Chem. 1986, 25, 11503-11511.
- 72. Huang, Z.-H.; Wu, J.; Roth, K. D. W.; Yang, Y.; Gage, D. A.; Watson, J. T. Anal. Chem. 1997, 69, 137-144.
- 73. Guettler, R. D.; Jones, G. C.; Posey, L. A.; Kirchner, N. J.; Keller, B. A.; Zare, R. N. J. Chem. Phys. 1994, 101, 3763-3771.
- 74. Cordero, M. M.; Houser, J. J.; Wesdemiotis, C. Anal. Chem. 1993, 65, 1594-1601.

- 75. Summerfield, S. G.; Whiting, A.; Gaskell, S. J. Int. J. Mass Spectrom. Ion Processes 1997, 162, 149-161.
- Schnier, P. D.; Price, W. D.; Jockusch, R. A.; Williams, E. R. J. Am. Chem. Soc.
 1996, 118, 7178-7189.
- 77. Graves, D. J.; Luo, S. J. Agric. Food Chem. 1987, 35, 439-442.
- 78. Roth, K. D. W.; Huang, Z.-H.; Sadagopan, N.; Watson, J. T. Mass Spectrom. Rev., 1998, 17, in press.
- 79. Papayannopoulos, I. A. Mass Spectrom. Rev. 1995, 14, 49-73.
- 80. Summerfield, S. G.; Cox, K. A.; Gaskell, S. J. J. Am. Soc. Mass Spectrom. 1997, 8, 25-31.
- 81. Downard, K. M.; Biemann, K. J. Am. Soc. Mass Spectrom. 1993, 4, 874-881.

